COUPLED DIFFUSIONAL/DISPLACIVE TRANSFORMATIONS

Shafiq Ahmad Mujahid

Darwin College

Cambridge

A dissertation submitted for the degree of

Doctor of Philosophy

at the University of Cambridge

July 1992

Dedicated to my parents, Saif–ur–Rehman and Mariam

Preface

This dissertation is submitted for the degree of Doctor of Philosophy at the University of Cambridge. The research work presented in this dissertation has been carried out at the Department of Materials Science and Metallurgy, University of Cambridge between April 1989 to July 1992, under the supervision of Dr. H. K. D. H. Bhadeshia. Except the places where acknowledgement and reference to previous work has been given, this work, to the best of my knowledge, is original and has not been submitted in whole or in part for a degree, diploma or other qualifications at any other University. This dissertation contains less than 60,000 words.

Parts of the results obtained in this research work have been published/submitted as follows:

(a) Mujahid, S. A. and Bhadeshia, H. K. D. H. (1992): Partitioning of carbon from supersaturated ferrite plates, *Acta Metallurgica*, **40**, 389–396.

(b) Mujahid, S. A. and Bhadeshia, H. K. D. H. (1991): Theoretical Analysis of Displacive Transformation of Austenite to Ferrite in Fe–Mn–Si–C Alloy, presented in the *Second International Symposium on Advanced Materials*, Islamabad, Pakistan, September, 15–19.

(c) Mujahid, S. A. and Bhadeshia, H. K. D. H. (1992): Coupled diffusional/displacive transformations: Effect of carbon concentration (*submitted to Acta Metallurgica for publication*).

Cambridge   Shafiq Ahmad Mujahid

July, 1992

Acknowledgements

Contents

Abstract

The displacive transformation of austenite to ferrite in steels containing both substitutional and interstitial elements has been studied. The aim was to establish the conditions under which plates of the product phase can form with a partial redistribution of the interstitial element during nonequilibrium nucleation and growth. An earlier model describing such 'coupled diffusional/displacive transformation' (CDDT) has been applied over a wide range of carbon concentrations, revealing a variety of discrepancies.

It was found that the theory correctly predicts the variation in the martensite–start temperature with carbon concentration, but fails to estimate the corresponding changes in the bainite–start temperatures of the same steels. Thus, the accuracy claimed by the original theory appears fortuitous for bainite. The failure is attributed to the fact that the model does not include any variation in the stored energy as a function of transformation temperature. The nature of the required variation in stored energy with temperature was calculated by fitting against available data and the CDDT model was modified appropriately. The estimated variation in stored energy is consistent with an expectation that when the yield strength is exceeded at a high enough temperature, plastic accommodation of the shape change should lead to a reduction in the stored energy. The modified model predicted a sharper transition from growth involving full partitioning of carbon, to diffusionless growth when applied to a number of alloyed steels. This abrupt transition from paraequilibrium to diffusionless growth is in fact consistent with experiments; Widmanstätten ferrite at all temperatures is known to grow at a rate controlled by the diffusion of carbon in the austenite ahead of the interface, whereas the growth rate of bainite subunits is much larger then might be expected from carbon diffusion–controlled growth. Considerable work is also reported on how bainite transformation might be described by the CDDT model, but significant difficulties remain.

Another model was developed to study the kinetics of the partitioning of carbon from supersaturated ferrite into residual austenite. The time required was estimated analytically and using a finite difference model. It was found that in all the cases investigated, the analytical solution underestimates the diffusion time, the discrepancy increasing at lower temperatures, or when the concentration of substitutional solutes which stabilise austenite is reduced. This is attributed to the fact that the analytical method fails to take account of the coupling of the diffusion fluxes that arise in both the austenite and the ferrite. The

results were first discussed in the context of displacive transformations in steels. The model was latter extended to the non–ferrous, Ag–44.9Cd at.% alloy. This alloy undergoes a $\beta_2 \rightarrow \alpha_1$ transformation which is sometimes called "bainite" by virtue of the fact that the plates appear to be different in composition from the parent phase. The α_1 plates could on the other hand, form without diffusion, the cadmium partitioning into the β_2 matrix after formation. The results are compared with published data, but they indicate that there is a need for more accurate diffusion data before definitive conclusions can be made on the mechanism of transformation.

Nomenclature and Abbreviations

α	ferrite
γ	austenite
G_{id}	Gibbs free–energy per unit volume, dissipated in the process of interfacial motion
G_{dd}	Gibbs free–energy per unit volume, dissipated in the diffusion of solute ahead of the transformation interface
ΔG	magnitude of Gibbs free–energy change per unit volume
x	carbon concentration (mole fraction)
x_I	carbon concentration in γ at γ/α interface (mole fraction)
x_m	maximum permissible carbon concentration in γ at the interface
x_α	carbon concentration in α at α/γ interface (mole fraction)
$\overline{x}$	average carbon concentration in alloy (mole fraction)
$x^{\alpha\gamma}$	equilibrium carbon concentration in α (mole fraction)
$x^{\gamma\alpha}$	equilibrium carbon concentration in γ (mole fraction)
θ	cementite
γ_{en}	enriched austenite
$\alpha_{ub,ss}$	supersaturated upper banite
$\alpha_{ub,us}$	unsaturated upper bainite
$\alpha_{lb,ss}$	supersaturated lower banite
$\alpha_{lb,us}$	unsaturated lower bainite
θ_f	cementite in ferrite
$\theta_{f/f}$	cementite between ferrite plates
ε_f	cementite in ferrite
V_i	velocity as calculated using the interfacial mobility law
V_d	velocity as calculated using the diffusion field velocity law
p	Péclet number
ρ	plate tip radius
D	diffusivity of carbon in γ
$\overline{D}$	weighted average diffusivity of carbon in γ
k	Boltzmann constant
Q_0	activation free–energy necessary to overcome the resistance to interfacial motion

	in the absence of an interfacial driving force
Q^*	activation free–energy for interfacial motion
V_0	pre–exponential velocity factor for thermally activated interfacial motion
$\hat{G}_{id}$	maximum glide resistance presented by obstacles to dislocation motion
μ	shear modulus of austenite
Ω	volume per atom
E	Young modulus
ν	Poisson ratio
N_0	Avodagro number
k_p	partition coefficient
k_e	equilibrium partition coefficient
λ	inersite distance
V_k	velocity as calculated using the Aziz solute trapping law
G_{el}	stored free–energy per unit volume, due to elastic strain
G_{surf}	stored free–energy per unit volume, due to interface
G_{α}	stored energy of α (where $G_{\alpha} = G_{el} + G_{surf}$)
M_s	martensitic–start temperature
B_s	bainite–start temperature
$\Delta G^{\gamma\alpha}$	driving force for diffusionless transformation
$\Delta G_{M_s}^{\gamma\alpha}$	driving force for diffusionless transformation at M_s temperature
ΔG_m	driving force for nucleation
G_N	universal function for displacive nucleation
w_{α}	width of the ferrite plate
t_d	time for decarburisation
D_c^{α}	diffusion of carbon in α
w_{γ}	width of slab of austenite
r_{γ}	grid parameter in the finite difference method for γ
r_{α}	grid parameter in the finite difference method for α
w'	normalised thickness used in the finite difference method
x'	normalised carbon concentration used in the finite difference method
t'	normalised value of time used in the finite difference method
$\overline{x}^{\alpha}$	mean carbon concentration in ferrite (mole fraction)
x_{α_1}	Cd composition in α_1–plate at α_1/β_2 interface (at.%)

x_I^{β} Cd composition in β_2 matrix at β_2/α_1 interface (at.%)

$x^{\alpha_1\beta_2}$ equilibrium cadmium concentration in α_1 (at.%)

$x^{\beta_2\alpha_1}$ equilibrium cadmium concentration in β_2 (at.%)

w_{α_1} width of the α_1–plate

D_{Cd} diffusivity of Cd

$D_{Cd}^{\alpha_1}$ diffusivity of Cd in α_1–plate

$D_{Cd}^{\beta_2}$ diffusivity of Cd in β_2 matrix

Q activation energy

w_{β_2} width of slab of β_2 matrix

r_{β_2} grid parameter in the finite difference method for β_2 matrix

r_{α_1} Grid parameter in the finite difference method for α_1–plate

$\overline{x}^{\alpha_1}$ average cadmium concentration in α_1–plate (at.%)

Chapter 1

Aspects of Phase Transformations

1.1 Introduction

Solid–state phase transformation is an important topic in physical metallurgy, since almost all industrial metals and alloys are heat–treated after casting to improve and optimise their properties. The heat treatment changes the microstructure of the alloy, either by a recovery and recrystallisation process, or by some type of a phase change. Two main types of transformations are found: polymorphic changes and precipitation reactions. In a polymorphic change, in for example elementary iron, cobalt or titanium, there is a change of crystal structure without a change of chemical composition. This affects all the atoms in the alloy and presents a tremendous scope for controlling the microstructure of the alloy. In precipitation reactions, which are crucial in alloys based on aluminium, copper and nickel, the main method of modifying the microstructure is to alloy with elements that are soluble in the base metal at high temperatures but precipitate out of solution at lower temperatures.

In both polymorphous and precipitation reactions, there is a migration of an interface between two crystalline phases, and there are two essential modes of interfacial migration. In the first of these modes, atoms make thermally activated random jumps across the interface, a "diffusive" mechanism. In the second mode, the daughter crystal grows into the parent, by a coordinated shear–type motion of all the atoms at the interface. Some transformations, such as those in iron–based alloys that are described as bainite, appear to have both a diffusive and martensitic character (Cahn and Haasen, 1983).

1.2 Modes of Phase Transformations

These can generally be divided into two catagories, 'displacive' and the 'reconstructive' transformations. These terms have a long–established usage, especially in non–metallurgical fields (Burger, 1951) and may seem more adaptable than their metallurgical equivalents (shear and diffusional). This classification, however, is rather closely linked to the concept

ite. This transformation is important and best known in connection with certain types of stainless steel, quenched and tempered steels and ball bearing alloys.

Important recent developments involving the martensitic transformation in steels include maraging steel (precipitation–hardened martensite), TRIP steels (transformation induced plasticity), ausforming steels (plastically deformed austenite prior to quenching) and dual phase steels (a mixture of ferrite + martensite obtained by quenching from the $\gamma + \alpha$ field).
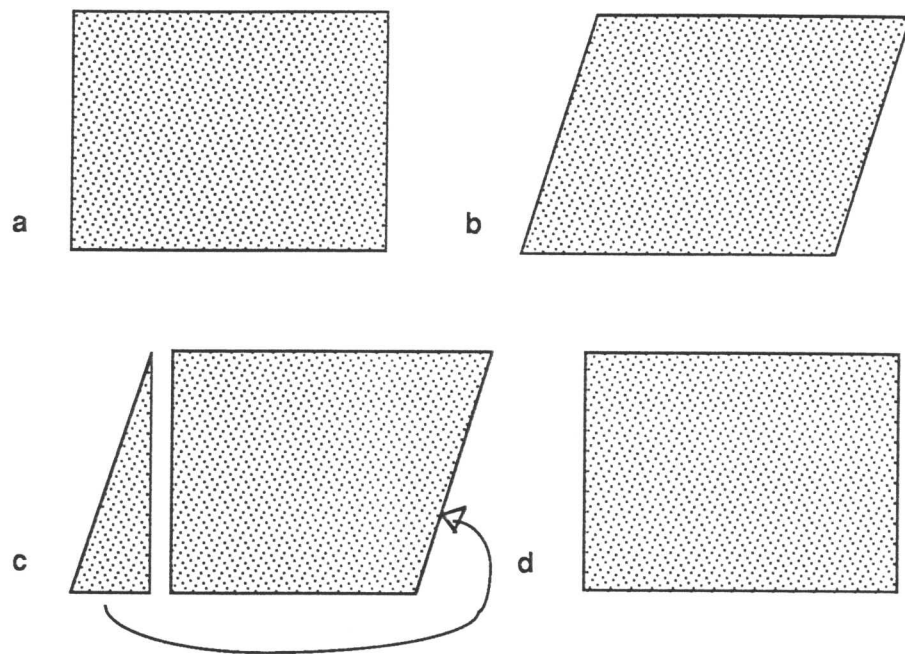
Figure 1.1: Transformation mechanism of reconstructive transformation. The lattice undergoes transformation shown from a to d. Displacive transformation stops at stage b.

In the study of displacive transformations, it is necessary to discuss the mobility of martensitic interfaces. Martensitic growth via slow interfacial motion makes an important contribution to overall transformation. Further, it is believed that the operational nucleating event in martensitic transformations is controlled by the motion of the interface of a supercritical nucleus (Olson and Cohen, 1976; 1982) and, consequently, its mobility is of fundamental importance to both nucleation and growth.

Boundaries in the solid state may conveniently be regarded as either glissile or non-glissile. A glissile boundary can migrate readily under the action of a suitable driving stress, even at very low temperatures, and its movement does not require thermal activation. Examples of the motion of glissile boundaries are provided by the growth of martensite plates or of a mechanical twin, or by the stress–induced movement of a symmetrical low angle tilt boundary. In all cases, the shape of the specimen changes as the boundary is displaced, so that the movement may be regarded as a form of plastic deformation. It follows that a suitable external mechanical stress should be able to produce displacement of any glissile interface.

The remaining types of boundary can move only with the assistance of thermal fluctuations. However mobile such a boundary may be at high temperatures, it must become virtually immobile at sufficiently low temperatures. We subdivide non–glissile boundaries into those in which there is no change of composition across the interface and those dividing regions of different composition. In the first group are any transformations from a metastable single phase to an equilibrium single phase (polymorphic changes), processes such as recrystallisation and grain growth which are entirely one–phase, and order–disorder reactions. In all these examples, the rate of growth is determined by atomic processes in the immediate vicinity of the interface, and we may describe such growth as "interface-controlled" (Christian, 1981).

Familiar examples of growth in which there is a composition difference across a moving interface are provided by precipitation from supersaturated solid solution and eutectoidal decompositions. The motion of the interface now requires longe–range transport of atoms of various species towards or away from the the growing regions, so that it is necessary to consider the diffusional processes which lead to the segregation. Two extreme cases can be distinguished in principle. In one of these we have a boundary which can move slowly, even under the influence of high driving forces. The rate of motion will then be largely independent of the diffusion rate, and we may again describe the growth as interface-controlled. The other extreme case is where the boundary is highly mobile when compared with the rate of diffusion, so that it will move as rapidly as the required segregation can be accomplished. The growth rate is then determined almost entirely by the diffusion conditions, and is said to be "diffusion–controlled" (Christian, 1981).

1.3 Rate Controlling Processes

The rate at which an interface moves depends both on its intrinsic mobility (related to the process of structural changes across the interface) and on the ease with which any solute elements partitioned during transformation diffuse ahead of the moving interface. The two processes are in series so that the interfacial velocity equals that computed from the diffusion of solute ahead of the interface (Olson *et al.*, 1989). Both of these processes dissipate the net free–energy available for interfacial motion, G_{id} being the amount dissipated in the interface process and G_{dd} the quantity dissipated in the diffusion process. The constant temperature free–energy curve is shown in Figure 1.2a. The two dissipations G_{id} and G_{dd} are related by the equation:

$$\Delta G = G_{id} + G_{dd}. \tag{1.1}$$

When $\Delta G \approx G_{dd}$, growth is said to be diffusion–controlled. Interface–controlled growth occurs when $\Delta G \approx G_{id}$. Mixed control arises when neither process dominates.

The diffusion field (composition versus position) that must move with the interface is of the form depicted in figure 1.2b, where x_I is the composition of γ–phase at the interface. In Figure 1.2, x_m is the carbon concentration of the austenite at the interface when $G_{id} = 0$ (*i.e.* when $\Delta G = G_{dd}$) and when the composition of the ferrite is α. This is consistent with the fact that a higher level of carbon in the austenite at the interface would cause an increase in free–energy as the interface moves during the $\gamma \to \alpha$ transformation.

1.4 Coupled Diffusional and Displacive Transformations

During phase transformation, the product phase sometimes grows with a nonequilibrium composition. Nonequilibrium growth may occur without any composition change, as in martensitic transformations, or some kind of a constrained equilibrium may exist at the transformation interface. An example of constrained equilibrium is paraequilibrium during the $\gamma \to \alpha$ transformation in alloy steels (Hultgren, 1951; Hillert, 1951; Rudberg, 1952; Aaronson *et al.*, 1966 and Bhadeshia, 1985b), in which the substitutional lattice may be considered to be configurationally frozen. The substitutional/iron atom ratio is then constant everywhere, but subject to this constraint, the carbon achieves equality of chemical potential in both phases.

A more general case of nonequilibrium transformation would be where none of the elements achieve a uniform chemical potential in all the phases even though, unlike martensitic reactions, there is some limited redistribution of alloying elements during transformation.

5
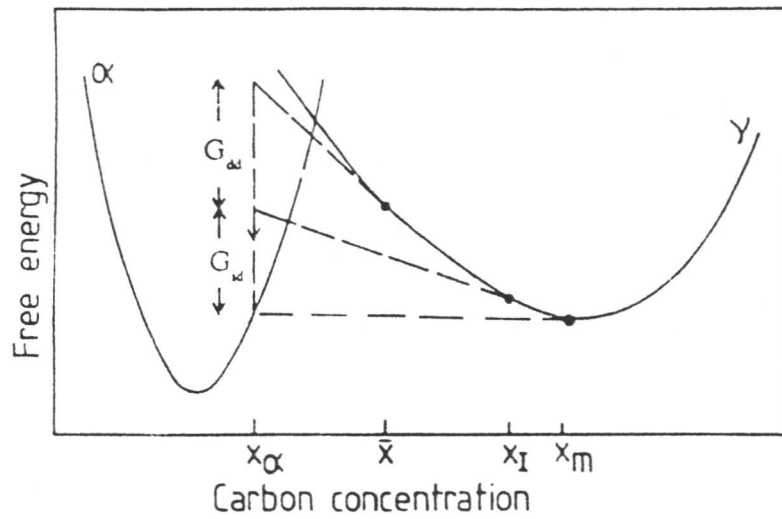
(a)
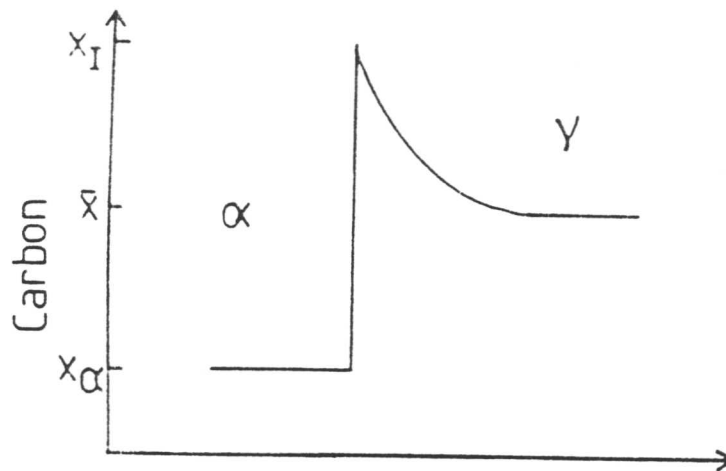
(b)

Figure 1.2: (a) Constant temperature free–energy curves for the case where the interface compositions are as illustrated in (b).

During such a process, there must naturally be a net reduction in free–energy, but in addition, the transfer of individual elements across the interface cannot be independent of the other elements (Baker and Cahn, 1971). The nonequilibrium may be better understood by looking at the schematic diagrams shown in Figure 1.3.

6
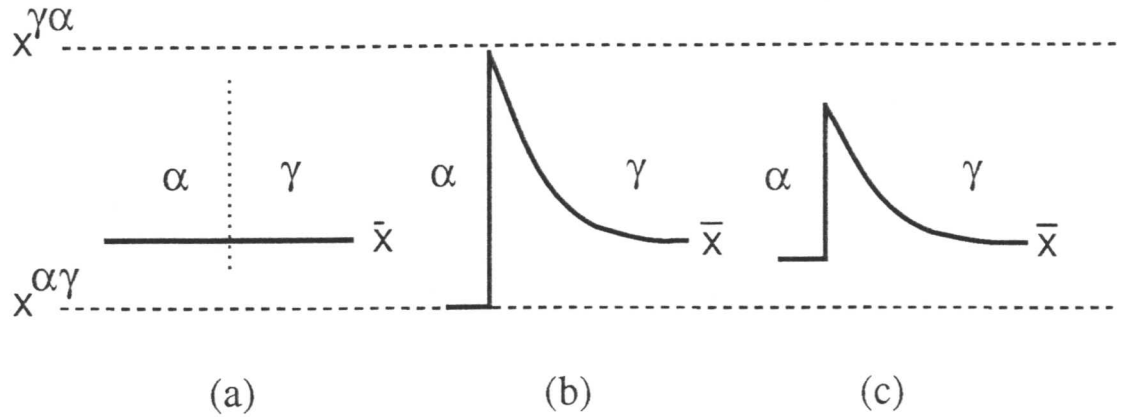
Figure 1.3: Possible carbon concentration profiles at the ferrite/austenite transformation interface during growth. (a) Diffusionless growth; (b) growth with diffusion–control; (c) growth with a partial supersaturation of carbon in the ferritic phase.

The diffusion–controlled growth profile (Figure 1.3b) represents the complete diffusional process where $x^{\alpha\gamma}$ and $x^{\gamma\alpha}$ are given by the phase diagram. Figure 1.3a is the case of a martensitic transformation which is displacive in nature where the carbon concentration is the same in both the γ and α phases and is equal to the average concentration of the alloy ($\overline{x}$). A possible example is the $\gamma \rightarrow \alpha + \gamma\prime$ transformation in a Fe–C alloy where the α has a carbon concentration (x_α) lower than the average concentration ($\overline{x}$), but higher than its equilibrium concentration $x^{\alpha\gamma}$ (Figure 1.3c). In these circumstances, the α is said to grow with a partial supersaturation of carbon (Olson et al., 1989).

The situation illustrated in Figure 1.3c is in principle unstable since any perturbation of the composition in the austenite at the interface, towards $x^{\gamma\alpha}$, should lead to a reduction in free energy. The profile should therefore tend to change towards that illustrated in Figure 1.3b. The instablility of the diffusion field during growth involving partial supersaturation can be illustrated using a mechanical analogy (Figure 1.4.).

Figure 1.4a represents the state of stable equilibrium. If the ball is infinitesimally perturbed, it will move to restore the equilibrium. The case of unstable equilibium is show in Figure 1.4b where the ball is stable but not to even the slightest purturbation. Nonequilibrium is like a ball located at the side of a hill (Figure 1.4c); a perturbation which lowers its potential energy is favoured, so that ball should collapse continuously towards

7

lowest energy position.

(a)   (b)   (c)
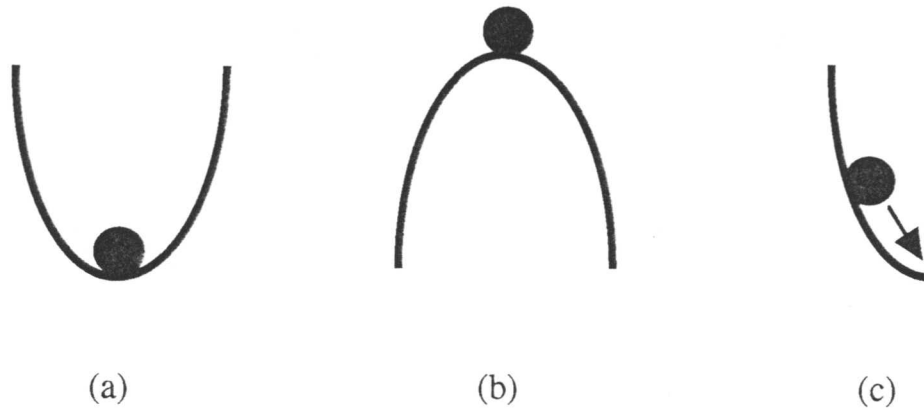
Figure 1.4: Schematic illustration of instability of diffusion field.

Since any diffusion field is by its very nature subject to random perturbations, opportunities must arise for the field to adjust towards lower free energy states. It follows that there will be a tendency for partial supersaturation to collapse towards equilibrium. Thus, it is necessary to introduce some other process which prevents the ball from falling down. In other words, growth involving partial supersaturation has to be stabilised by some process which occurs in series with the diffusion of solute (Christian and Edmonds, 1984). One such stabilising process is already there in the form of structural changes across the interface (Olson *et al.*, 1989). The schematic diagrams in Figure 1.5 show how the nonequlibrium can be made stable.

There are two processes which determine the compositions at the interface; the diffusional process (Figure 1.5a) and the mobility of the interface *i.e.* the structural changes across the interface (Figure 1.5b). Since these two processes are in series, therefore the stable nonequlibrium illustrated in Figure 1.5c can be acheived. If the temperature is sufficient to allow some degree of atomic diffusion, solute partitioning between the two phases could increase the operative driving force and allow interfacial motion (Olson and Cohen, 1986).

1.5 Kinetics of Bainite

A major reason for the examination of growth involving partial supersaturation is to see whether that represents the bainite transformation in steels. Hence, a brief overview of

8

the relevant points is presented below – a detailed survey can be found in Bhadeshia (1988).

(a)   (b)   (c)
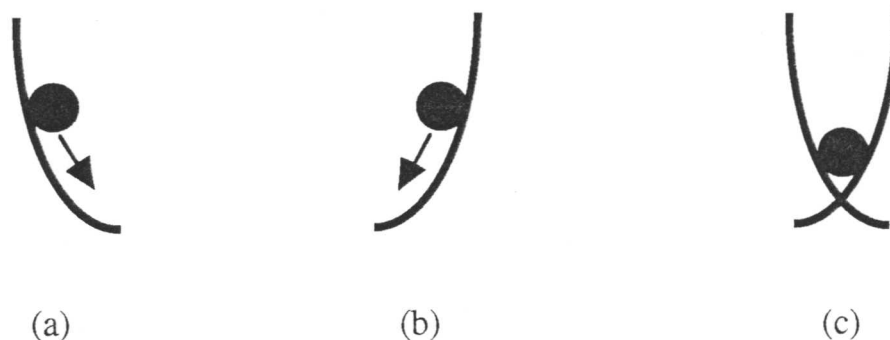
Figure 1.5: Schematic illustration of stability of nonequilibrium due to two processes operating in series (c).

A key problem in the study of bainite is to determine the carbon concentration of bainitic ferrite during its growth. If a platelet of bainitic ferrite grows with the composition of the parent austenite, and subsequently rejects its excess carbon into residual austenite, then the next platelet would have to form from γ which is enriched in carbon. A reaction like this would stop prematurely when the carbon concentration of the residual austenite becomes high enough to prevent composition invariant transformation i.e., when x_γ reaches the T_0 curve on the phase diagram (Bhadeshia, 1988).

In steels where the bainite transformation can be studied without interference from other reactions, it is found that the maximum volume fraction of bainite obtained during isothermal transformation from austenite increases from zero as the transformation temperature decreases below the bainitic start temperature, B_s (Hehemann, 1970; Christian and Edmonds, 1984). The fact that bainite is not obtained at all for $T > B_s$, together with the observation that for $T < B_s$, the transformation ceases well before the carbon concentration of the residual austenite reaches the equilibrium or paraequilibrium $\alpha + \gamma/\gamma$ phase boundary is the essence of the incomplete reaction phenomenon (Bhadeshia, 1988).

Kinetic data obtained from various resources confirm that bainite grows with a supersaturation of carbon, since the lengthening rates of sheaves and subunits far exceed those calculated on the basis of paraequilibrium, carbon diffusion–controlled growth (Bhadeshia,

9

1984; 1985a).

Since bainitic ferrite grows with a noneqilibrium concentration of carbon, the carbon should tend at some stage to partition into the residual austenite where it has a lower chemical potential. The time needed to decarburise the ferrite is intuitively expected at least to be comparable to that required for a subunit to complete its growth. If the decarburisation time is small relative to the time required to relieve the carbon supersaturation by the precipitation of carbides within the ferrite, the upper bainite is obtained; otherwise, lower bainite forms (Bhadeshia, 1988).

1.5.1 Carbides and Bainite

The variation of the carbon concentration in bainitic ferrite during transformation is very important in determining the kinetics of carbide precipitation. The formation of bainite does not involve the co-operative growth of bainitic ferrite and carbides. The ferritic component of bainite forms first; the excess carbon in this thermodynamically unstable, supersaturated bainitic ferrite is then removed by either of two competing processes. These processes are the partitioning of carbon into the residual austenite or its precipitation (in form of carbides) within the bainitic ferrite. At relatively high temperatures, the rejection of carbon into the residual austenite is rapid, so that any carbide precipitation occurs from the carbon enriched residual austenite and the final microstructure obtained is upper bainite. At lower temperatures, carbide precipitation within the bainitic ferrite is predominant, resulting in lower bainite. The distribution of carbon in the residual austenite is not, in general, homogeneous after isothermal transformation to bainite. The austenite is enriched to a greater extent in the immediate vicinity of bainite platelets or in regions trapped between platelets (Matas and Hehemann, 1961; Schrader and Wever, 1952). The sequence of transformation can be summarised as follows (Bhadeshia, 1988; Bhadeshia, 1989, Bhadeshia and Christian, 1990).

1. Upper bainite

$$\gamma \rightarrow \gamma + \alpha_{ub,ss} \rightarrow \alpha_{ub,us} + \gamma_{en} \rightarrow \alpha_{ub,us} + \alpha + \theta$$
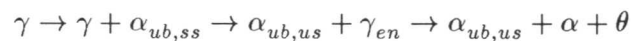
where γ, θ and γ_{en} are austenite, cementite and enriched austenite respectively. α, $\alpha_{ub,ss}$ and $\alpha_{ub,us}$ are the ferrite, supersaturated upper banite and unsaturated upper bainite repectively.

2. Lower bainite: the dislocation density of lower bainite has an effect on the free energy of carbon in the bainitic ferrite and hence can influence the carbide precipitation sequence,

10

determining in particular whether ε–carbide forms before the growth of cementite.

(i) high dislocation density

$$\gamma \rightarrow \gamma + \alpha_{lb,ss} \rightarrow \theta_f + \alpha_{lb,us} + \gamma_{en} \rightarrow \alpha_{lb,us} + \alpha + \theta_{f/f} + \theta_f$$
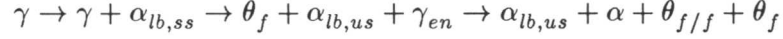
where $\alpha_{lb,ss}$ and $\alpha_{lb,us}$ are the supersaturated lower banite and unsaturated lower bainite repectively. θ_f and $\theta_{f/f}$ are cementite in ferrite and cementite between ferrite plates respectively.

(ii) low dislocation density

$$\gamma \rightarrow \gamma + \alpha_{lb,ss} \rightarrow \varepsilon_f + \alpha_{lb,us} + \gamma_{en} \rightarrow \alpha_{lb,us} + \varepsilon_f + \alpha + \theta_{f/f} \rightarrow \alpha_{lb,us} + \theta_f + \theta_{f/f} + \alpha$$
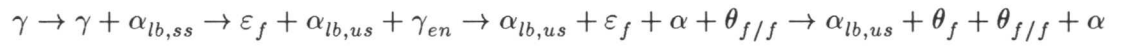
where ε_f is the cementite in ferrite.

1.6 Summary

A brief literature review of some of the relevant aspects of phase transformations has been presented. In steels and some other alloys, the bainite transformation appears to have both diffusional and displacive characteristics. The martensitic transformations which is displacive in nature, represents an extreme instance of nonequilibrium transformation in which there is no diffusion at all. Within the category of displacive transformations, Widmanstätten ferrite similarly represents the other extreme, whereby iron and substitutional solute atoms do not diffuse during transformation, but subject to that constraint, the carbon achieves equality of chemical potential in all phases. Widmanstätten ferrite therefore never has an excess carbon concentration. In between these two bounds of nonequilibrium transformation, there may exist situations in which growth occurs with a partial supersaturation of carbon. Some of the carbon would then be trapped whereas the remainder would be partitioned into the residual austenite.

Chapter 2

Coupled Diffusional/Displacive Transformations:
Effect of Carbon Concentration

2.1 Introduction

Martensitic transformations in steels are well established to be diffusionless (Christian, 1965b). The growth of Widmanstätten ferrite, on the other hand, occurs by a mechanism in which the structural change is accomplished by displacive transformation, but interstitial carbon partitions between the parent and product phases. Thus, martensite represents an extreme instance of nonequilibrium transformation in which there is no diffusion at all. Within the category of displacive transformations, Widmanstätten ferrite similarly represents the other extreme, whereby iron and substitutional solute atoms do not diffuse during transformation, but subject to that constraint, the carbon achieves equality of chemical potential in all phases (Bhadeshia, 1985a). The Widmanstätten ferrite therefore never has an excess carbon concentration.

It is feasible that between these two bounds of nonequilibrium transformation, there exist situations in which growth occurs with a partial supersaturation of carbon (Hillert, 1960; Bhadeshia, 1981a; Olson *et al.*, 1989; Agren, 1989). Some of the carbon would then be trapped whereas the remainder would be partitioned into the residual austenite (Figure 1.3). A situation like this is at first sight unstable because any perturbation in the carbon concentration of the ferrite which takes it nearer to equilibrium would lead to a reduction in free energy (Bhadeshia, 1981a). The process should then tend to collapse towards equilibrium growth as illustrated in Figure 1.4. However, the diffusion of carbon is not the only process occurring during ferrite growth; other processes acting in series could in principle stabilise nonequilibrium growth involving partial supersaturation (Christian and Edmonds, 1984).

The processes which act in series in order to accomplish transformation include the diffusion of carbon ahead of the interface, the transfer of atoms across the interface, and the trapping of solute atoms in the product phase (Olson *et al.*, 1989; 1990). Each of

these is associated with a dissipation of a fraction of the available free energy change. The dissipation can, with an appropriate model, be related to an interface response function, such as the diffusion field velocity, interfacial mobility or a solute trapping velocity. Since there is only one interface moving, the dissipations must be chosen in such a way that all the interface response functions give the same velocity. It is this condition which permits the evaluation of velocity, supersaturation and interfacial composition from the simultaneous solution of the three interface response functions.

The first two response functions i.e. diffusion–field velocity and interface mobility are in analogy with the electrical circuit where two resistors are connected in series as shown in Figure 2.1a. The potential difference (driving force) at each resistor gives different characteristic curve (voltage versus current). Since the resistors are in series the current passing through the system must be same. Thus the point of intersection of both curves (Figure 2.1b) will give the value of current passing through the circuit. Similarly in the present model two curves of driving force versus velocity can be drawn by using the process of mobility of the interface and diffusion field velocity. The point of intersection gives the velocity of the interface as shown in Figure 2.1c. Therefore, it is necessary to solve the following two equations simultaneously to determine the actual velocity:

$$V_i = \xi(G_{id}) \tag{2.1}$$

$$V_d = \psi(G_{dd}) \tag{2.2}$$

where ξ and ψ are response functions relating velocity to the Gibbs free energy per unit volume dissipated in the processs of interfacial motion and the diffusion of solute ahead of interface respectively.

Since the two processes are in series, putting correct values of G_{id} and G_{dd} in equations (2.1) and (2.2) give $V = V_i = V_d$, where V_i and V_d are the interface mobility and diffusion field velocity respectively. A third process (solute trapping) also exists in the transformation which provides the calculation of solute trapping velocity. The purpose of the present study was to investigate the effect of defining bainite in a way consistent with diffusionless growth using the coupled diffusional/displacive transformation (CDDT) model. It was also intended to extend the results to a range of carbon concentrations rather than just the Fe–0.4C wt.% alloy examined previously.

13
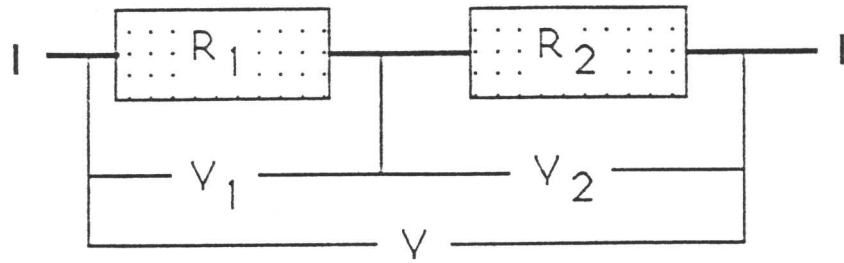
(a)
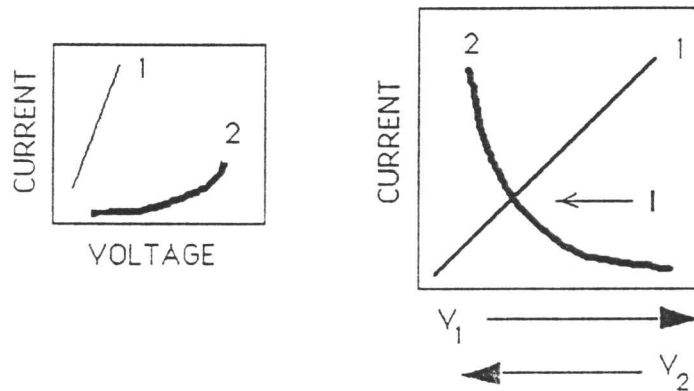
(b)
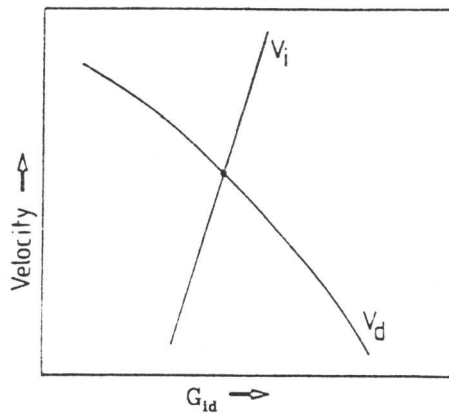
(c)

Figure 2.1: Interface response functions. (a) an analogy with electrical circuit (b) voltage versus current curve (c) coupled diffusional/displacive transformation (Olson *et al.*, 1989): diffusion–field velocity (for edge–wise growth of plate–shaped particle) and dislocation–interface velocity versus interfacial dissipation, identifying stable steady–state velocity for the coupled process.

2.2 The Response Functions

It is necessary to solve for three unknowns: the carbon supersaturation in the ferrite, the interface velocity, and the composition of the austenite at the interface. This can be done by considering three interface response functions for the processes which occur in series, and solving them simultaneously for a given transformation temperature and alloy. The three functions are the diffusion–field velocity, the interface mobility (describing the transfer of atoms across the interface) and the solute trapping function.

2.2.1 Diffusion-field Velocity

The lengthening rate, V_d, for steady state growth at a temperature, T, as a function of the diffusion of carbon in the austenite ahead of interface, can be approximated by the Ivantsov solution for a parabolic cylinder (Ivantsov, 1947):

$$\frac{(\overline{x} - x_I)}{(x_\alpha - x_I)} = (\sqrt{\pi p}) \exp(p) \mathrm{erfc}(\sqrt{p}) \tag{2.3}$$

where $\overline{x}$ is the mean carbon concentration of the alloy, x_I is the carbon concentration of the austenite at the interface, x_α is the carbon concentration in the growing ferrite and p is the Péclet number given by:

$$p = \frac{V_d \rho}{2\overline{D}}. \tag{2.4}$$

The Péclet number is a dimensionless velocity and ρ is the effective plate tip radius. Since the diffusion coefficient D of carbon in austenite depends on the carbon concentration x, a weighted average diffusion coefficient ($\overline{D}$) is used (Trivedi and Pound, 1967):

$$\overline{D} = \int_{x_I}^{\overline{x}} D\{x, T\} \frac{dx}{(\overline{x} - x_I)} \tag{2.5}$$

2.2.2 Interface Mobility

The interfacial velocity V_i, as dependent on the mobility of atoms across the transformation front, is calculated by using the dislocation models of interfacial structure (Grujicic et al., 1985a; 1985b; 1985c) based on the theory of thermal activated dislocation motion, which can be written as

$$V_i = V_0 \exp(-Q^*/kT) \tag{2.6}$$

where Q^* is the free energy of activation, V_0 is pre-exponential factor (m s^{-1}), k is the Boltzmann constant and T is the absolute temperature. The activation energy is given by the following integral

$$Q^* = \int_{G_{id}}^{\hat{G}_{id}} v^* dG \tag{2.7}$$

15

where G_{id} is the driving force dissipated in the transfer of atoms across the interface, $\hat{G}_{id}$ is maximum glide resistance, and v^* is the activation volume swept by the interface during the thermally activated event. For a wide range of obstacle interactions, the function Q^* can be written (Kocks *et al.*, 1975):

$$Q^* = Q_0 \left\{ 1 - \left(\frac{G_{id}}{\hat{G}_{id}} \right)^y \right\}^z \tag{2.8}$$

where Q_0 is the total activation free-energy necessary to overcome the resistance to dislocation motion without the aid of an interfacial driving force. Q_0 is given by (Olson, unpublished research)

$$Q_0 = 0.31 \mu \Omega \tag{2.9}$$

where μ is shear modulus of matrix and Ω is the volume per atom. The value of the shear modulus of matrix μ (in N m^{-2}) is given by;

$$\mu = \frac{0.5E}{(1 + \nu)} \tag{2.10}$$

where ν is Poisson ratio. The Young's Modulus (E) for different temperature ranges (Aaronson *et al.*, 1975) is given by

$$E = -18.8T + 52400 \qquad 25 \leq T(^\circ C) \leq 540$$

$$E = -37.6T + 62300 \qquad 540 \leq T(^\circ C) \leq 705$$

For our desired range of temperatures from 298 K to 813 K, the Young modulus in units of N m^{-2} can be written as

$$E = -78772000(T' - 273) + 2.1956 \times 10^{11} \qquad 298 \leq T'(K) \leq 813 \tag{2.11}$$

The value of ν for different temperature ranges (Aaronson *et al.*, 1975) is given by

$$\nu = 3.6 \times 10^{-5}T + 0.284 \qquad 260 \leq T(^\circ C) \leq 595$$

$$\nu = 9.9 \times 10^{-5}T + 0.246 \qquad 595 \leq T(^\circ C) \leq 705$$

For the temperature range of interest from 533 K to 868 K, ν can be written as

$$\nu = 3.6 \times 10^{-5}(T' - 273) + 0.284 \qquad 533 \leq T'(K) \leq 868 \tag{2.12}$$

16

Therefore by putting the values of E and ν in equation (2.10), we get the following equation for the shear modulus (μ) in the units of N m^{-2}.

$$\mu = \frac{-78772000(T' - 273) + 2.1956 \times 10^{11}}{3.6 \times 10^{-5}(T' - 273) + 1.284} \tag{2.13}$$

The molar volume of martensite Ω (in m^{3}mol^{-1}) is given by (Kaufman $et\ al.$, 1963)

$$\Omega = 6.679 \times 10^{-6}(1 + 7.89 \times 10^{-5}T') \tag{2.14}$$

where T' is in units of K. Putting the values of μ and Ω from equations (2.13) and (2.14) in equation (2.9), the value of Q_0 (in J mol^{-1}) may be obtained. For calculating the value in J atom^{-1}, we use the following equation

$$Q_0 = 0.31\frac{\mu\Omega}{N_0} \tag{2.15}$$

where N_0 is the Avogadro's number having the value of 6.023×10^{23}.

The quantities y and z define the shape of the force–distance function for solid–solution interactions. The following values of these constants are assumed (Nabarro, 1982)

$$y = 0.5$$

$$z = 1$$

Based on the behaviour of Fe–Ni–C alloys (Nabarro, 1982), the following value of $\hat{G}_{id}$ (in N m^{-2} or J m^{-3}) can be taken

$$\hat{G}_{id} = 1.22 \times 10^{-3}\mu \tag{2.16}$$

For calculating the value of $\hat{G}_{id}$ we need to find the value of shear modulus of austenite (μ) in J mol^{-1} and that can be calculated by the following equation

$$\mu = \frac{-78772000(T' - 273) + 2.1956 \times 10^{11}}{3.6 \times 10^{-5}(T' - 273) + 1.284}\Omega/N_0 \tag{2.17}$$

Putting all these values in equation (2.7), activation energy can be written as

$$Q^* = Q_0\left\{1 - \left(\frac{G_{id}}{\hat{G}_{id}}\right)^{0.5}\right\} \tag{2.18}$$

Putting this value in equation (2.6), the following equation for the interfacial mobility is obtained

$$V_i = V_0\exp\left[\frac{Q_0}{kT}\left\{1 - \left(\frac{G_{id}}{\hat{G}_{id}}\right)^{0.5}\right\}\right] \tag{2.19}$$

17

where $V_0=30$ m s^{-1} (Grujicic, 1985b).

2.2.3 The Solute Trapping Law

If the interface advance rapidly into the austenite then the carbon may not be able to diffuse away as required thermodynamically; it would then be trapped behind the advancing interface, in the ferrite, where its chemical potential is higher. This is solute trapping. The partitioning coefficient, k_p, is given by Aziz (1982) as:

$$k_p = \frac{x_\alpha}{x_I} \tag{2.20}$$

where x_α and x_I are the solute concentrations in ferrite and in austenite at the interface respectively. When the two concentration terms represent the respective equilibrium concentration of the phases concerned, then we have

$$k_p = k_e \tag{2.21}$$

where k_e is the equilibrium partitioning coefficient. The velocity function for solute trapping is (Aziz, 1982):

$$V_k = \frac{D\{x_I\}}{\lambda} \left(\frac{k_p - k_e}{1 - k_p} \right) \tag{2.22}$$

where λ is taken to be 0.25 nm. $D\{x_I\}$ is the carbon diffusivity in austenite of composition x_I. $D\{x_I\}/\lambda$ is the diffusion velocity of carbon. Trapping becomes significant as the actual interface velocity approaches this value.

2.3 Numerical Calculations

The model calculates the values of G_{dd} and G_{id} for different levels of supersaturation (*i.e.* for different values of x_α) using the concept of driving force (Olson *et al.*, 1989). Then it becomes possible to produce the curves of G_{id} (J mol^{-1}) versus x_I (mole fraction) for different x_α which are shown in Figure 2.2. The calculations for the velocity of the interface for different free energies have been carried out for both nucleation and growth for a variety of temperatures for low alloy carbon steels. The plots of velocity (V) versus free energy ($G_{id} + G_{el} + G_{surf}$) at different temperatures for Fe–0.2C wt.% alloy are shown in Figure 2.3.

The model, then calculates the point of intersection of each curve (in Figure 2.3) with the nucleation (dashed curve in Figure 2.3) and growth curves (chain–link curve in Figure

2.3). The equations for the diffusion curves (Figure 2.3) were obtained by curve fitting and are given by

$$V = B_1 + B_2 G'$$ (2.23)

where

$$G' = G_{id} + G_\alpha = (G_{id} + G_{el} + G_{surf})$$
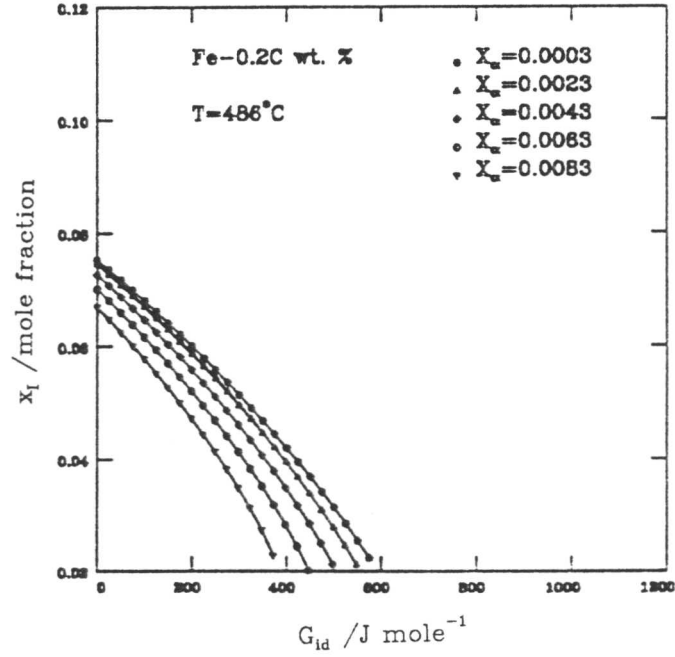
Figure 2.2: Illustration of the dependence of interfacial composition x_I on the interfacial dissipation G_{id} for a Fe–0.2C wt.% transformed at 486 °C .

B_1 and B_2 are the coefficients of the polynomial. The ordinate of the point of intersection of curve (Figure 2.3) with the growth curve (chain–link curve in Figure 2.3) can be found by the following transcendental equation

$$B_1 + B_2 G' = V_0 \exp\left[\frac{Q_0}{kT}\left\{1 - \left(\frac{G' - 700}{\hat{G}_{id}}\right)^{0.5}\right\}\right]$$ (2.24)

Hence the growth velocity (V) can be calculated by using equations 2.23 and 2.24. Similarly the ordinate of the point of intersection of the curve (Figure 2.3) with the nucleation curve (dashed curve in Figure 2.3) is calculated by the following transcendental equation

$$B_1 + B_2 G' = V_0 \exp\left[\frac{Q_0}{kT}\left\{1 - \left(\frac{G' - 2 \times 10^{-3}\mu}{\hat{G}_{id}}\right)^{0.5}\right\}\right]$$ (2.25)

19

where μ is in the units of J mol^{-1}. Hence the nucleation velocity can also be calculated using equation 2.23 and 2.25. The plot of velocity (V) versus concentration of carbon in ferrite at the interface (x_α) for both nucleation and growth for different temperature for Fe–0.2C wt.% is shown in Figure 2.4. Superimposed on these curves, are the data obtained using the solute trapping model.

The partitioning coefficient k_p can be determined using equation 2.20, given values of x_α, and related values of x_I. Using the data of G_{id}, corresponding x_I value could be calculated from the relationship between x_I and G_{id}, illustrated in Figure 2.2. The equilibrium partitioning coefficient k_e were calculated using the following equation:

$$k_e = \frac{x^{\alpha\gamma}}{x^{\gamma\alpha}} \tag{2.26}$$

where $x^{\alpha\gamma}$ is the equilibrium carbon concentration in ferrite, and $x^{\gamma\alpha}$ is the equilibrium carbon concentration in austenite. The latter was calculated using the Bhadeshia model (Bhadeshia, 1981a; 1981b; 1981c).

Finally, the points of intersection of the curves (Figure 2.4) for both nucleation and growth were used to draw the supersaturation curves (normalised supersaturation, $x_\alpha/\bar{x}$, versus temperature, T) for different low carbon alloy steels. Hence time–temperature–transformation (TTT) diagrams can be drawn accordingly.

2.4 Results and Discussion

The results of calculations performed for a series of carbon concentrations, using the original Olson *et al.* model (1990), are being considered. As a typical example, every intersection obtained from the first two response functions (diffusion field velocity and interface mobility) for Fe–0.2C wt.% alloy at a variety of temperatures for different levels of supersaturation is shown in Figure 2.3. These points of intersection correspond to a solution for velocity where interfacial velocity (V_i) equals diffusion field (V_d). The other two curves (chain–link and dashed), in Figure 2.3, correspond to growth at a stored energy (G_α) of 700 (J mol^{-1}) and nucleation event at a stored energy of $2 \times 10^{-3}\mu$ (J mol^{-1}) respectively. The stored energy, $G_\alpha = G_{el} + G_{surf}$, where G_{el} and G_{surf} are the elastic strain energy and surface energy respectively. The value of stored energy of nucleation event ($2 \times 10^{-3}\mu$ J mol^{-1}), corresponds to the plate tip radius (ρ) of 1.5 nm. These values of stored energy has been taken from the previous work (Olson *et al.*, 1989; 1990).

This difference of stored energy leads to different nucleation and growth kinetics. In the work of Olson *et al.* (1989), the simultaneous solution of the interface mobility and the diffusion–field velocity functions for a specified temperature led to the curves of velocity versus supersaturation for Fe–0.4C wt.% alloy. Superimposed on these curves, are the data obtained using the solute trapping model. In Figure 2.4, the intersection of two curves (solute trapping and the curve representing the simultaneous solution of diffusion field velocity and interface mobility curves) gives the velocity of the interface corresponding to nucleation and growth. The variation in the ferrite carbon supersaturation as a function of transformation temperature is illustrated in Figure 2.5a–d, for both the nucleation and growth processes. These data were used to calculate the martensite–start temperature as the temperature where both nucleation and growth become diffusionless. In order to assess these results, they were compared against estimates made with alternative more empirical (and less informative) models (Bhadeshia, 1981a; 1981b; 1981c) which are known to represent experimental data to within ±10 °C for a wide variety of steels. Figure 2.6 shows that the CDDT model is in excellent agreement with "experimental" data for the M_s temperatures. This is in spite of the fact that the parameters used in the interface response functions *etc.* are independently measured or derived; the results thus indicate that the methodology of the CDDT model is intrinsically correct.

The CDDT model was also used to calculate the bainite–start temperatures, using two methods. The first is that of Olson *et al.* where B_s is given by the highest temperature of the calculated "C" curve of the TTT diagram for displacive transformation. As pointed out earlier, this makes no assumptions about the carbon concentration of the bainitic ferrite during growth, whereas there are considerable data to indicate that the growth of bainite is indeed diffusionless. The second method, therefore, assumes that B_s is the highest temperature where growth becomes diffusionless, although the nucleus may grow with little or no supersaturation of carbon. Both of these assumptions led to an unsatisfactory results (Figure 2.7). The comparison of results is given in Table 2.1.

The original model gave the wrong trend for the B_s temperature as a function of the carbon concentration. The alternative assumption of diffusionless growth at a constant stored energy of $700\,\mathrm{J\,mol^{-1}}$ gave the correct trend but underestimated the B_s temperature. This last result is not surprising given that the stored energy value is appropriate for martensite in steels (Christian, 1979), but not for bainite. The latter is known to be associated with a smaller stored energy of the order of $400\,\mathrm{J\,mol^{-1}}$ (Bhadeshia, 1981a;

Table 2.1: Comparison of M_s and B_s values.

Alloy	Description	M_s (°C)	B_s (°C)
Fe–0.1C wt.%	Olson *et al.* (1990)	523	620
	Present Estimates	523	570
	Bhadeshia model	523	636
Fe–0.2C wt.%	Olson *et al.* (1990)	486	610
	Present Estimates	486	539
	Bhadeshia model	484	609
Fe–0.3C wt.%	Olson *et al.* (1990)	440	600
	Present Estimates	440	508
	Bhadeshia model	411	577
Fe–0.4C wt.%	Olson *et al.* (1990)	410	590
	Present Estimates	410	470
	Bhadeshia model	396	546

Olson *et al.*, 1989; Agren, 1989; Olson *et al.*, 1990; Christian and Edmonds, 1984).

The incubation time has been calculated using the relation $t = 10^{-5}/V$, where V is the velocity in ms^{-1} (Olson, 1989; Olson and Cohen, 1986). A comparison of the predicted time–temperature–transformation (TTT) diagrams with that obtained from the Bhadeshia model (Bhadeshia, 1981a; 1981b; 1981c) for Fe–0.1C, Fe–0.2C, Fe–0.3C wt.% and Fe–0.4C wt.% is shown in Figure 2.8.

2.5 Conclusion

A mathematical model for the coupled diffusional and displacive has been applied to a series of iron–carbon alloys to examine the displacive growth of partially carbon supersaturated ferrite plates. On the basis of the calculations, the following conclusions for a low alloy steels can be reached:

(a) It is in principle possible to envisage displacive growth involving a partial supersaturation of interstitial carbon.

(b) The level of supersaturation increases steadily as the transformation temperature is decreased. It is therefore possible to imagine the growth of ferrite plates with an equilibrium carbon concentration at high temperatures, and diffusionless martensitic transformation at low temperatures.

22

(c) Because during nucleation the surface to volume ratio of the nucleus is rather large, extra free energy is required to account for the corresponding surface energy. Thus, the level of carbon supersaturation that can be sustained in the nucleus tends in general to be less than during growth at the same temperature.

The trend of variation in B_s temperature as a function of carbon concentration can be satisfactorily estimated if it is assumed that the bainite–start temperature can be identified with the highest temperature at which diffusionless growth becomes possible. However, absolute agreement is found to be unsatisfactory. This problem will be addressed in Chapter 3.
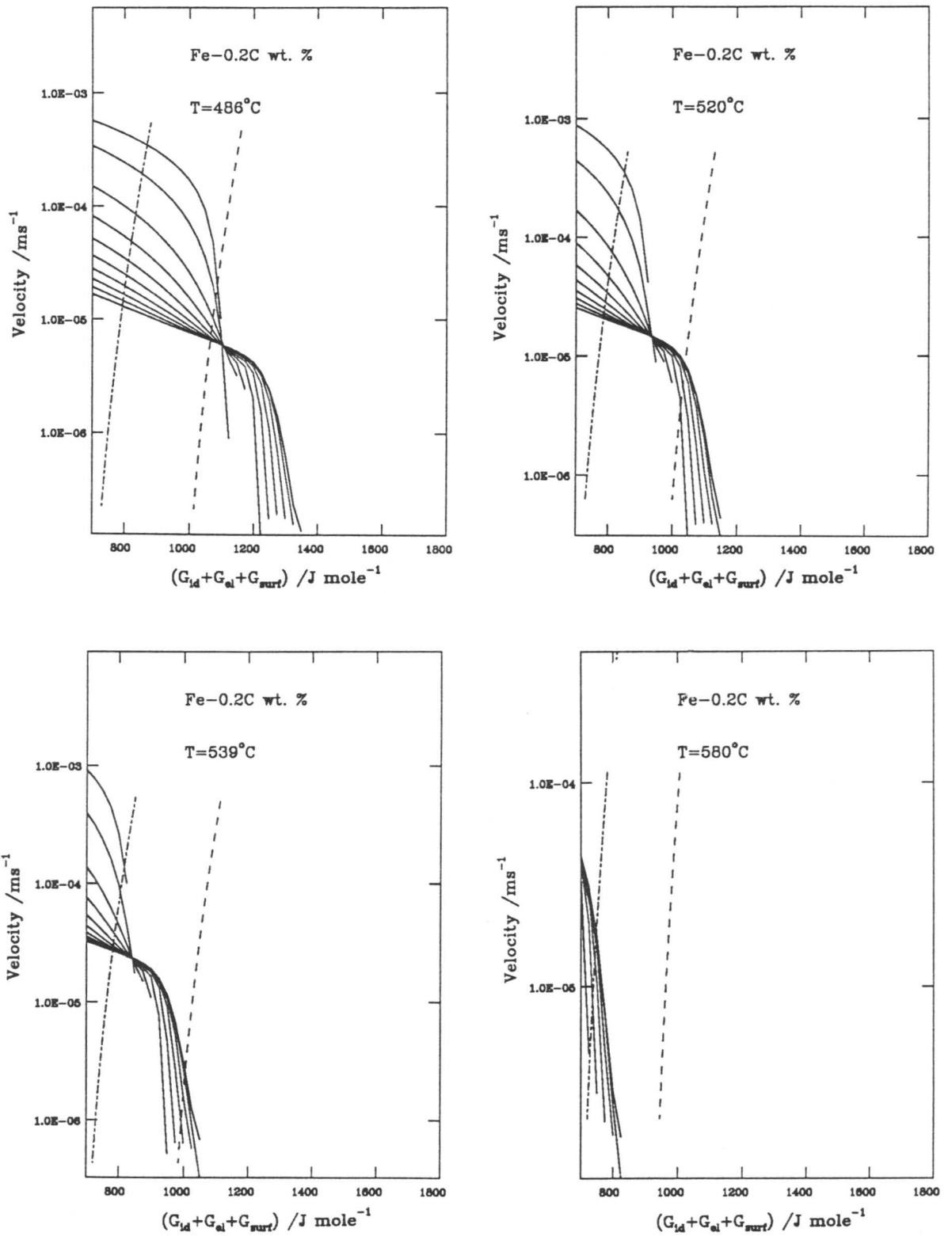
Figure 2.3: Plot of velocity versus free energy for Fe–0.2C wt.%. Different curves correspond to the diffusion field velocity for different levels of supersaturation. The chain–link curve corresponds to the velocity for growth and the dashed curve to the velocity for nucleation events.

24
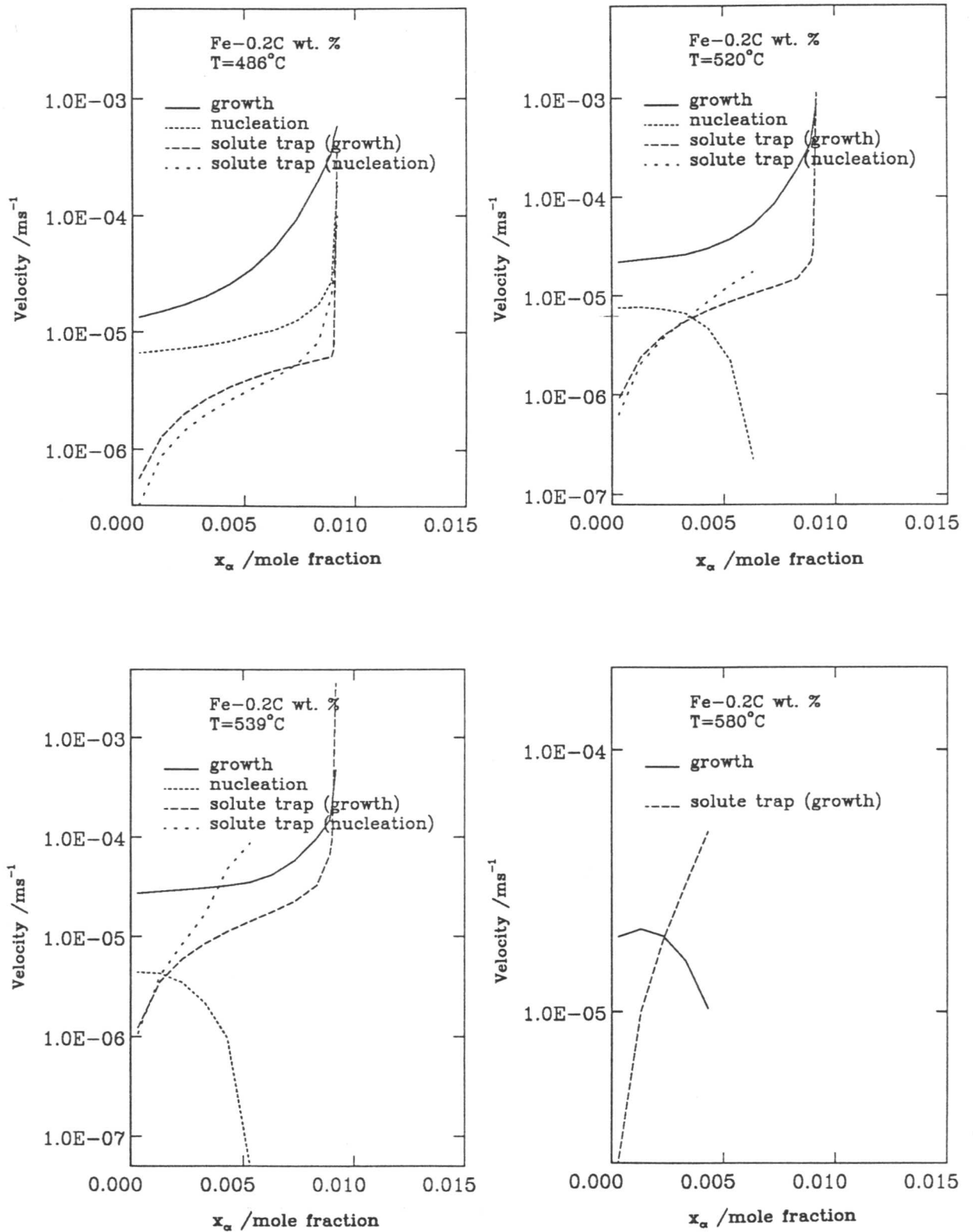
Figure 2.4: Plot of velocity versus carbon concentration in ferrite for all cases where $V_i = V_d$, and the solute trapping functions. The results are for Fe–0.2C wt.% at a variety of temperatures and similar kind of graphs were obtained for Fe–0.1C, Fe–0.3C and Fe–0.4C wt.% alloys.
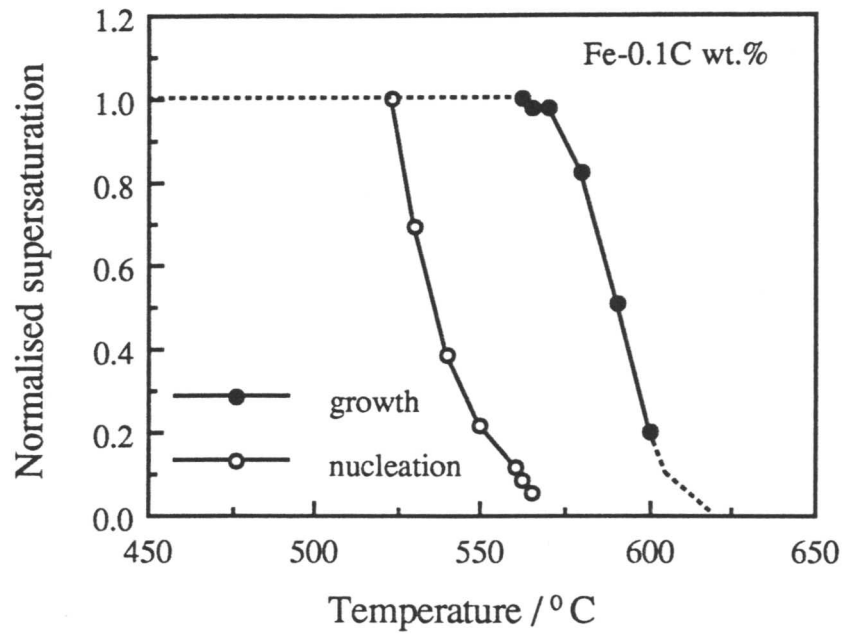
(a)
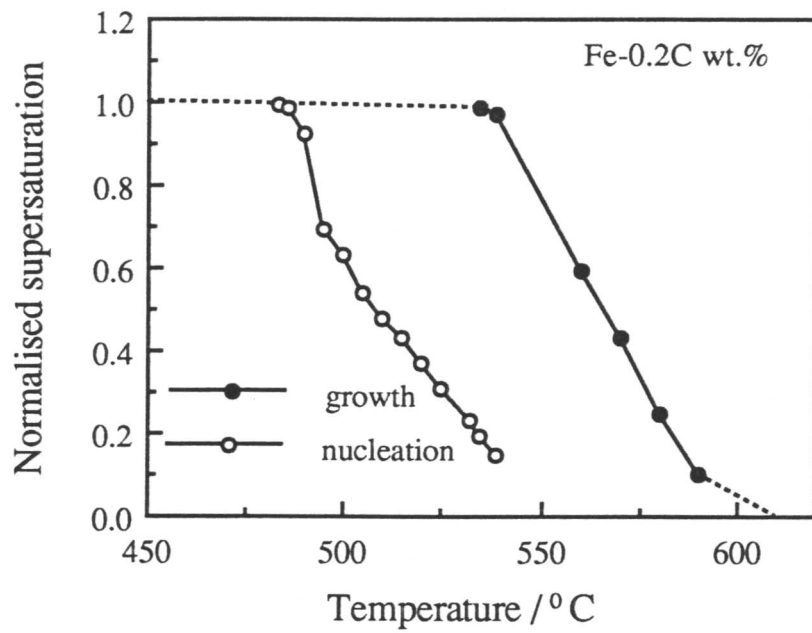
(b)

Figure 2.5: The variation in the degree of carbon supersaturation in the growing ferrite, as a function of the transformation temperature and carbon concentration. The calculations are according to the CDDT model (Olson *et al.*, 1990) (a) Fe–0.1C (b) Fe–0.2C wt.%.
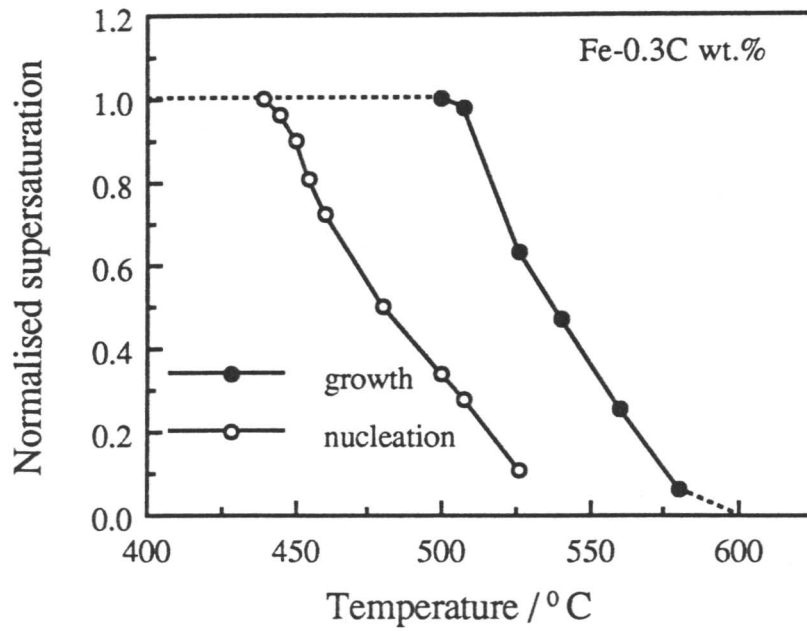
(c)
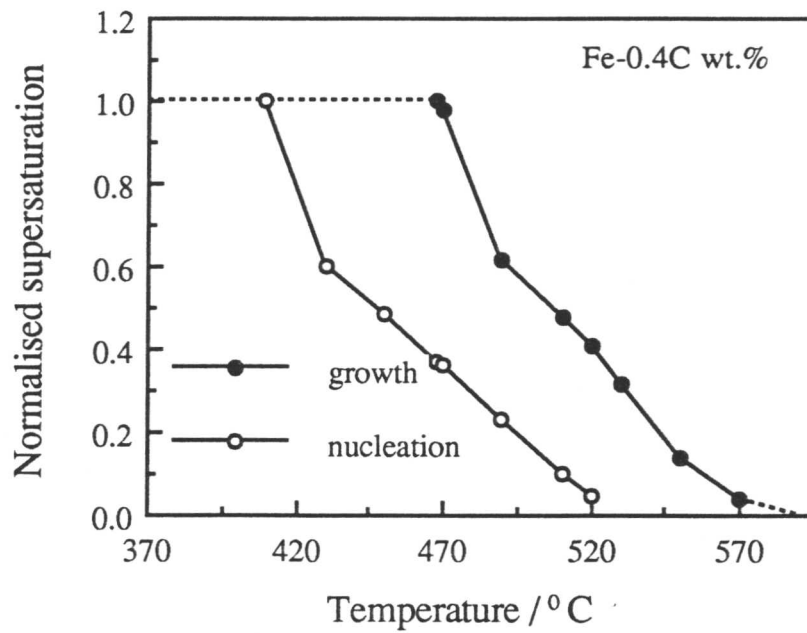
(d)

Figure 2.5: Continued. (c) Fe–0.3C and (d) Fe–0.4C wt.%.
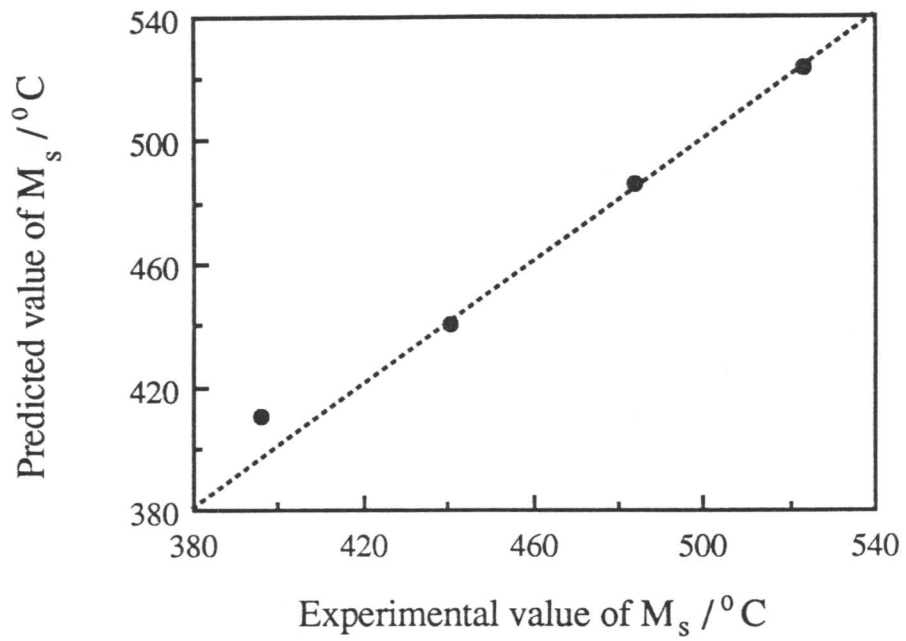
Figure 2.6: The agreement between the M_s as calculated using the CDDT model, and the "experimental" data, as discussed in the text.
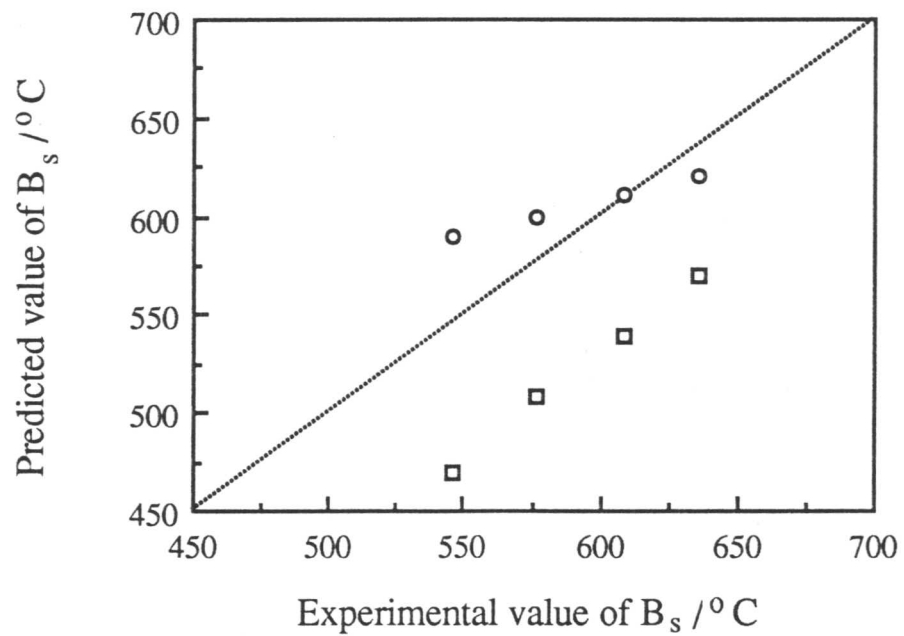
Figure 2.7: The B_s as calculated using the CDDT model, versus the "experimental" data, as discussed in the text. The circles are calculated on the basis of the assumption for bainite as used in (Olson *et al.*, 1990), whereas the squares are based on the assumption that bainite growth is diffusionless.
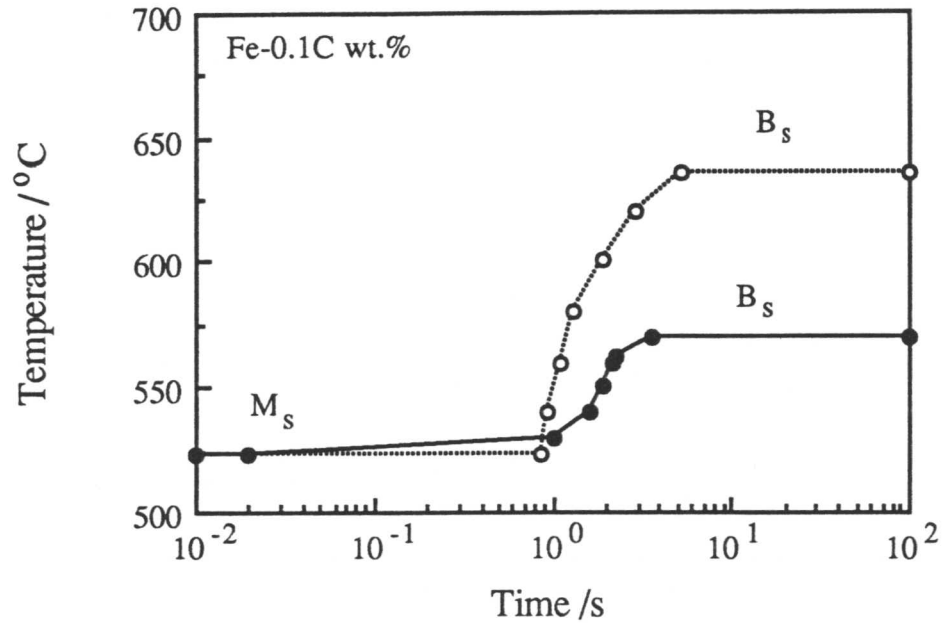
(a)
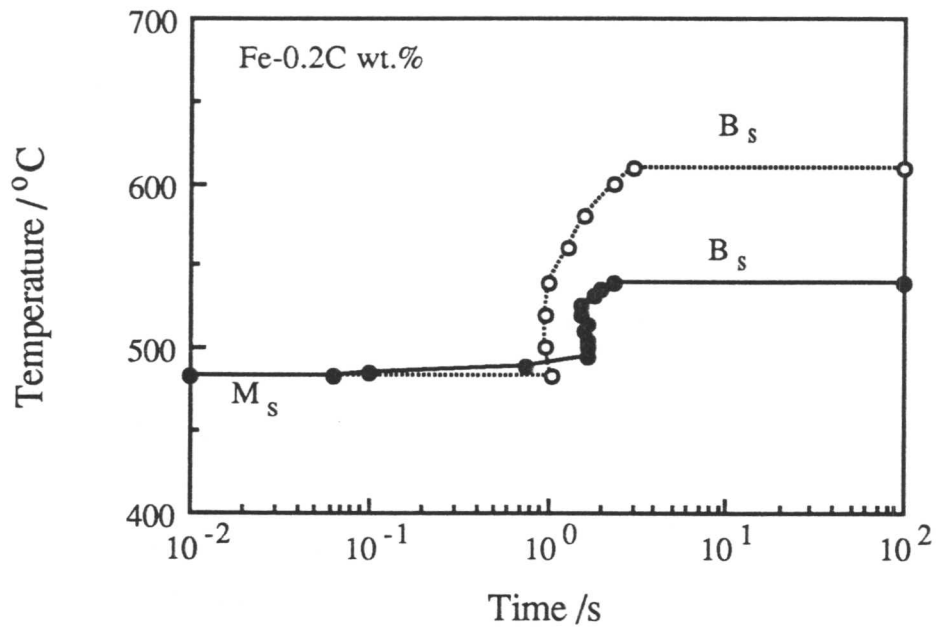
(b)

Figure 2.8: Comparison of the calculated TTT diagram (solid line) with that calculated using the Bhadeshia model (dotted line) for (a) Fe–0.1C (b) Fe–0.2C wt.%.

remain constant at $700 \, \text{J mol}^{-1}$ for all temperatures below about 740 K. This is necessary in order to ensure the correct prediction of the martensite–start temperature for concentrated alloys.

Table 3.1: Values of the stored energies at B_s for different alloys.

Alloy	"experimental" B_s (°C)	Stored energy at B_s ($J \, mol^{-1}$)
Fe–0.1C wt.%	636	335
Fe–0.2C wt.%	609	335
Fe–0.3C wt.%	577	308
Fe–0.4C wt.%	546	325
Fe–0.5C wt.%	512	297
Fe–0.43C–2Si–1.6Mn wt.%	468	652

3.3 Results and Discussion

The calculations using the CDDT model which allows the variation in the stored energy of the growing phase is presented here. The nature of the required variation in stored energy has been calculated by fitting against available data (Figure 3.1). The form of the curve illustrated in Figure 3.1 in fact seems physically reasonable. At low temperatures, the stored energy is about $700 \, \text{J mol}^{-1}$ because the shape change is elastically accommodated, so that the plate can thicken and achieve an aspect ratio large enough to be consistent with thermoelastic equilibrium even when its lengthening is stifled. At high temperatures, it is conceivable that the plastic yielding of the matrix prevents such thickening and hence reduces the stored energy both by the relaxation of elastic strains and by preventing the aspect ratio from being as large as that of martensite, to approximately $325 \, \text{J mol}^{-1}$. This, of course, is consistent with reported values of the stored energy of bainite (Bhadeshia, 1981a; Christian and Edmonds, 1984). It is also interesting that the elastic and plastic

33

accommodation regimes are separated by a fairly sharp transition region in the temperature range 450–500 °C, as might be expected from a yield phenomenon. The variation of supersaturation with temperature and carbon concentration, as calculated using the CDDT model modified to allow for the variation of stored energy is illustrated in Figure 3.2.
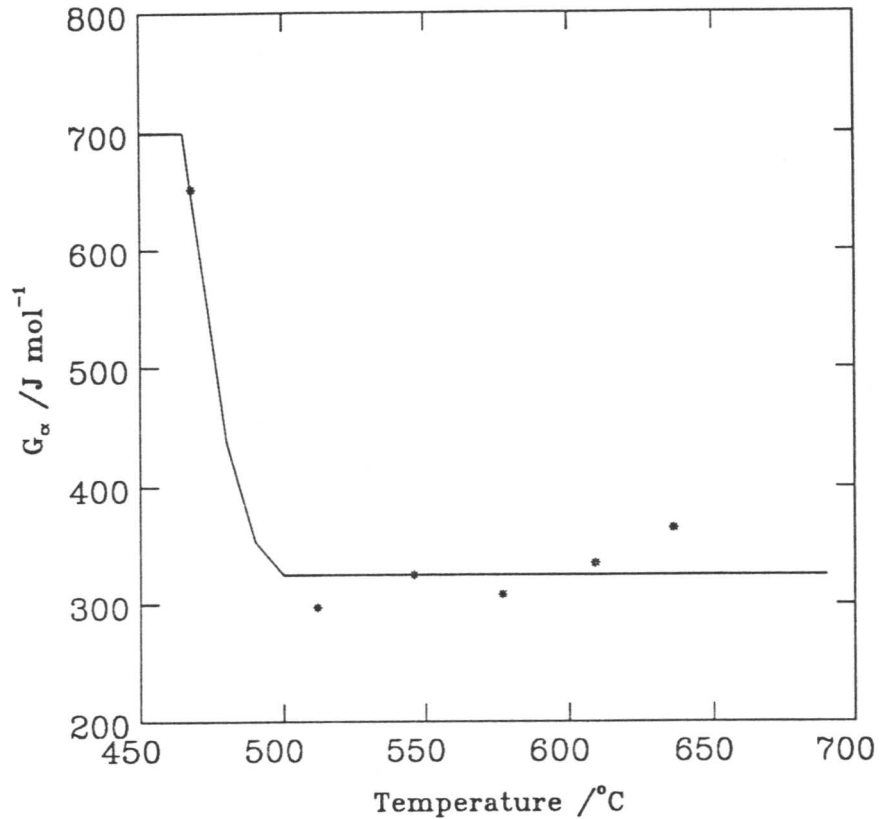
Figure 3.1: Calculated variation in the stored energy for growth, as a function of the transformation temperature.

The most striking feature is that there is now a much sharper transition from growth involving full partitioning of carbon, to diffusionless growth – the temperature range for the transition is typically 10–50 °C, compared with 50–100 °C for the earlier calculations presented in Figure 2.5. An abrupt transition from paraequilibrium to diffusionless growth is in fact consistent with experiments; Widmanstätten ferrite at all temperatures grows at a rate controlled by the diffusion of carbon in the austenite ahead of the interface (Bhadeshia, 1985a), and the growth rate of bainite subunits is much larger than diffusion–controlled growth (Bhadeshia, 1984; Ali and Bhadeshia, 1989). These values obtained from

34

the following two methods are given in Table 3.2.

(a) Original CDDT model with a fixed stored energy of 700 J mol^{-1} but with the assumption that the bainite–start temperature (B$_s$) is the highest temperature at which the plates grow with full supersaturation of carbon (*i.e.* $x_\alpha/\bar{x} = 1$) even though carbon may partition during the nucleation.

(b) The CDDT model which allows variation in stored energy during growth.

Table 3.2: Comparison of the predicted M$_s$ and B$_s$ values with the experimental data (Bhadeshia, 1981a; 1981b: 1981c).

Alloy	Description	M$_s$ (°C)	B$_s$ (°C)
Fe–0.1C wt.%	Present Estimates	523	640
	experimental	523	636
Fe–0.2C wt.%	Present Estimates	486	620
	experimental	484	609
Fe–0.3C wt.%	Present Estimates	440	583
	experimental	411	577
Fe–0.4C wt.%	Present Estimates	410	549
	experimental	396	546

The agreement between the "experimental" and calculated transformation temperatures is illustrated in Figure 3.3 and in Figure 3.4. The predicted and experimental time–temperature–transformation (TTT) diagrams for various low carbon alloys are shown in Figure 3.5.

3.4 Conclusion

A coupled diffusional/displacive transformations (CDDT) model has been applied to the calculation of transformation temperatures of a series of iron–carbon alloys. Using the assumption that martensitic nucleation and growth are both diffusionless, it has been found possible to accurately calculate the martensite–start temperatures. This is in spite of the fact that all the parameters used in implementing the interface response functions

were independently derived. This suggests that the approach used in the CDDT model is intrinsically correct.

The variation in B_s temperature as a function of carbon concentration can be satisfactorily estimated if it is assumed that the bainite–start temperature can be identified with the highest temperature at which diffusionless growth becomes possible. Good absolute agreement can be obtained if it is further assumed that the stored energy of the growing ferrite varies with temperature. The necessary variation appears to be physically reasonable.
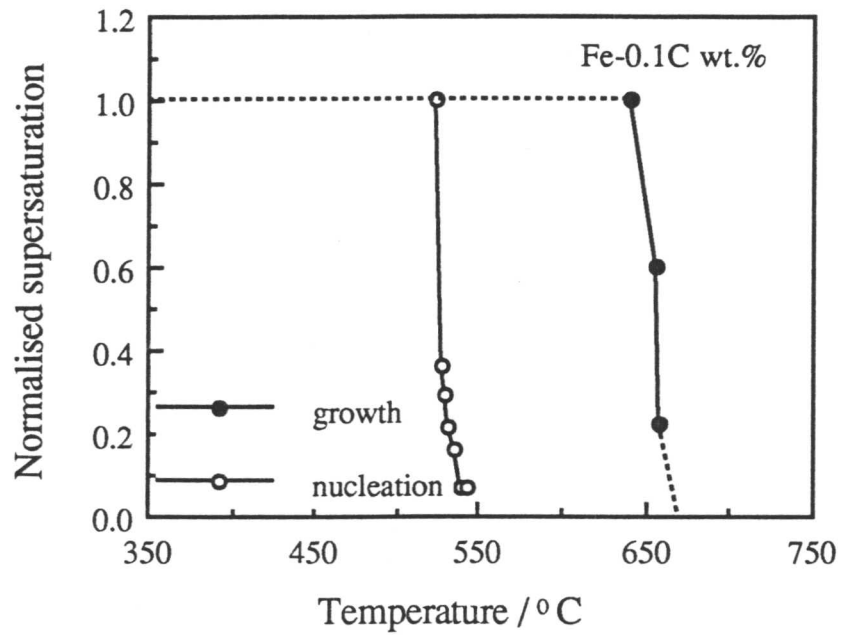
(a)
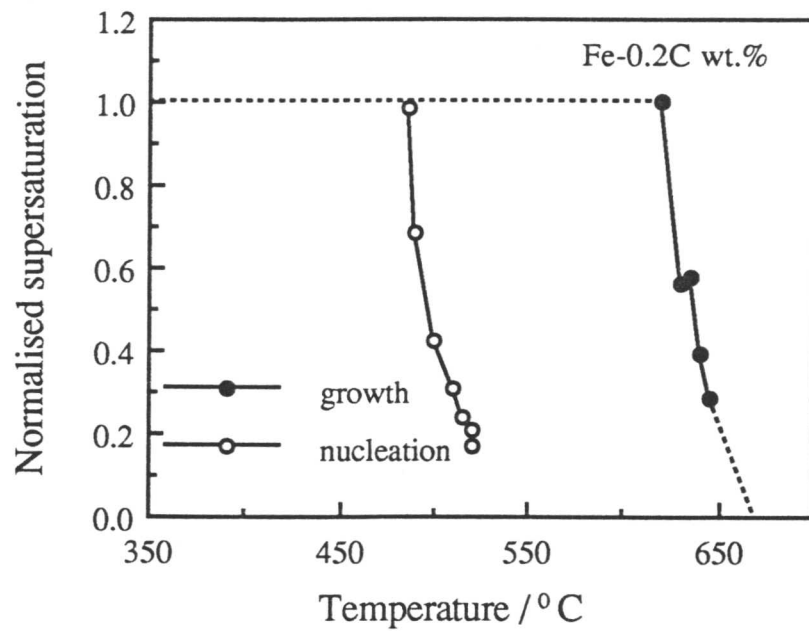
(b)

Figure 3.2: The variation in the degree of carbon supersaturation in the growing ferrite, as a function of the transformation temperature and carbon concentration. The calculations are according to the CDDT model with stored energy variation (a) Fe–0.1C (b) Fe–0.2C wt.%.
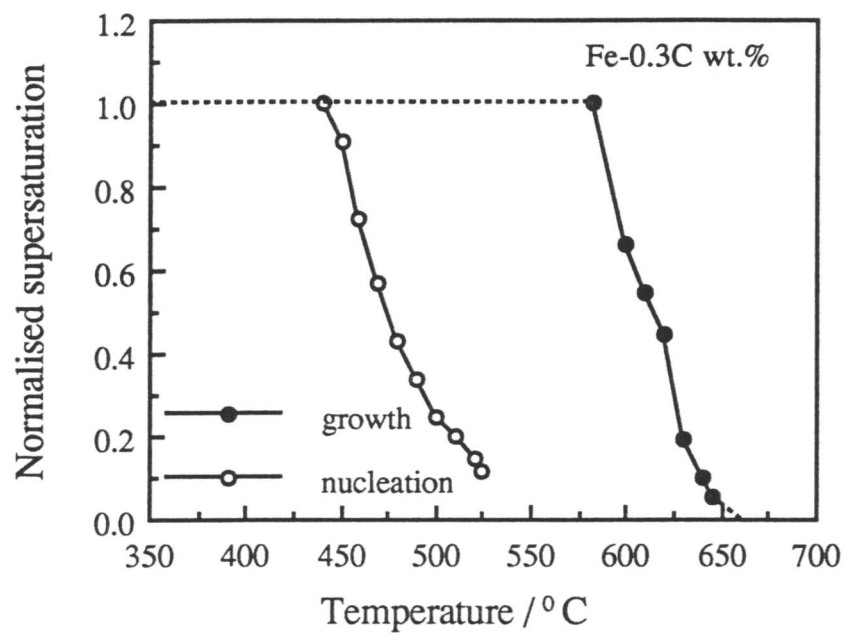
(c)
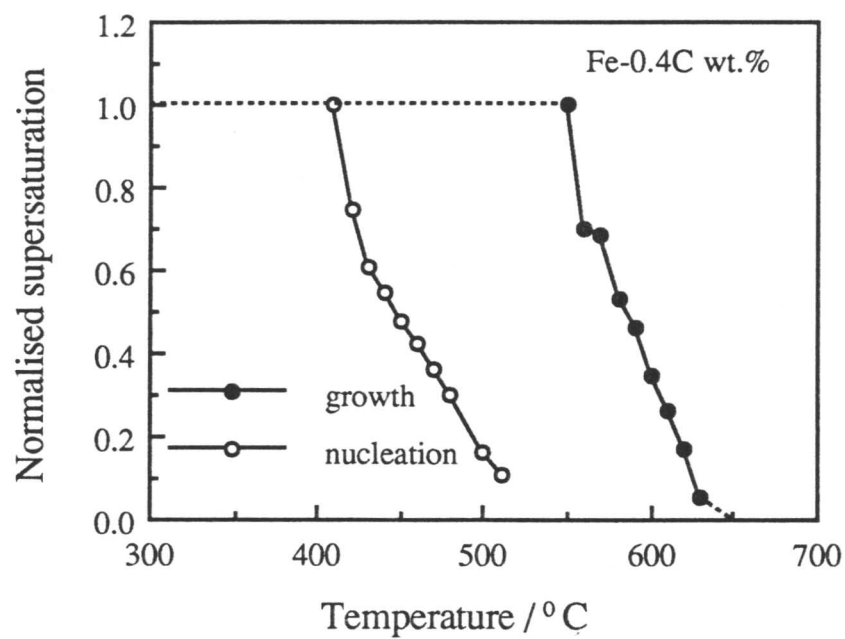
(d)

Figure 3.2: Continued. (c) Fe–0.3C and (d) Fe–0.4C wt.%.
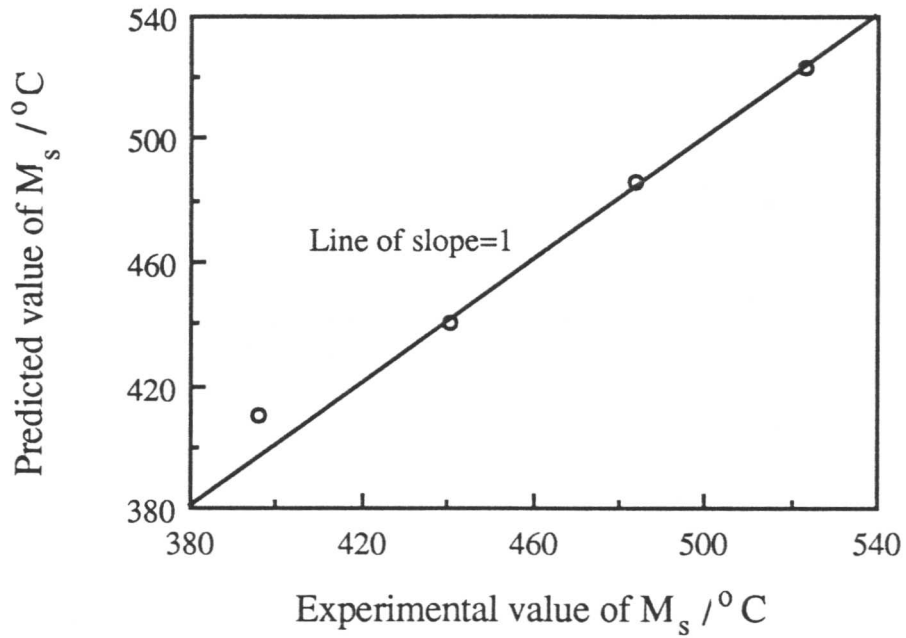
Figure 3.3: The agreement between the M_s as calculated using the CDDT model (with the stored energy function illustrated in Figure 3.1), and the "experimental" data, as discussed in the text.
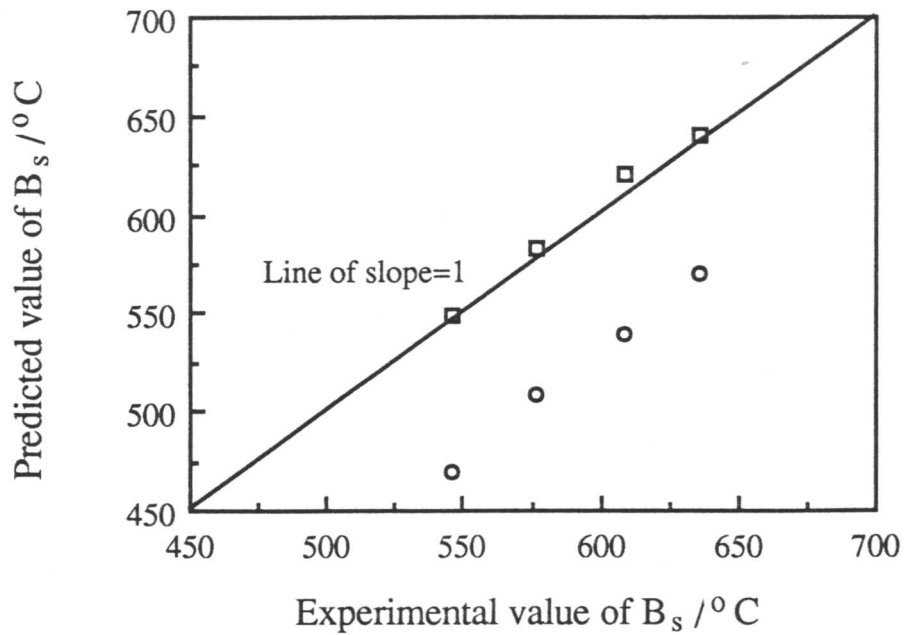
Figure 3.4: The B_s as calculated using the CDDT model and assuming that bainite growth is diffusionless, versus the "experimental" data, as discussed in the text. The circles represent calculations carried out with a constant stored energy for growth ($700 \, J \, mol^{-1}$) whereas the squares allow the stored energy to vary as in Figure 3.1.

39
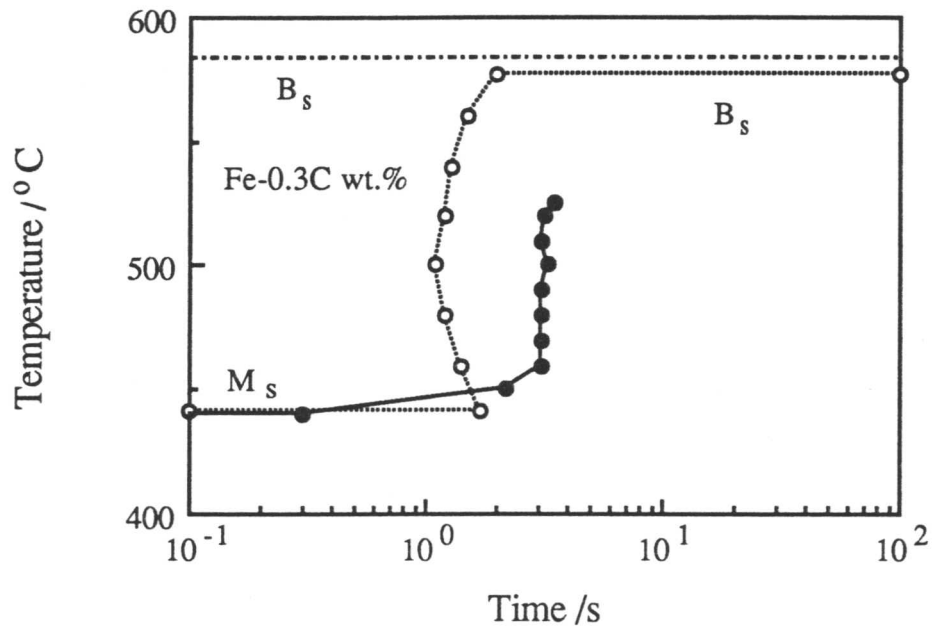
(c)
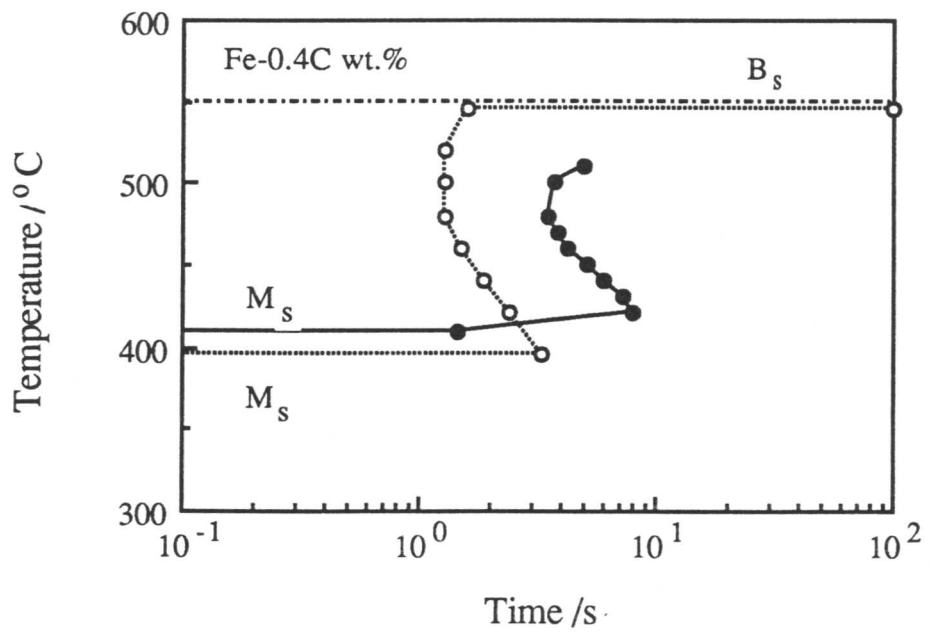
(d)

Figure 3.5: Continued. (c) Fe–0.3C (d) Fe–0.4C wt.%.

41

Chapter 4

Addition of Substitutional Alloying Elements

4.1 Introduction

Solid–state phase transformations in steels can involve both substitutional and interstitial atoms. It is conceivable that the former do not diffuse during transformation, whereas the much more mobile interstitial atoms are able to partition between the parent and product phases. Thus, the lattice change could be accomplished by displacive transformation as far as the substitutional solute and iron atoms are concerned. There would then be an invariant–plane strain shape change (with a large shear component) associated with the growth of a thin–plate shaped product. The extent to which the carbon atoms partition during the growth of ferrite plates by this mechanism can in principle be between equilibrium and full supersaturation (*i.e.* zero partitioning).

As discussed in earlier chapters, an attempt has recently been made to model such growth involving some partitioning of carbon (Olson *et al.*, 1989; 1990), the rest being trapped as the α/γ interface advances. Whilst it is appreciated that models like these are currently less than satisfactory in predicting experimental behaviour (Bhadeshia and Christian, 1990), they are the only ones capable of giving some idea of the growth rates involved during displacive transformations which occur above the martensite–start temperature. The coupled diffusional/displacive transformation (CDDT) model has already been extended further to deal with a variety of plain carbon steels (Chapters 2 and 3). The purpose of the present work is to apply the modified CDDT model to a number of alloyed steels and to compare the results with the experimental data of Steven and Haynes (1956) in order to check whether the model can be applied to alloyed steels. It was intended at the outset of this work to compare some of the overall results of such modelling with alternative, tried and tested but less informative methods of calculating transformation characteristics. Throughout this chapter, an approximation is made that the solid solution strengthening caused by the introduction of relatively small concentrations of substitutional solute can be

neglected. The interface mobility function is therefore indentified with that used for plain carbon steels.

4.2 Results and Discussion

4.2.1 Martensite–start Temperature

There are several methods for the prediction of martensite–start temperatures in steels, especially when the alloy concentration is small. The most commonly used method (Steven and Haynes, 1956) is completely empirical and works rather well, with M_s being given, for example, by

$$M_s(^\circ C) = 561 - 474C - 33Mn - 17Ni - 17Cr - 21Mo \qquad (4.1)$$

where the concentrations are all stated in weight percent. Using this relation, the M_s temperature can be calculated within $\pm$ 20–25 °C with a 90% certainty within the following limits of chemical composition.

C 0.1–0.5 wt.%	Cr Trace–3.5 wt.%	Mn 0.2–1.7 wt.%
Mo Trace–1.0 wt.%	Ni Trace–5 wt.%	

A more general method which has its origins in the work by Kaufman and Cohen (1956, 1958) assumes that martensite forms at a temperature where the driving force for diffusionless transformation $\Delta G^{\gamma\alpha}$ reaches a critical value $\Delta G^{\gamma\alpha}_{M_s}$ (Figure 4.1) Thus, alloying elements lead to a change in M_s simply as a consequence of their effect on the thermodynamic stabilities of the γ and α crystals.

Bhadeshia (1981b) used this method with experimental M_s data, to calculate $\Delta G^{\gamma\alpha}_{M_s}$ for a series of Fe–C alloys and found that external driving force is a function of the carbon concentration (Figure 4.2). This function was then used empirically to predict the M_s temperatures for substitutionally alloyed steels (Bhadeshia, 1981c), assuming that M_s is given by the temperature where $\Delta G^{\gamma\alpha}\{Fe - C - X, M_s\} = \Delta G^{\gamma\alpha}_{M_s}\{Fe - C\}$. The method works extremely well, but there is no justification for the particular way in which $G^{\gamma\alpha}_{M_s}\{Fe - C\}$ varies with the concentration of carbon.

The CDDT method can in principle avoid all of the empirical assumptions discussed above. The experimental data of Steven and Haynes (1956) provide a rich source of carefully measured M_s temperatures as a function of the alloy chemistry (Tables 4.1 and 4.2). Assuming only that martensite forms when nucleation and growth become diffusionless,

43

the CDDT model with the temperature dependent stored energy was applied to the Steven and Haynes data. The results are illustrated in Figure 4.3; the level of agreement between the experimental data and those calculated is impressive and gives confidence in the CDDT model. During barrierless nucleation, the dependence of stored energy on M_s temperature is shown in Figure 4.4. The variation in the driving force at M_s with M_s temperature is shown in Figure 4.5. The predicted variation of $\Delta G^{\gamma\alpha}\{Fe - C, M_s\}$ with carbon concentration is compared against the Bhadeshia (1981b) results is shown in Figure 4.6.

4.2.2 The Bainite-start Temperature

Again, for bainite, there are empirical equations for the variation in the B_s temperature with alloy chemistry (Steven and Haynes, 1956);

$$B_s(°C) = 830 - 270C - 90Mn - 37Ni - 70Cr - 83Mo \tag{4.2}$$

where the concentrations are all stated in weight percent. This relation calculates the B_s temperature within $\pm$ 20–25 °C with a 90% certainty within the following limits of chemical composition.

| C | 0.1–0.5 wt.% | Cr | Trace–3.5 wt.% | Mn | 0.2–1.7 wt.% |
| Mo | Trace–1.0 wt.% | Ni | Trace–5 wt.% | | |

However, the precision with which such equations represent B_s is known to be poor when compared with corresponding equations for M_s temperature. Part of the reason for this is that the B_s temperature is much more difficult to measure. In some low–alloy steels, there is an overlap of several reactions in the vicinity of the bainite transformation temperature range, and this can confuse measurements. Secondly, as pointed out in a detailed analysis by Bhadeshia (1981a), some authors confuse the onset of Widmanstätten ferrite growth with that of bainite.

A more fundamental method for estimating B_s is given by Bhadeshia; it sets two conditions for the formation of bainite:

(1) That the driving force for diffusionless growth must exceed the stored energy of bainite ($\simeq 400$ J mol^{-1})

$$|\Delta G^{\gamma\alpha}| > 400 \quad \text{J mol}^{-1}$$

(2) That the driving force for nucleation ΔG_m (during which carbon partitions between the parent phases) must exceed a value $G_N\{T\}$

44

$$|\Delta G_m| > |G_N\{T\}|$$

G_N is a universal function for displacive nucleation and is independent of alloy chemistry – it has been defined by Bhadeshia (1981a). The method is illustrated in Figure 4.7. When these two conditions are simultaneouly satisfied, bainite transformation becomes feasible.

The method works quite well in predicting the B_s temperature. Although the function G_N is based on and consistent with the physical properties of displacive nucleation theory, there is a certain amount of fitting involved in deriving certain constants for practical applications.

The CDDT model was again applied to Steven and Haynes B_s data, the conditions for bainite being that;

(1) Growth must be diffusionless.

(2) Carbon may partition during nucleation.

(3) The stored energy must be temperature dependent, of the form given in Chapter 3.

The results are presented in Figure 4.8 which reveals serious discrepencies, the calculations on average underestimating the B_s temperatures by some 100 °C . The scatter is in fact far greater than would be expected from Chapter 3 where the B_s temperature was fully accurately estimated for Fe–C alloys. The reasons for these discrepencies are not clear but it is useful that there is a general trend as function of alloy content. The variation in stored energy with the experimental B_s temperatures of Steven and Haynes data is shown in Figure 4.9.

4.3 Conclusion

The CDDT model is able to accurately predict the martensite–start temperature of alloyed steels, the level of accuracy matching any previous empirical analysis. On the other hand, significant difficulties remain as far as the bainite–start temperatures are concerned, the reason for which is not clear. The calculations consistently underestimate the experimental data. The trend in B_s temperatures nevertheless appears to be roughly predicted.

Table 4.1: Chemical composition of steels analysed. The "En" number used to be the common identification terminology incorporated in British Standards.

Reference No.	B. S. En No.	Chemical Composition wt.%								
		C	Si	Mn	S	P	Ni	Mo	Cr	V
1	12	0.34	0.20	1.06	0.040	0.037	0.75	0.02	0.08	...
2	12	0.33	0.21	0.62	0.025	0.022	0.89	0.05	0.10	...
3	13	0.19	0.14	1.37	0.012	0.026	0.56	0.31	0.20	...
4	14	0.29	0.26	1.67	0.030	0.033	0.21	0.04	0.12	...
5	15	0.33	0.23	1.54	0.024	0.021	0.18	0.05	0.15	...
6	16	0.33	0.18	1.48	0.028	0.028	0.26	0.27	0.16	...
7	17	0.38	0.25	1.49	0.028	0.036	...	0.41	...	...
8	18	0.39	0.16	0.89	0.025	0.027	0.25	Nil	0.88	...
9	18	0.48	0.25	0.86	0.021	0.023	0.18	0.04	0.98	...
10	19	0.41	0.31	0.64	0.017	0.030	0.18	0.38	1.24	...
11	19	0.41	0.23	0.67	0.016	0.015	0.20	0.23	1.01	...
12	21	0.33	0.23	0.74	0.027	0.031	3.47	...	0.07	...
13	22	0.40	0.26	0.62	0.005	0.007	3.45	0.10	0.28	...
14	23	0.33	0.23	0.57	0.007	0.005	3.26	0.09	0.85	...
15	23	0.32	0.28	0.61	0.031	0.018	3.22	0.22	0.63	0.03
16	24	0.36	0.22	0.52	0.005	0.007	1.52	0.27	1.17	...
17	24	0.38	0.20	0.67	0.010	0.017	1.58	0.26	0.95	...
18	25	0.32	0.27	0.56	0.012	0.018	2.37	0.51	0.74	...
19	25	0.31	0.20	0.62	0.012	0.018	2.63	0.58	0.64	...
20	26	0.38	0.15	0.56	0.005	0.011	2.42	0.46	0.74	...
21	26	0.42	0.31	0.67	0.022	0.029	2.53	0.48	0.72	...
22	28	0.32	0.19	0.51	0.009	0.013	3.02	0.48	1.37	0.18
23	28	0.25	0.15	0.52	0.024	0.010	3.33	0.65	1.14	0.16
24	30A	0.35	0.14	0.44	0.008	0.016	4.23	0.13	1.43	...
25	30B	0.33	0.17	0.51	0.009	0.013	4.16	0.31	0.44	...
26	30B	0.32	0.29	0.47	0.020	0.022	4.13	0.30	1.21	0.01
27	40B	0.26	0.21	0.55	0.022	0.010	0.25	0.54	3.34	...
28	45A	0.55	1.74	0.87	0.037	0.038	...	...	...	...
29	47	0.51	0.27	0.72	0.020	0.021	0.15	0.05	0.094	0.20
30	100	0.40	0.24	1.38	0.031	0.033	0.74	0.16	0.53	...
31	100	0.40	0.21	1.34	0.027	0.028	1.03	0.22	0.53	...
32	110	0.44	0.23	0.58	0.004	0.029	1.40	0.11	1.26	...
33	110	0.39	0.23	0.62	0.018	0.021	1.44	0.18	1.11	...
34	111	0.35	0.13	0.65	0.032	0.035	1.27	Nil	0.55	...
35	111	0.37	0.28	0.89	0.035	0.025	1.24	0.05	0.63	...
36	160	0.41	0.13	0.48	0.043	0.016	1.75	0.22	0.17	...
37	32A	0.14	0.19	0.50	0.043	0.031	0.19	0.06	0.16	...
38	33	0.10	0.25	0.46	0.006	0.007	3.00	0.12	0.13	...
39	34	0.25	0.16	0.40	0.021	0.019	1.78	0.27	0.23	...
40	35	0.24	0.17	0.42	0.005	0.010	1.84	0.20	0.18	...
41	36	0.14	0.19	0.46	0.009	0.006	3.55	0.12	1.11	...
42	36	0.15	0.25	0.41	0.008	0.020	3.02	0.15	0.90	...
43	37	0.09	0.33	0.33	0.031	0.018	4.87	0.08	0.13	...
44	38	0.11	0.21	0.30	0.004	0.014	5.04	0.30	0.13	...
45	39B	0.15	0.20	0.38	0.018	0.027	4.33	0.17	1.16	...
46	39B	0.14	0.28	0.45	0.017	0.016	4.11	0.24	1.11	...
47	39B	0.15	0.23	0.33	0.015	0.015	4.25	0.25	1.11	...
48	320	0.14	0.22	0.50	0.015	0.010	2.13	0.18	2.00	...
49	325	0.20	0.11	0.53	0.005	0.026	1.75	0.25	0.50	...
50	352	0.20	0.15	0.71	0.018	0.032	1.13	0.05	0.80	...
51	353	0.18	0.26	0.93	0.008	0.016	1.34	0.11	1.11	...
52	354	0.19	0.21	0.90	0.015	0.017	1.97	0.18	1.08	...
53	...	0.40	0.23	0.52	0.004	0.008	1.83	1.00	1.25	0.15
54	...	0.31	0.13	0.54	0.025	0.011	1.67	0.24	1.24	
55	...	0.41	0.35	0.58	0.020	0.013	1.43	0.31	1.27	...
56	...	0.49	0.17	0.52	0.022	0.013	1.50	0.29	1.28	...
57	...	0.38	0.33	0.55	0.021	0.010	0.16	0.31	1.25	...
58	...	0.38	0.12	0.56	0.024	0.017	3.00	0.29	1.21	...
59	...	0.38	0.12	0.57	0.023	0.010	4.95	0.29	1.22	...
60	...	0.41	0.15	0.52	0.027	0.016	1.46	0.29	2.10	...
61	...	0.37	0.12	0.52	0.026	0.012	1.51	0.29	2.90	...
62	...	0.40	0.30	0.55	0.025	0.011	1.47	0.52	1.22	...
63	...	0.36	0.16	0.56	0.029	0.009	1.46	0.31	1.22	0.13
64	...	0.39	0.26	0.20	0.022	0.009	1.66	0.26	1.22	...
65	...	0.40	0.27	0.84	0.025	0.012	1.75	0.27	1.23	...

Table 4.2: Comparison of predicted values of M_s and B_s with the experimental data (Steven and Haynes, 1956) for a variety of alloys.

Reference No.	B. S. En No.	Experimental		Using CDDT model	
		M_s (° C)	B_s (° C)	M_s (° C)	B_s (° C)
1	12	345	...	365	420
2	12	370	...	385	520
3	13	420	600	410	535
4	14	380	560	361	427
5	15	340	...	350	...
6	16	340	580	350	418
7	17	320	550	335	398
8	18	320	560	345	396
9	18	300	560	310	356
10	19	320	540	335	397
11	19	330	570	335	402
12	21	310	570	330	386
13	22	280	540	303	401
14	23	300	500	323	380
15	23	320	520	325	387
16	24	325	530	339	400
17	24	320	530	335	381
18	25	335	510	340	402
19	25	330	500	335	349
20	26	305	520	315	373
21	26	290	480	295	349
22	28	315	440	305	366
23	28	330	470	325	392
24	30A	290	420	285	342
25	30B	295	420	285	343
26	30B	295	420	300	355
27	40B	360	450	347	411
28	45A	290	...	310	367
29	47	290	560	298	351
30	100	300	530	310	371
31	100	300	520	295	365
32	110	300	520	310	361
33	110	320	520	325	382
34	111	347	...	360	415
35	111	315	600	340	395
36	160	320	...	342	397
37	32A	...	...	...	...
38	33	...	...	...	...
39	34	...	...	...	...
40	35	...	640	...	542
41	36	415	550	385	362
42	36	415	580	402	534
43	37	...	...	...	...
44	38	390	550	395	452
45	39B	365	500	365	430
46	39B	390	500	375	435
47	39B	380	500	372	434
48	320	415	520	400	456
49	325	390	620	410	545
50	352	415	600	410	545
51	353	400	560	395	530
52	354	410	530	380	443
53	...	275	450	295	354
54	...	365	530	350	411
55	...	300	490	315	371
56	...	260	480	...	343
57	...	320	550	355	412
58	...	280	450	295	351
59	...	260	370	...	312
60	...	...	430	...	353
61	...	280	400	290	349
62	...	320	450	330	374
63	...	300	500	325	387
64	...	310	540	340	394
65	...	270	450	300	356
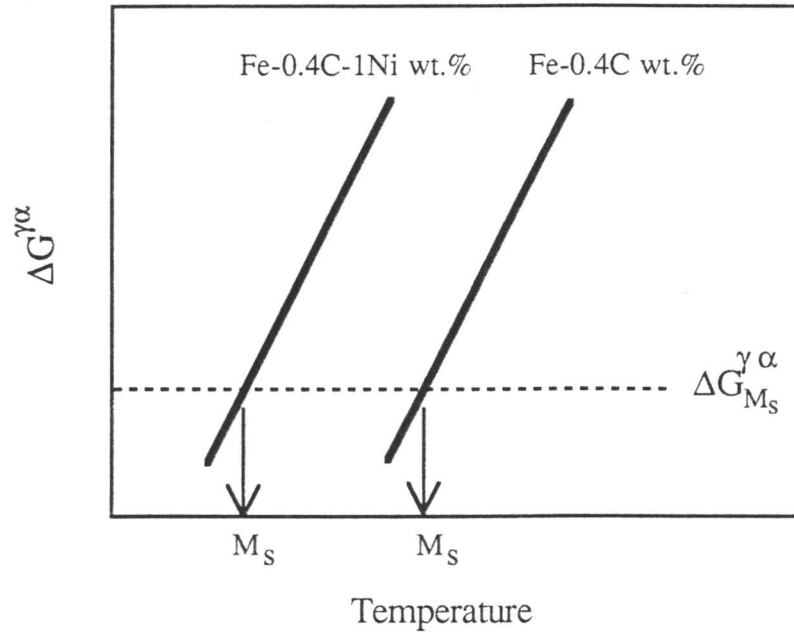
Figure 4.1: Schematic free energy curve illustrating the martensite formation at a critical value of free energy and the effect of alloying element.
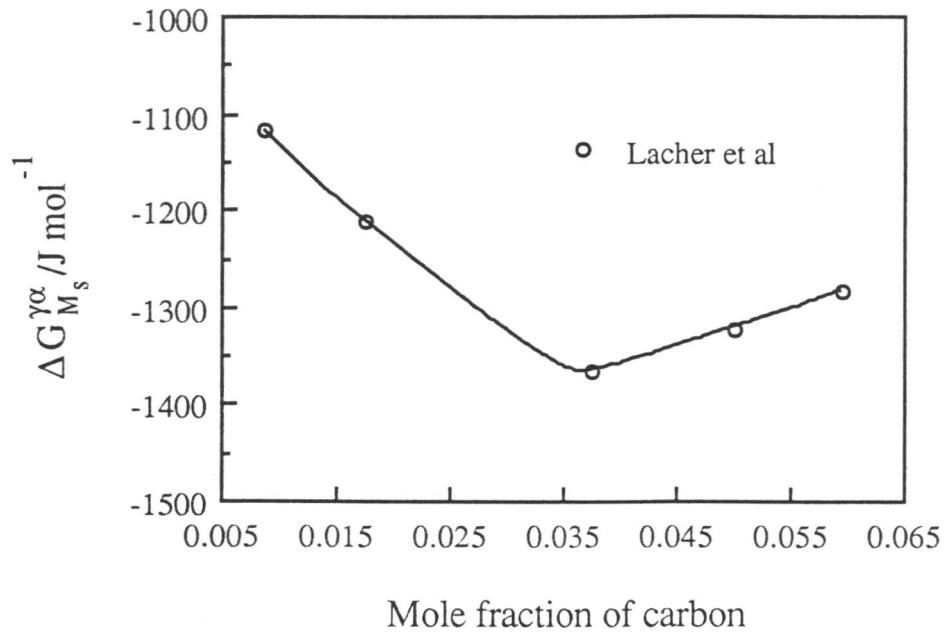
Figure 4.2: Variation of free energy change (accompanying martensitic transformation at M_s temperature) as a function of carbon content (Bhadeshia, 1981b).
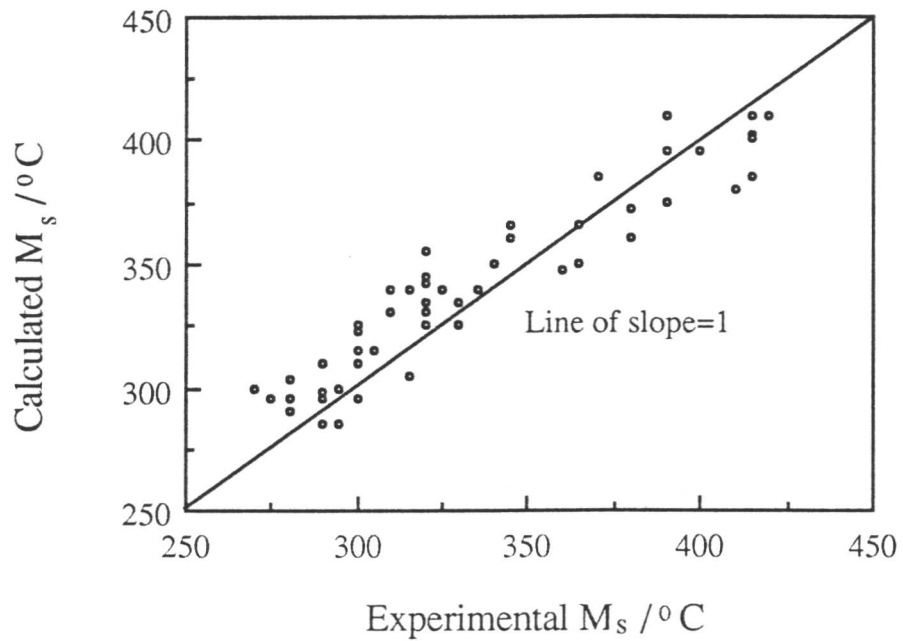
Figure 4.3: The agreement between the M_s as calculated using the CDDT model (with variable stored energy), and the experimental data of Steven and Haynes, 1956.
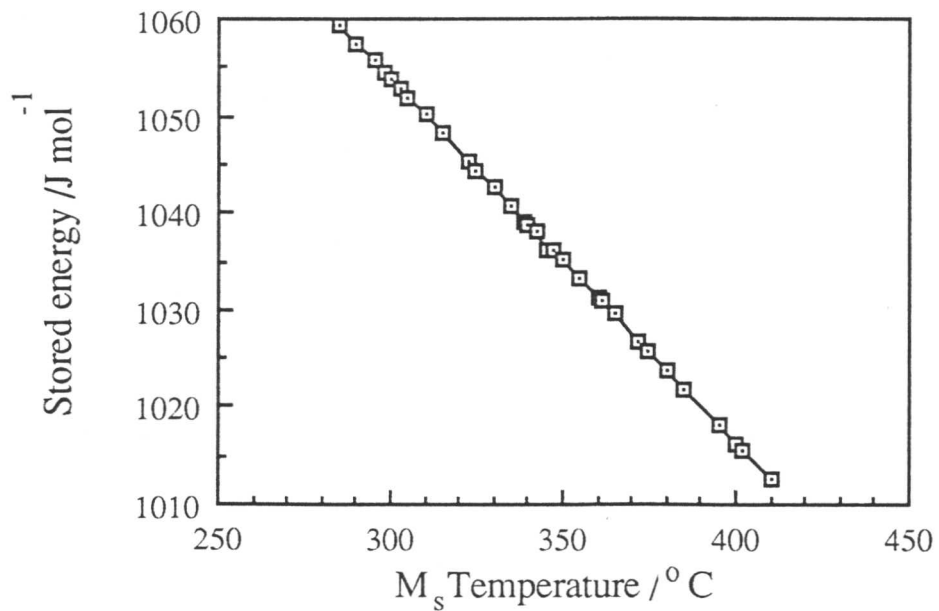
Figure 4.4: Variation of stored energy during nucleation at M_s versus M_s temperature of each alloy.
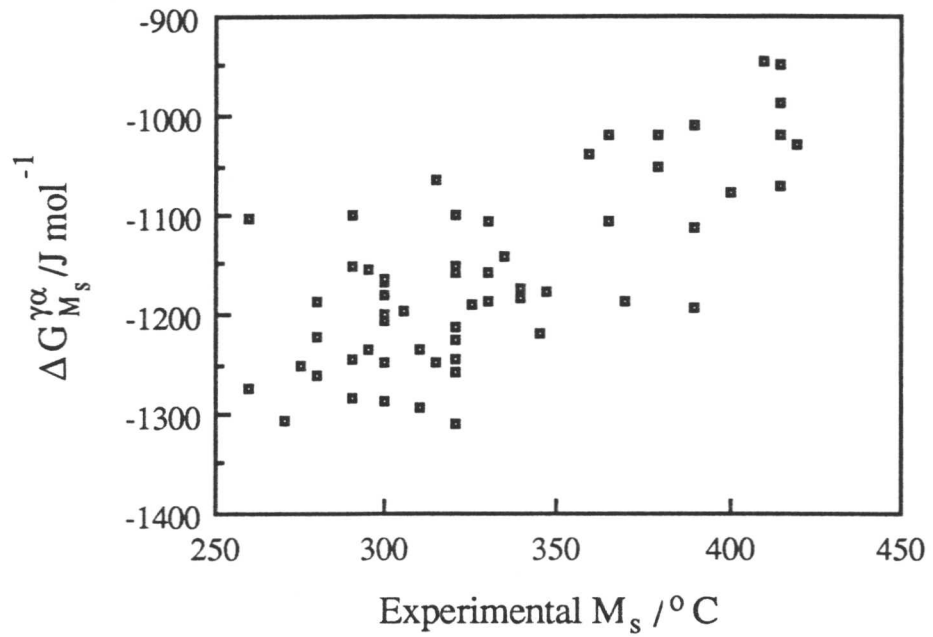
Figure 4.5: Plot of driving force at M_s versus M_s temperature of each alloy.
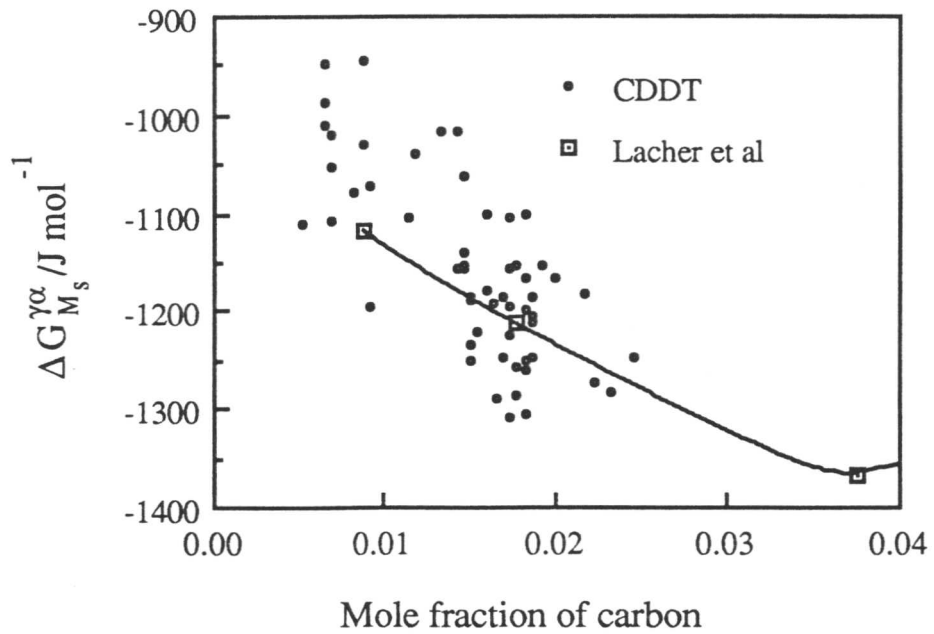
Figure 4.6: Comparison of the variation of free energy change (accompanying martensitic transformation at M_s temperature) as a function of carbon content between the predicted and the curve by Bhadeshia (1981b).
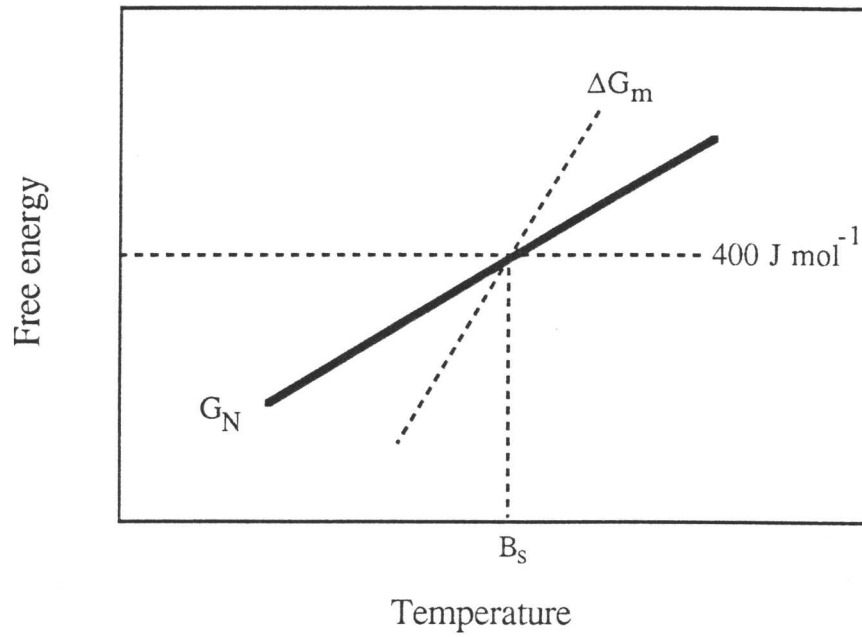
Figure 4.7: Schematic free energy versus temperature curve illustration showing the conditions of determining bainite start temperature.
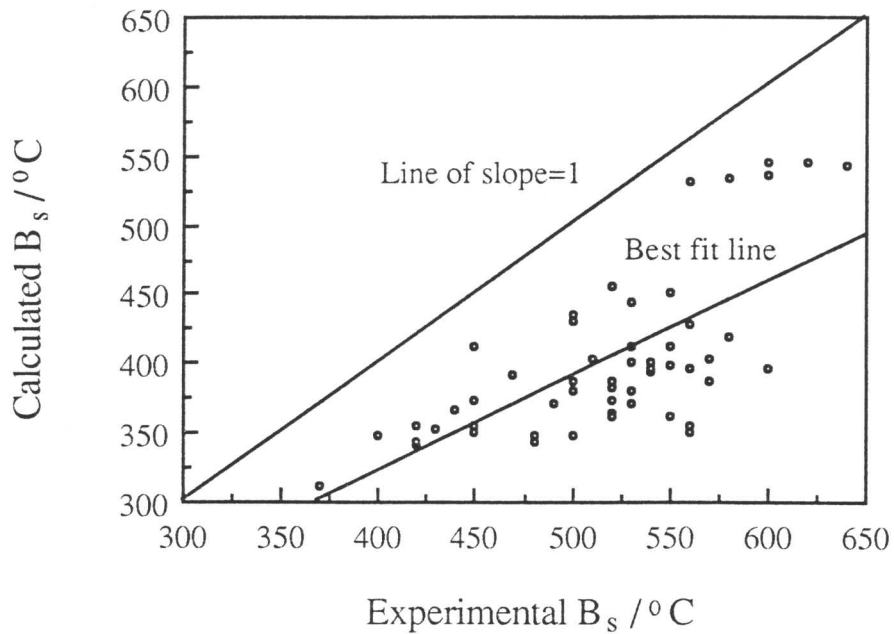
Figure 4.8: The B_s as calculated using the CDDT model (with variable stored energy) and assuming that bainite growth is diffusionless, versus the experimental data of Steven and Haynes, 1956.
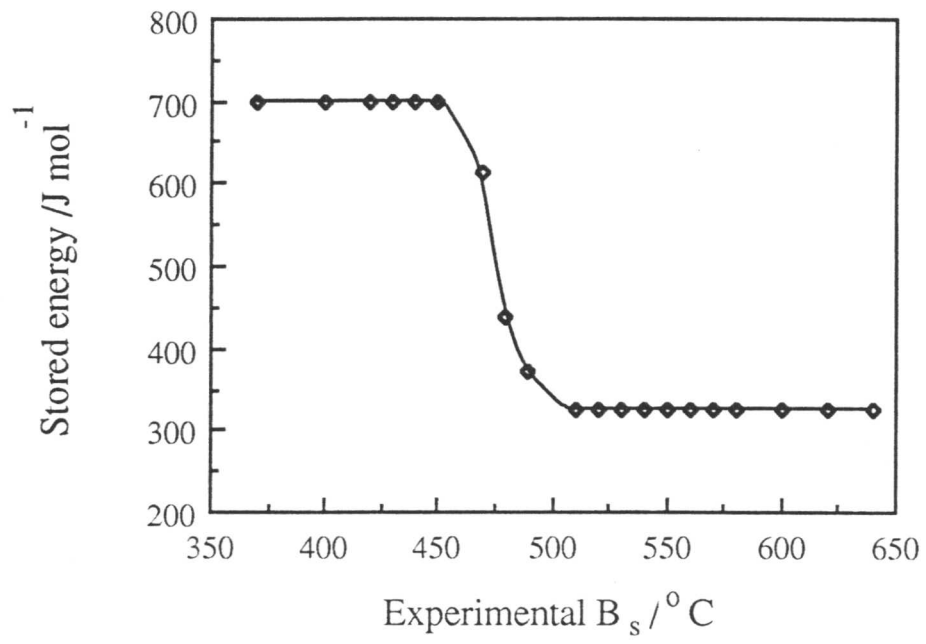
Figure 4.9: Plot of stored energy at experimental values of B_s (Steven and Haynes, 1956) for each alloy.

Chapter 5

Partitioning of Carbon from Supersaturated
Ferrite Plates

5.1 Introduction

The equilibrium solubility of carbon in ferrite is extremely limited, and is typically far less than the average carbon concentration of commercial steels. Excess carbon can, during transformation, be forced into solid solution in the ferrite if the transformation interface moves so rapidly as to *trap* the carbon into the ferrite before it can diffuse away from the advancing interface. This causes the chemical potential of the carbon to increase on transfer across the interface, and this nonequilibrium phenomenon is known as "solute trapping" (Baker and Cahn, 1969; 1971). When martensite forms in steels, the mobility of the carbon atoms during transformation is sufficiently small to enable all the carbon to be trapped into the martensite, making the reaction diffusionless. The situation is not so clear for bainite, which occurs at relatively higher temperatures where atomic mobilities are also larger. Even if the growth of bainitic ferrite involves the complete or partial trapping of carbon, the carbon could redistribute rapidly into the residual austenite immediately after transformation, making it difficult to assess the situation that existed during growth.

There is therefore, a particular experimental difficulty with the bainite transformation, that in the case of upper bainite at least, it is impossible to say anything about the initial carbon content of the ferrite because the time taken for any carbon to diffuse into austenite can be very small. Even though direct observations have demonstrated quantitatively that the post transformation carbon content of bainitic ferrite tends to be significantly higher than equilibrium (Bhadeshia and Waugh, 1981, 1982; Stark *et al.*, 1988; 1990; Josefsson and Andren, 1988), the data may underestimate the concentration in the ferrite during the early stages of growth.

Early research tended to suggest that the time, t_d, taken to decarburise a fully supersaturated plate of ferrite is of the order of a few milliseconds (Kinsman and Aaronson, 1967). A more recent analysis (Bhadeshia, 1988) shows that it can in fact be much longer,

the time for decarburisation being given by:

$$t_d = \frac{w_\alpha(\overline{x} - x^{\alpha\gamma})\pi^{0.5}}{4\overline{D}^{0.5}(x^{\gamma\alpha} - \overline{x})} \tag{5.1}$$

where $\overline{D}$ is a weighted average diffusivity of carbon in austenite (discussed later), $\overline{x}$ is the average mole fraction of carbon in the alloys, $x^{\alpha\gamma}$ and $x^{\gamma\alpha}$ are the paraequilibrium carbon concentrations in the ferrite and austenite respectively, and w_α is the width of the ferrite plate. It has pointed out that even this analysis may not be completely satisfactory given that it does not allow for the coupling of fluxes in the ferrite and austenite, since the model is based on the assumption that diffusion is so rapid in the ferrite that it is unnecessary to consider its role in determining the decarburisation time (Bhadeshia, 1988). It therefore contains nothing about diffusion in the ferritic phase.

The purpose of the present work was to re-examine the partitioning of carbon from supersaturated ferrite into adjacent austenite using a numerical method. This should in principle enable the treatment of diffusion in both the ferrite and austenite phases, and at the same time permit "soft–impingement" effects to be treated relatively easily. The overlap of the diffusion or temperature fields of adjacent particles, or from active regions of the same particle, is called soft–impingement (Christian, 1975).

5.2 Method

5.2.1 The Diffusion Coefficients

While it is well established that the octahedral interstices represent the most favoured sites for carbon atoms dissolved in body–centered cubic iron, it has been demonstrated (Mclellan et al., 1965) that discrepancies in the diffusion data gathered over a wide range of temperatures can be resolved if it is assumed that a small but significant fraction of carbon atoms reside in the tetrahedral interstices. The actual diffusion coefficient is then a function of three different coefficients, each representing one of the three diffusion paths $T - T$, $T - o - T$ or $o - T - o$ involving the octahedral (o) and tertrahedral interstices (T):

$$D_c^\alpha = \phi D^{o-T-o} + (1 - \phi)f D^{T-T} + (1 - \phi)(1 - f)D^{T-o-T} \tag{5.2}$$

where ϕ is the fraction of carbon atoms which occupy the octahedral interstices, and is given by:

$$\phi = 1 - \left(\frac{1}{2}\exp\frac{\Delta E}{RT}\exp-\frac{\Delta S}{R} + 1\right)^{-1}$$

54

with $\Delta E = 3.017 \times 10^5$ J mol^{-1} and $\Delta S/R = -4.4$. R is the universal gas constant. Of all the atoms which occupy the tetrahedral interstices, f represents the fraction which diffuse by jumping directly between adjacent tetrahedral sites, rather than by the $T - o - T$ route. Mclellan *et al.* found that $f = 0.86$ and that the diffusion coefficients are given by:

$$D^{o-T-o} = D^{T-o-T} = 3.3 \times 10^{-7} \exp\{-Q_1/RT\} \quad \text{m}^2\,\text{s}^{-1} \tag{5.3}$$

$$D^{T-T} = 3.0 \times 10^{-4} \exp\{-Q_2/RT\} \quad \text{m}^2\,\text{s}^{-1} \tag{5.4}$$

$$Q_1 = 19.3 \times 10^3 \times 4.184 \quad \text{Jmol}^{-1}$$

$$Q_2 = 14.7 \times 10^3 \times 4.184 \quad \text{Jmol}^{-1}$$

The diffusion coefficient of carbon in austenite is very sensitive to the carbon concentration (Wells *et al.*, 1950; Smith, 1953) and this has to be taken into account in treating the large concentration gradients that develop in the austenite. Trivedi and Pound (1967) first considered this problem in detail and found that a weighted average diffusivity $\overline{D}$ can be substituted into the kinetic equations without any loss of accuracy:

$$\overline{D} = \int_{x_I}^{\overline{x}} D^\gamma\{x, T\} dx/(\overline{x} - x_I) \tag{5.5}$$

where x_I is the carbon concentration in the austenite at the γ/α interface. Although this equation is strictly valid only for steady–state growth, it can to a very good approximation be used in circumstances such as the present, where the diffusion profile actually varies with time. The function $D^\gamma\{x, T\}$ adopted in this work is based on the theory of Siller and McLellan (1970) and Bhadeshia (1981d).

5.2.2 Finite Difference Analysis

The method used here is a standard finite difference technique, which has been discussed fully by Crank (1975). The austenite–ferrite aggregate is treated as a composite diffusion couple in which flat slabs of austenite, each of thickness w_γ are welded on either side of a slab of ferrite of thickness w_α Figure 5.1. As a first stage in the analysis, the slab dimensions were chosen to avoid the possibility of soft–impingement in the austenite, while at the same time keeping the computing time required to a minimum and maintaining a realistic thickness for the ferrite plate, with $w_\gamma = 0.2\ \mu$m and $w_\alpha = 0.4\mu$m. For austenite, soft–impingement occurs when the carbon concentration in the austenite at the furthest point away from the α/γ interface rises beyond the initial concentration $\overline{x}$, and can be avoided in spite of the
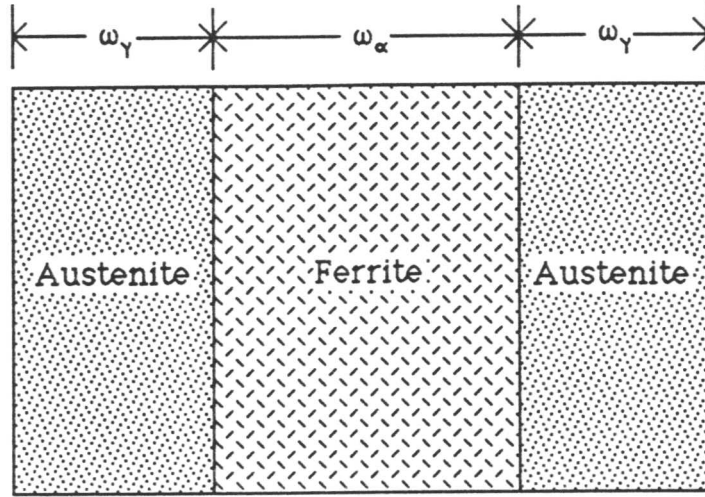
Figure 5.1: Schematic illustration of the ferrite/austenite diffusion couple.

rather small value of w_γ because the diffusivity of carbon in austenite is much smaller than in ferrite. Thus, the ferrite becomes decarburised long before the carbon concentration profile has penetrated all regions of the austenite. The diffusion process considered is one–dimensional (normal to the α/γ interface), and is symmetrical about the centerline so that only half the couple needs to be considered in the finite difference analysis. The austenite and ferrite regions were for the purposes of numerical analysis, divided into a number of slices n_γ and n_α respectively, with

$$w_\gamma^s = w_\gamma/n_\gamma \qquad (5.6)$$

$$w_\alpha^s = w_\alpha/(2n_\alpha) \qquad (5.7)$$

The choice of the number of slices into which each phase may be divided is not entirely arbitrary since the diffusion processes in the two phases are coupled. The larger the number of slices, the greater the accuracy of the method, although the calculations are then more expensive in terms of computing time. The choice of n_γ is initially made arbitrarily, so that w_γ^s can be calculated. This in turn leads to the time t, representing the interval between successive recalculations of the concentration profile of the whole diffusion couple:

$$t = r_\gamma \frac{(w_\gamma^s)^2}{D} \qquad (5.8)$$

where r_γ is a grid parameter in the finite difference method, which can be set to a smaller value for higher accuracy. Having thus fixed the interval t, the thickness of the ferrite slice

56

follows as:

$$w_\alpha^s = (tD_c^\alpha/r_\alpha)^{(0.5)}. \tag{5.9}$$

r_α is another dimensionless grid parameter, this time for ferrite, which in the present work is taken to be the same as r_γ. The implications of choosing different values of the grid parameter are discussed later. Note that since the diffusivity in ferrite is much larger than in austenite, the number of slices in the austenite has to be much larger than in ferrite in order to ensure that $w_\alpha^s \ll w_\alpha$.

The finite difference analysis is carried out using nondimensional variables, the concentrations, x, and distances, w, being normalised with respect to average concentration in the alloy and the thickness of austenite respectively (Crank, 1975). The normalised variables are defined as follows:

$$w' = w/w_\gamma \tag{5.10}$$

$$x' = x/\overline{x} \tag{5.11}$$

$$t' = Dt/(w_\gamma)^2 \tag{5.12}$$

where D is the diffusion coefficient. Since the ferrite occupies the space $0 \leq w' \leq (w_\alpha/2w_\gamma)$, the region is covered by a grid of rectangles of sides $\delta w'$ and $\delta t'$. The coordinates of a grid point (w', t') can be written $(i\delta w', j\delta t')$, where i and j are integers. The normalised concentration at that point (for phase γ) is written $x_{i,j}'^\alpha$.

The explicit finite difference formula is then given by (Crank, 1975):

$$x_{1,j+1}'^\alpha = x_{i,j}'^\alpha + r_\alpha(x_{i-1,j}'^\alpha - 2x_{i,j}'^\alpha + x_{i+1,j}'^\alpha) \tag{5.13}$$

where the $r_\alpha = \delta t'/(\delta w')^2$ is grid parameter for the finite difference parameter. The normalised concentration $x_s'^\alpha$ in the α at the α/γ interface has been taken as $x^{\alpha\gamma}/\overline{x}$. The relationship (5.13) has been used to calculate the value of x at all points along successive time rows of the grid, for the initial conditions that $x_{0,0}'^\alpha = x^{\alpha\gamma}/\overline{x}$, and $x_{i,0}'^\alpha = 1$ for all $i > 0$.

A similar analysis was carried out for the austenite, and the diffusion processes in the ferrite and austenite were related by using the mass conservation condition which ensures that the amount of carbon leaving the ferrite at any instant is identical to that entering the austenite (*i.e.* the fluxes to and from the interface must be equal):

$$\overline{D}(x_{0,j}'^\gamma - x_{i,j}'^\gamma) = D_c^\alpha(x_{1,j}'^\alpha - x_{0,j}'^\alpha) \tag{5.14}$$

57

where $x_{i,0}'^\gamma = 1$ for all $i > 0$. Thus the value of $x_{0,j}'^\gamma = 1$ can be obtained by using the above equation.

The concentrations in the slices with $i = i_{max}$ are not significantly affected during the early stages of diffusion, but soft–impingement must eventually occur in both phases, the ferrite first since $D_c^\alpha \gg D_c^\gamma$. When soft–impingement does occur, the concentrations in these limiting slices can be calculated by reflecting the concentration profile across an imaginary boundary located at i_{max}; the finite difference formula is then given by:

$$x_{i_{max},j+1}'^\gamma = x_{i_{max},j}'^\gamma + 2r_\gamma(x_{i_{max}-1,j}'^\gamma - x_{i_{max},j}'^\gamma) \tag{5.15}$$

5.3 Results and Discussion

The calculations were carried out for Fe–0.4C and Fe–0.4C–2Mn wt. % alloys over the temperature range 280–480 °C at 40 °C intervals. The plain carbon steel was chosen for its simplicity and the Fe–C–Mn alloy to illustrate the effect of making a solute addition which increases the stability of austenite. The calculated transformation–start temperatures are listed in Table 5.1; the method used for the calculations is due to Bhadeshia and Edmonds (1980) and Bhadeshia (1981a–c). The paraequilibrium $(\alpha+\gamma)/\gamma$ Ae3' phase boundaries are presented in Figure 5.2, calculated using the method described in (Aaronson *et al.*, 1966; Bhadeshia and Edmonds, 1980). The Ae3" boundary refers to the corresponding paraequilibrium austenite composition when the ferrite is associated with 400 J mol^{-1} of stored energy, consistent with the strain energy due to the shape deformation accompanying the growth of bainite (Bhadeshia, 1981a). Most of the calculations were carried out without incorporating the stored energy term, since plastic deformation or elastic interactions between adjacent sheaves could lead to a lowering of the magnitude of the stored energy. The equilibrium or paraequilibrium carbon concentration of bainitic ferrite is always very small, and was taken in all cases to be given by the thermodynamically extrapolated $\alpha/(\alpha+\gamma)$ Ae1 phase boundary for plain carbon steels (Bhadeshia, 1982).

Table 5.1: Chemical compositions (wt.%) of the alloys used in this investigation.

Alloy	M_s (°C)	B_s (°C)
Fe-0.4C wt.%	396	546
Fe-0.4C-2Mn wt.%	298	440

Figure 5.3 shows the calculations for a Fe–0.4C wt.% alloy, using both the analytical solution and the finite difference method; the time for decarburisation is that required for the ferrite to uniformly achieve its equilibrium concentration. The finite difference calculations were repeated using many different values of the grid parameter (with $r_\alpha = r_\gamma$), the aim being to find the point where a reduction in r makes little difference to the results. Figure 5.3 shows that the calculations with different r values begin to converge as r falls below about 0.16. Thus, all subsequent calculations were conducted with the grid parameter set to 0.04 in order to ensure high numerical accuracy while at the same time keeping the computing time involved within reasonable bounds.

It is also apparent from Figure 5.3 that the analytical solution persistently underestimates the diffusion time, the discrepancy with the numerical analysis increasing as the temperature decreases. This is because the analytical equation does not allow for the coupling of fluxes in the austenite and ferrite. It is based on the assumption that the diffusivity in the ferrite is so large, that any concentration gradients within the ferrite remain extremely small. This assumption must fail as the carbon concentration in the austenite at the interface rises (*i.e.* as the transformation temperature is reduced) because of the need to satisfy the mass conservation condition at the interface (equation 5.14). The diffusivity of carbon in ferrite is much larger than in austenite, so that the composition x^α in the ferrite at the interface will almost always deviate from equilibrium ($x^{\alpha\gamma}$) in order to maintain compatibility with the mass conservation condition, and will only reach the equilibrium value towards the end of the partitioning process. As $x^{\gamma\alpha}$ increases, the concentration gradients in the ferrite must also increase, and the partitioning process becomes to an increasing extent limited by diffusion within the ferrite. As a consequence, the diffusion process time as predicted by the finite difference method becomes larger than that estimated by the analytical equation when the transformation temperature is reduced. Typical concentration gradients that develop during the partitioning process are illustrated in Figure 5.4, and confirm that diffusion in the ferrite becomes more of a limiting factor as the equilibrium concentration in the austenite at the interface rises. Hence, concentration gradients within the ferrite at 450 °C are seen to virtually vanish after just 0.04s, whereas substantial gradients are apparent for the 330 °C heat treatment after the much longer time interval of 1.1s.

This is also illustrated by the fact that the difference in the carbon concentration in the middle of the ferrite plate, compared with that at the α/γ interface, increases as the temperature decreases (Figure 5.5). At any specified temperature, the gradients in

59

the ferrite are largest at the beginning of the decarburisation process and diminish as the partitioning process slows down with the build up of carbon in the austenite ahead of the α/γ boundary (Figure 5.4).

A reduction in the paraequilibrium carbon concentration $x^{\gamma\alpha}$ at a constant temperature must lead to an increase in the time required to achieve a specified level of partitioning, since the driving force for diffusion is reduced. Thus, an addition of 2 wt.% Mn to the plain carbon steel shifts the Ae3' phase boundary to lower carbon concentrations (Figure 5.2) and the diffusion times increase significantly (Figure 5.6) when the comparison is made at the same temperature. Since a lowering of $x^{\gamma\alpha}$ also causes a concomitant decrease in any concentration gradients in the ferrite, the discrepancy between the analytical and finite difference calculations decreases as the concentration of austenite stabilising element increases (c.f. Figures 5.6a, 5.6b). The effect of alloy chemistry on the decarburisation time is of vital importance in rationalising the upper bainite, lower bainite and martensite reactions in steels. Without such an alloy effect, it would not be possible to explain, for example, why the temperature at which lower bainite grows in a given steel might be higher than that at which upper bainite forms in another steel (Takahashi and Bhadeshia, 1990).

Figure 5.6c illustrates the effect of the 400 J mol^{-1} of stored energy, on the diffusion times calculated for the Fe–0.4C wt.% alloy. The stored energy term manifests in the calculations via $x^{\gamma\alpha}$, which is given by the Ae3" curve instead of the Ae3' curve utilised in all the other calculations. The effect is significant but does not alter any trends and is neglected for the reasons stated earlier.

The analytical approach indicates that the mean carbon concentration in the ferrite should decrease parabolically with time, i.e. $(\overline{x}^{\alpha} - x^{\alpha\gamma}) \propto t^{0.5}$ in the absence of soft–impingement effects. Figure 5.7 illustrates this variation, as calculated using the finite difference method; it is evident that the parabolic relation is still valid, since in all cases the deviations from linearity are found to be negligible. This might be a consequence of the speed with which the concentration gradients in the ferrite collapse after an initial transient.

5.3.1 Soft–impingement in the Austenite

In all of the cases discussed above, the concentration in the austenite far from the α/γ interface never rose significantly above $\overline{x}$. This is because the diffusion coefficient for carbon in austenite is far smaller than that in ferrite. For the purposes of the decarburisation process, the austenite therefore remained essentially semi–infinite in extent in the direction of the diffusion flux, even though the total thickness of the austenite on either side of the

60

ferrite plate was taken to be identical to the full thickness of the ferrite plate ($0.4\,\mu$m).

There are in practice many circumstances where plates of ferrite grow in close proximity, with only small regions of austenite trapped between the ferrite plates. This is particularly the case for bainitic transformation where platelets of supersaturated ferrite grow in parallel formations called "sheaves", adjacent platelets being separated by rather thin films of austenite. The intervening austenite films tend to become thinner as the undercooling below the equilibrium transformation temperature increases, probably because the plate nucleation rate then rises. A similar situation arises during martensitic transformation in steels, when large numbers of supersaturated plates form at rates much faster than the time needed for the diffusion of carbon into the austenite. The films of austenite between the plates of martensite are then extremely thin ($< 20\,$nm, Sarikaya *et al.*, 1982). In such circumstances, the composition of the austenite in all regions is likely to rise beyond $\overline{x}$ during the decarburisation process, even in the furthest regions from the ferrite/austenite interface. Thus, soft–impingement in the austenite is likely to occur before the ferrite has completely decarburised.

The soft–impingement phenomenon was investigated by progressively reducing the thickness of the austenite slabs adjacent to the ferrite plate (Figure 5.8). For a ferrite plate of fixed thickness $0.4\,\mu$m, the thickness of the two austenite slabs in contact with the plate was progressively reduced from $0.2\,\mu$m towards zero, and the time taken for diffusion within the ferrite to cease was computed. For the particular circumstances considered, the austenite behaves as if it is of semi–infinite extent down to a thickness of about $0.05\,\mu$m. Hence, for larger austenite thicknesses, the time plotted on Figure 5.8 is that taken for $x^{\alpha} = x^{\alpha\gamma}$. As the thickness is reduced below $0.05\,\mu$m, the time for diffusion to stop in the ferrite goes through a maximum, because the austenite is no longer able to accommodate all the excess carbon within the ferrite (it saturates at the concentration $x^{\gamma\alpha}$). This can be concluded from the fact that the carbon concentration in the ferrite when diffusion in the ferrite stops, rises towards $\overline{x}$ as w_{γ} decreases. The maximum in the time occurs because initially, soft–impingement in the austenite leads to a reduction in the diffusion flux from the ferrite. As the austenite thickness is decreased further, it becomes impossible to accommodate all the carbon that is rejected from the ferrite; the austenite achieves its paraequilibrium carbon concentration before the ferrite has been decarburised, and diffusion ceases even though $\overline{x}^{\alpha} > x^{\alpha\gamma}$. The time required to saturate the austenite decreases with w_{γ}, giving the maximum observed in Figure 5.8.

The results prove that if the plates of supersaturated ferrite form sufficiently rapidly, and leave very limited regions of austenite untransformed, then it becomes impossible to partition all of the excess carbon into the residual austenite. The carbon must remain in solution or precipitate as carbides within the ferrite. This is exactly what happens during martensitic transformations in low–alloy steels, where only minute quantities of retained austenite are to be found in the microstructure obtained by quenching to ambient temperature.

5.4 Conclusions

The factors controlling the time required to partition excess carbon from a super-saturated ferrite plate have been examined using a finite difference method. The results have been compared with an earlier analytical approximation, which is found to give a poor representation of the diffusion problem when the concentration in the austenite at the interface becomes large (*i.e.* when the concentration gradients in the ferrite become significant). The analytical model in general underestimates the decarburisation time, the discrepancy increasing with lower temperatures or with alloys containing smaller quantities of austenite stabilising elements. The basic trends are, however, found to be similar for the two models, both models predicting much larger times than has been generally accepted in the past. Soft–impingement in the austenite is found to reduce the rate at which carbon in partitioned from supersaturated ferrite. There are also circumstances where the amount of austenite available is inadequate to fully absorb the excess carbon in the ferrite, in which case diffusion stops even though the ferrite is supersaturated with carbon.
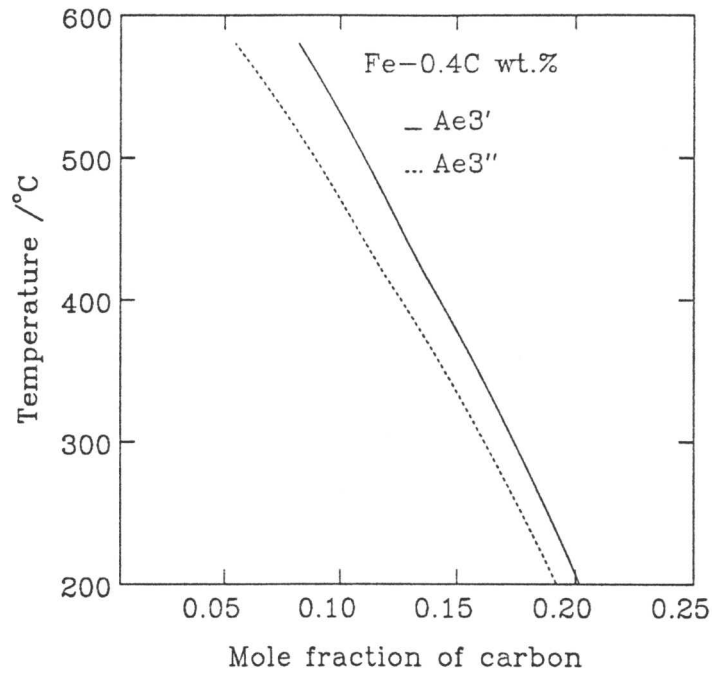
(a)
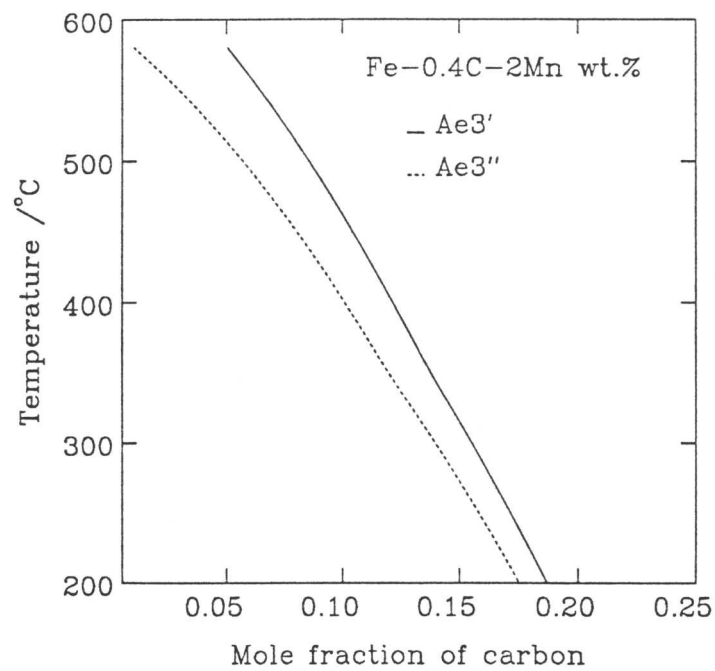
(b)

Figure 5.2: Calculated paraequilibrium $(\gamma + \alpha)/\gamma$ phase boundaries for the steels studied. The curves are labelled Ae3' to identify them as being for paraequilibrium, although for the plain carbon steel, the Ae3' curve is identical to the conventional Ae3 curve of the phase diagram. The Ae3" curve is the paraequilibrium phase boundary calculated assuming a stored energy for ferrite of 400 J mol^{-1}. (a) Fe–0.4C wt.%. (b) Fe–0.4C–2Mn wt.%.
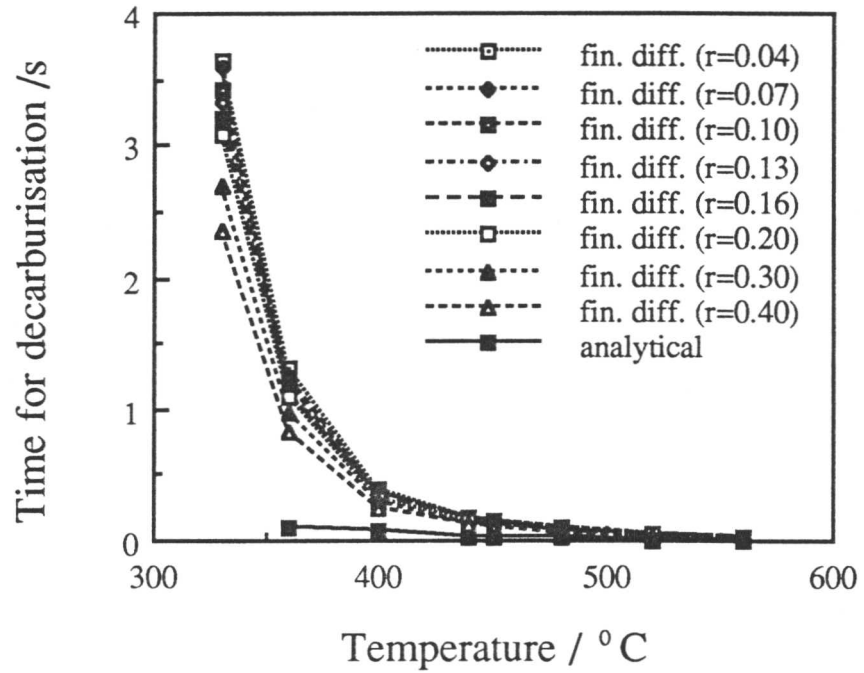
Figure 5.3: Calculated times required to decarburise a supersaturated plate of ferrite of thickness (0.4μ m) as a function of temperature in a Fe–0.4C wt.% steel. The calculations include those carried out using the analytical solution, and using different grid parameters for the finite difference method.
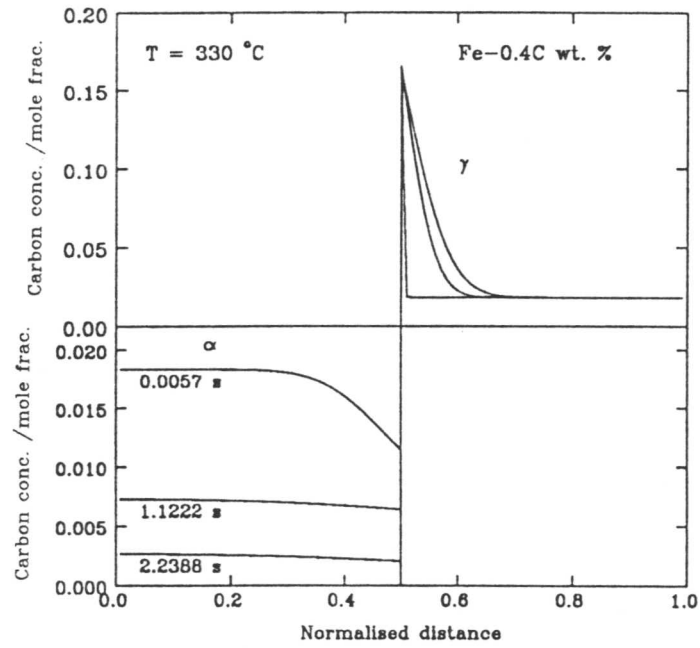
(a)
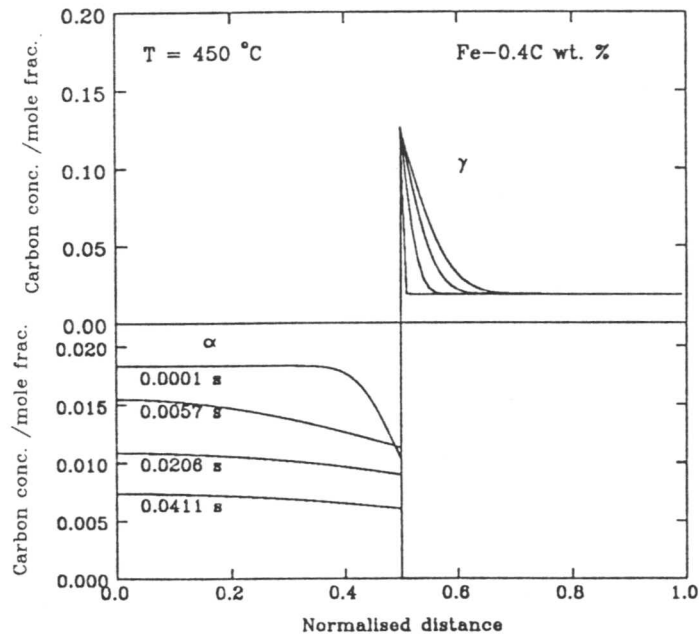
(b)

Figure 5.4: An illustration of the calculated composition profiles that develop within the ferrite and austenite during the partitioning of carbon. (a) 330 °C, the different curves within a given phase representing calculations carried out at time intervals of 1.117 s. (b) 450 °C, 0.021 s time intervals.
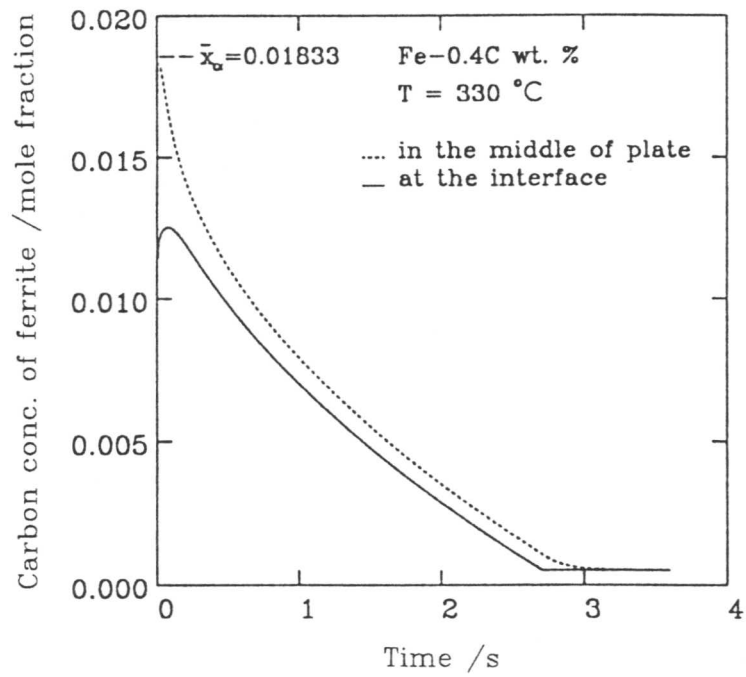
(a)
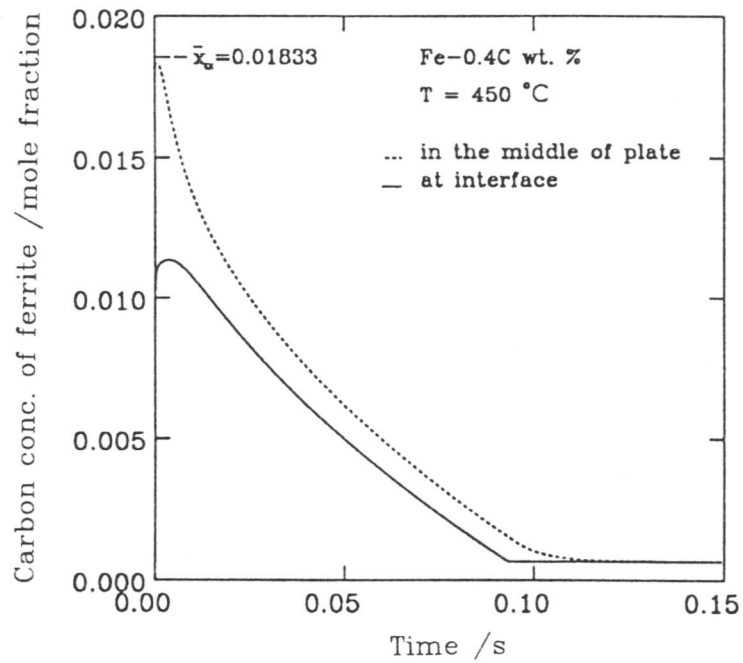
(b)

Figure 5.5: Comparison of the carbon concentrations in ferrite at the centre and edge of the plate during the partitioning of carbon. (a) 330 °C. (b) 450 °C.
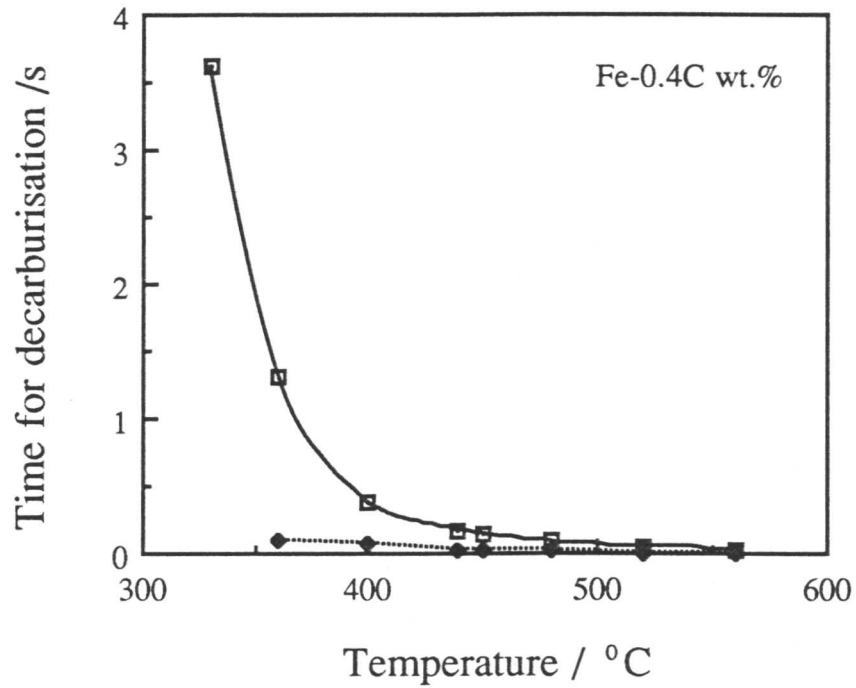
(a)
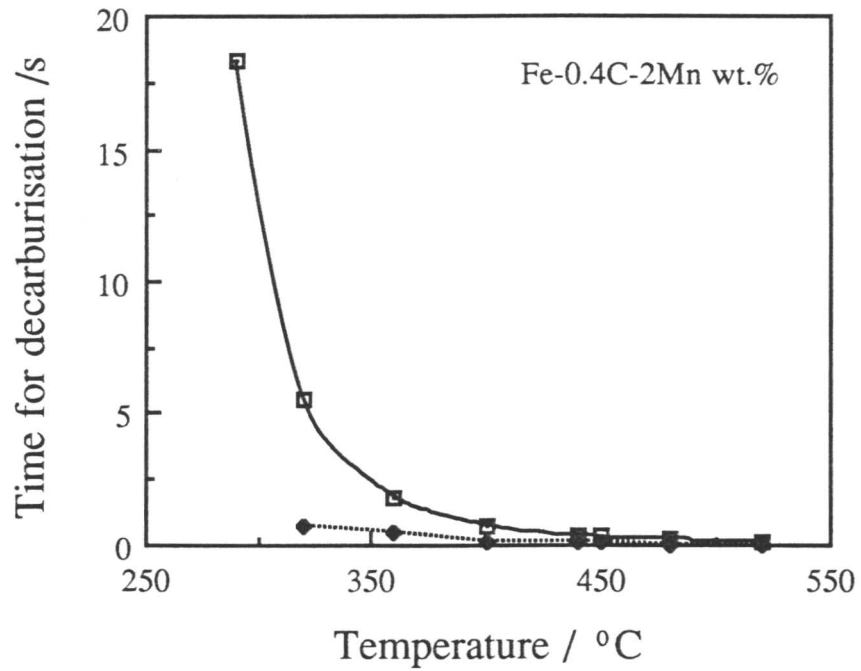
(b)

Figure 5.6: Decarburisation time as a function of temperature. The dashed curves represent calculations carried out using the approximate analytical solution, whereas the continuous curves were calculated using the finite difference method. (a) Fe–0.4C wt.%. (b) Fe–0.4C–2Mn wt.%.
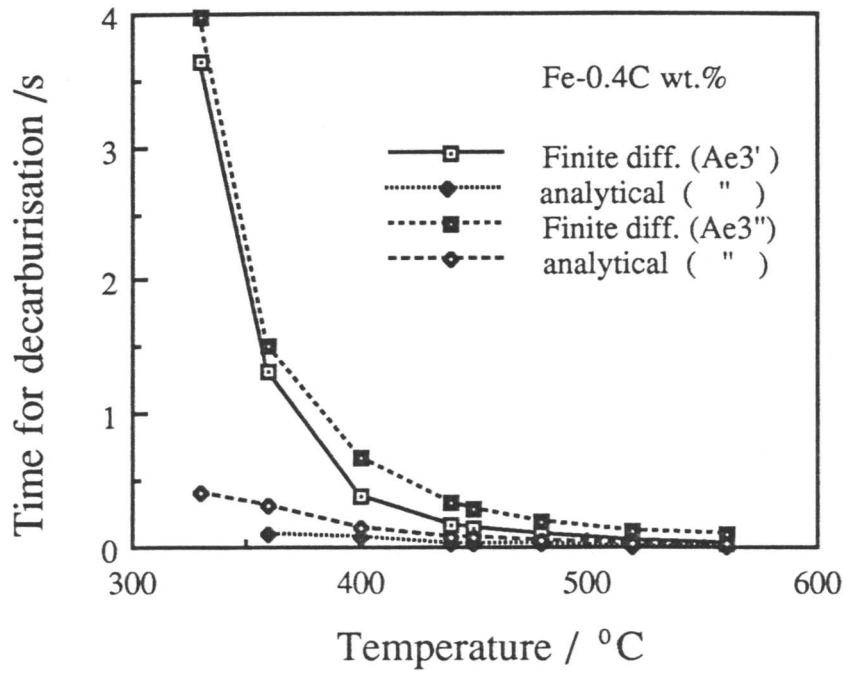
(c)

Figure 5.6: Continued. (c) Fe–0.4C wt.%; the solid curve refers to calculations using the Ae3' curve for $x^{\gamma\alpha}$, whereas the other curve is based on Ae3" which includes a $400\,\mathrm{J\,mol^{-1}}$ of stored energy in the ferrite.

(a)

(b)
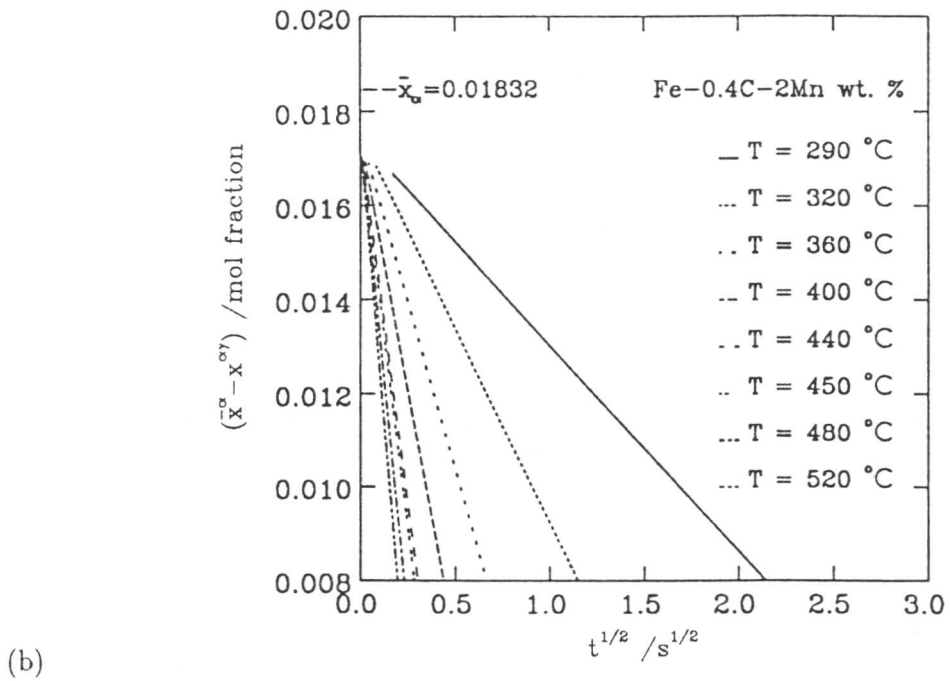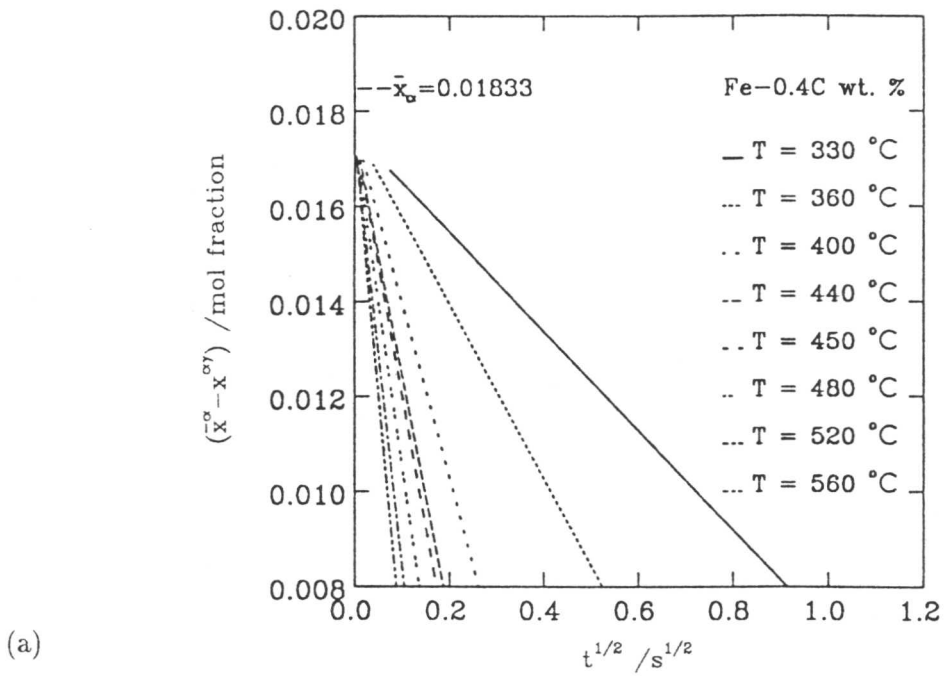
Figure 5.7: Variation in the mean carbon concentration of the ferrite as a function of time and temperature. (a) Fe–0.4C wt.%. (b) Fe–0.4C–2Mn wt.%.

69
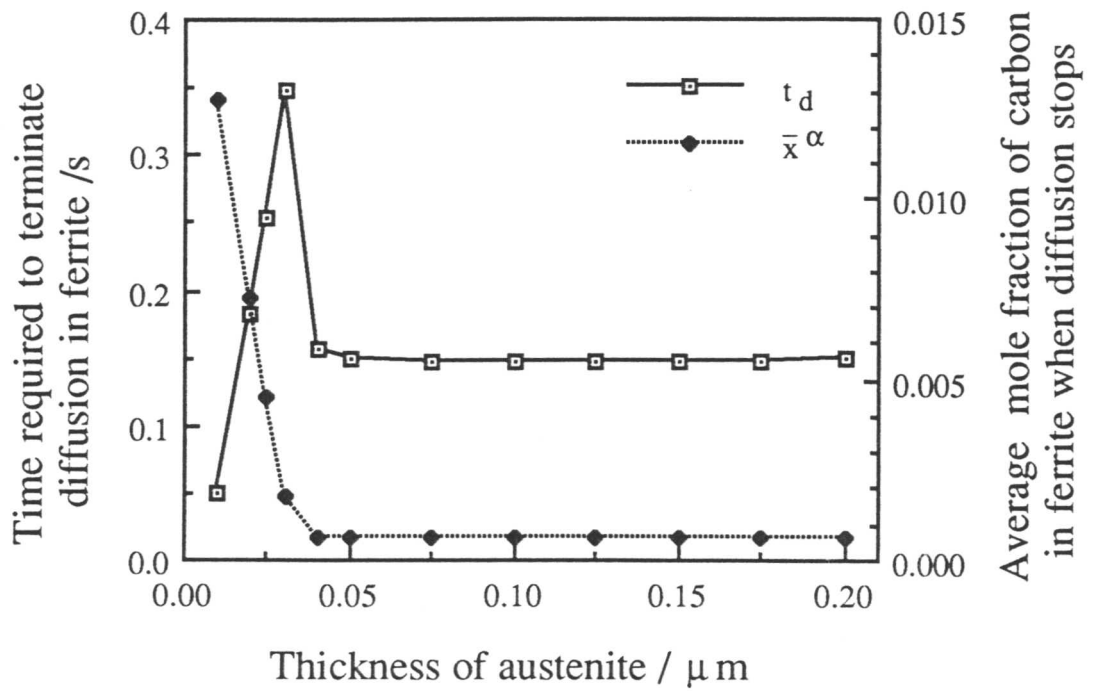
Figure 5.8: Plot of the time required to terminate the diffusion process within the ferrite, versus the thickness of the adjacent austenite slab. Note that there are two such slabs of austenite per ferrite plate, one on each side of the ferrite plate. The discontinuous curve represents the carbon concentration in the ferrite at the point where diffusion stops.

Chapter 6

An Analysis of Compositional Data on α_1 Plates in an Ag–44.9Cd at.% Alloy

6.1 Introduction

The structure of the parent phase, in an Ag–44.9Cd at.% alloy at elevated temperatures is disordered body–centered cubic (bcc). With decreasing temperature, the alloy undergoes a disorder–order transition to β_2 with the CsCl structure (Masson and Barrett, 1958). It has been reported that in an Ag–Cd alloy, a platelike phase, "bainite", will precipitate during ageing after quenching from a high temperature. The incubation time on a time–temperature–transformation (TTT) diagram has been measured to be 200 seconds at 160 °C and was found to decrease with an increase in temperature (Kostic $et\ al.$ 1976). During the $\beta_2 \rightarrow \alpha_1$ transformation two forms of precipitates are commonly observed and the conditions of their formation depend on the alloy composition and the transformation temperature (Flewitt and Towner, 1967; Hornbogen and Warlimont, 1967; Srinivasan and Hepworth, 1971; Cornelis and Wayman, 1974; Kostic and Hawbolt, 1979). At the higher end of the transformation temperature range, a rod–shaped Widmanstätten ferrite form of the equilibrium α phase is formed while at the lower temperatures, a metastable plate–like product, often referred to as substitutional bainite α_1 is found (Garwood, 1954–1955; 1965).

The alloy under consideration undergoes a solid state phase transformation in which the metastable product phase exhibits the geometry and crystallography of a displacive transformation although formation of the equilibrium α phase requires a composition change involving long range diffusion (Wu $et\ al.$ 1988). The controversy arises in the formation of fcc α_1 plates from the metastable β_2 phase (ordered bcc, B2 structure) in Ag–Cd and Cu–Zn as to whether shear or diffusional growth is the operating mechanism and whether or not the plates fulfil all the criteria presently accepted for martensite. If not then the growth mechanism is presumably diffusional (Lorimer $et\ al.$ 1975). In the case of interstitial solid solutions, the argument has been made that the interstitial solute can diffuse while the substitutional atoms undergo a shear mechanism (Christian, 1965a; Olson $et\ al.$ 1989;

1990). No such mechanism should, however, be possible when both phases are substitutional (Lorimer, 1975).

It has also been reported that plates of the α_1 phase exhibiting chevron–shaped surface traces were found to form isothermally above room temperature in the β_2 phase of several Cu– and Ag–based alloys (Garwood, 1954–55; Garwood and Hull, 1958; Flewitt and Towner, 1967; Hornbogen and Warlimont, 1967; Srinavasan and Hepworth, 1971; Agers and Massalski, 1972; Massalski *et al.* 1972). These plates have been considered to be bainite by analogy with bainite in ferrous alloys. Flewitt and Towner (1967) and Cornelis and Wayman (1973) observed the bainite plates in a Cu–Zn alloy. According to them the bainite plates were formed initially without a change in composition, and the partitioning of Cu and Zn atoms occurred only after the plates had formed. According to the analysis of Kostic, Hawbolt and Brown (1976) the bainite plates which formed in the β_2 phase of a Ag–44.9Cd at.% alloy at temperatures 160 to 300 °C, grew rapidly to a given length and maintained the length for extended transformation times although they continued to thicken. They claimed that the thickening displayed parabolic kinetics in agreement with the Frank (1950) and Zener (1949) model for volume diffusion–controlled precipitate growth. The lengthening of the plates was then analysed using Trivedi (1970a; 1970b) model. It was established that the plates lengthened at a rate approximately 180 times longer than permitted by volume diffusion and no explanation was given for this rapid lengthening of plates. It has been argued that despite the implications of the geometry and crystallographic evidence, the α_1 phase forms with the composition of the equilibrium α phase (Lorimer *et al.* 1975).

The present work was started to investigate the hypothesis that α_1 plates are formed with an excess of Cd and if enough time is given after their formation, cadmium can diffuse into the neighbouring β_2 matrix. In the analysis of Wu *et al.*, (1988) the ageing time utilised was very small and that probably may not have been sufficient to see any diffusion take place. Since the movement of the interface is much faster than permitted by diffusion, the cadmium is probably trapped during transformation. According to the Aziz model (1982, 1983) for solute trapping the partitioning coefficient can be written as:

$$k_p = \frac{x_{\alpha_1}}{x_I^{\beta_2}} = \frac{1 + \eta K_e}{1 + \eta} \tag{6.1}$$

where $\eta = D_{Cd}/\lambda V$. x_{α_1} and $x_I^{\beta_2}$ are the Cd compositions in α_1–plate and in the β_2 matrix at the interface. The equilibrium partitioning coefficient is:

$$k_e = \frac{x^{\alpha_1 \beta_2}}{x^{\beta_2 \alpha_1}} = 0.864 \tag{6.2}$$

where $x^{\alpha_1\beta_2}$ and $x^{\beta_2\alpha_1}$ are the equilibrium Cd composition in the α_1–plate and β_2 matrix respectively. Using the values of diffusivity of Cd in Ag–Cd (D_{Cd}), interatomic spacing (λ) and interface velocity (V) as 6.377×10^{-16} m^{2}s^{-1} (discussed later), 0.25 nm (Aziz, 1982; 1983) and 2.27×10^{-7} ms^{-1} (Kostic $et\ al.$ 1976) respectively, the following values of partitioning coefficient have been calculated.

$$k_p = 0.953 \approx 1 \qquad (6.3)$$

This means that there is almost no partitioning of cadmium during the growth of α_1–plates. Thus it is reasonable to think that in the $\beta_2 \rightarrow \alpha_1$ transformations, plates of α_1 are formed with an excess of cadmium. The cadmium then diffuses to the neighbouring β_2 matrix during ageing.

An analytical model presented by Bhadeshia (1988) can be applied to the non–ferrous alloys of interest. According to this model the time taken to diffuse all of the excess cadmium from α_1 plate in Ag–Cd alloy can be witten as:

$$t_d = \frac{w_{\alpha_1}(\overline{x} - x^{\alpha_1\beta_2})\pi^{0.5}}{4(D_{Cd}^{\beta_2})^{0.5}(x^{\beta_2\alpha_1} - \overline{x})} \qquad (6.4)$$

where $D_{Cd}^{\beta_2}$ is diffusivity of cadmium in β_2 matrix (discussed in next section), $\overline{x}$ is the average at.% of cadmium in the alloys, $x^{\alpha_1\beta_2}$ and $x^{\beta_2\alpha_1}$ are the equilibrium cadmium concentrations in the α_1–plate and β_2 matrix respectively, and w_{α_1} is the width of the α_1–plate. The values of equilibrium concentrations for different temperatures were taken from the references (Hansen, 1958; Binary Alloy Phase Diagrams, 1990). The data are given in Table 6.1.

Table 6.1: Equilibrium concentration of Cd in α_1–plate ($x^{\alpha_1\beta_2}$) and in β_2 matrix ($x^{\beta_2\alpha_1}$) in Ag–Cd alloy (Hanson, 1958; Binary Alloy Phase Diagrams, 1990).

Temperature (°C)	$x^{\alpha_1\beta_2}$ (at.%)	$x^{\beta_2\alpha_1}$ (at.%)
160	40.5	49.7
180	40.7	49.5
200	41.0	49.2
220	41.5	48.6
240	42.0	48.6

Ag–Cd phase diagram (Hansen, 1958; Binary Alloy Phase Diagrams, 1990) is shown in Figure 6.1. As in the case of ferrous alloys, it has pointed out that even this analysis may not be completely satisfactory given that it does not allow for the coupling of fluxes in the plate and matrix (Bhadeshia, 1988). It therefore contains nothing about diffusion in the α_1–plate.

The purpose of the present work was to re-examine the partitioning of cadmium from supersaturated α_1–plate into the adjacent β_2 matrix using a numerical method. This should in principle enable the treatment of diffusion in both the plate and matrix, and at the same time permit "soft-impingement" effects to be treated relatively easily. The overlap of the diffusion or temperature fields of adjacent particles, or from active regions of the same particle, is called soft–impingement (Christian, 1975).

6.2 The Diffusion Coefficients

The diffusivity of Cd in Ag–Cd has been calculated from the data available from three different sources given below. In all of these cases the diffusivity of Cd in α_1 plate ($D_{Cd}^{\alpha_1}$) and in β_2 matrix ($D_{Cd}^{\beta_2}$) are assumed to be identical *i.e.*

$$D_{Cd}^{\alpha_1} = D_{Cd}^{\beta_2} = D_{Cd}. \tag{6.5}$$

This assumption was made for the reason that diffusion data for α_1 and β_2 phases in Ag–Cd alloy are not available separately for the individual phases.

6.2.1 Radiotracer diffusion

Lexcellent *et al.*, (1989) performed measurements of creep rates and the radiotracer diffusion coefficients in equiatomic β_2 Ag–Cd over the temperature range of 440 to 610 °C. The empirical relation for the temperature dependence of diffusivity (in m²s⁻¹) is given by:

$$D_{Cd}^{\beta_2} = 0.77 \times 10^{-4} \exp(-Q/RT) \quad T > 773\text{K} \tag{6.6}$$

Where activation energy, $Q = 9.2004 \times 10^4$ J mol⁻¹. The diffusion data did not obey an Arrhenius equation over the whole experimental temperature range explored in Ag–Cd but it bends to lower values of diffusivity at lower temperatures. The value of Ag–Cd at 240 °C has been calculated by extrapolation of the bent part of the curve to 240 °C as shown in Figure 6.2. A least square fit of the data to the bent part yielded the following relations for the temperature dependence of the diffusion coefficient of Cd;

$$\ln D_{Cd}^{\beta_2} = -0.26155 - 1.8128 \times 10^4/T$$

74

or

$$D_{Cd}^{\beta_2} = 0.7698 \exp(-1.5068 \times 10^5 / RT) \quad T < 775K \tag{6.7}$$

where $D_{Cd}^{\beta_2}$ is in the units of $m^2 s^{-1}$.

6.2.2 Potentiostatic Dissolution

Pchelnikov *et al.*, (1985) deduced the diffusivity of Cd in β_2 Ag–Cd at room temperature from potentiostatic dissolution experiments by assuming that the rate of dissolution was governed by solid state diffusion (Diffusion and Deffect Data, 1986). They reported the value of diffusivity of Cd in Ag–30Cd at.% as 1.4×10^{-17} $m^2 s^{-1}$.

6.2.3 Self–diffusion

The diffusion coefficient of cadmium in Ag–44.9Cd at.% at 240 °C (513 K) has been calculated by extrapolating data based on self–diffusion experiments (Gardner *et al.* 1968; Diffusion Data, 1969). Using the serial sectioning technique, Gardner *et al.* studied the self–diffusion of Cd^{115} in various Ag–Cd alloys. The data are given in Table 6.2.

Table 6.2: Self–diffusion of Cd^{115} in various Ag–Cd alloys (Gardner *et al.* 1968; Diffusion Data, 1969).

Temperature (°C)	Cd composition (at.%)	Diffusivity ($m^2 s^{-1}$)
563.7	37.20	4.33×10^{-14}
	33.02	4.12×10^{-14}
	30.50	2.41×10^{-14}
634.9	38.12	2.81×10^{-13}
	33.75	2.18×10^{-13}
	29.90	1.10×10^{-13}
681.9	37.82	5.83×10^{-13}
	32.99	4.64×10^{-13}
	30.05	2.87×10^{-13}

The extrapolated curves of Cd composition versus diffusivity at different temperatures are shown in Figure 6.3a. The natural log of the estimated values of diffusivity for 44.9Cd at.% ($\ln D_{Cd}$) were then plotted versus corresponding temperatures as shown in Figure 6.3b. The final value of diffusivity was then estimated by fitting the curve shown in Figure 6.3b. The empirical relation obtained by curve fitting is given by:

$$\ln D_{Cd} = -9.0877 - 1.8088 \times 10^4 / T$$

or

$$D_{Cd} = 8.171 \times 10^{-10} \exp(-1.503 \times 10^5/RT) \tag{6.8}$$

where T and D_{Cd} are in the units of Kelvin and m^2s^{-1} respectively.

6.3 Finite Difference Analysis

The method used here is a standard finite difference technique, which has been discussed fully by Crank (1975). The same technique has also been used in Chapter 5 (Mujahid and Bhadeshia, 1992). The matrix–plate aggregate is treated as a composite diffusion couple in which flat slabs of matrix, each of thickness w_{β_2} are welded on either side of a slab of plate of thickness w_{α_1}, Figure 6.4. The slab dimensions were chosen to avoid the possibility of soft–impingement in the matrix and to compare the results with earlier published work (Wu *et al.* 1988). A number of plate thicknesses in the range 60–300 nm were chosen, while the matrix thickness was taken as 400 nm. However the averaging of Cd composition in the matrix was done at 20 nm interval in order to make comparison with the results by Wu *et al.*, (1988). In the matrix, soft–impingement occurs when the cadmium concentration in the matrix at the furthest point away from the α_1/β_2 interface rises beyond the initial concentration $\bar{x}$. It was found that, the plate looses all of the excess cadmium long before the cadmium concentration profile has penetrated all regions of the matrix. The diffusion process considered is one–dimensional (normal to the α_1/β_2 interface), and is symmetrical about the centerline so that only half the couple needs to be considered in the finite difference analysis (Chapter 5). The matrix and plate regions were divided into a number of slices n_{β_2} and n_{α_1} respectively, with

$$w_{\beta_2}^s = w_{\beta_2}/n_{\beta_2} \tag{6.9}$$

$$w_{\alpha_1}^s = w_{\alpha_1}/(2n_{\alpha_1}). \tag{6.10}$$

A compromise has to be made between accuracy and computer time in the choice of the number of slices. The larger the number of slices, the greater the accuracy of the method, although the calculations are then more expensive in terms of computing time. The choice of n_{β_2} is initially made arbitrarily, so that $w_{\beta_2}^s$ can be calculated. This in turn leads to the time t, representing the interval between successive recalculations of the concentration profile of the whole diffusion couple:

$$t = r_{\beta_2} \frac{(w_{\beta_2}^s)^2}{D_{Cd}^{\beta_2}} \tag{6.11}$$

where r_{β_2} is a grid parameter in the finite difference method, which can be set to a smaller value for higher accuracy. Having thus fixed the interval t, the thickness of the α_1–plate follows as:

$$w_{\alpha_1}^s = (tD_{Cd}^{\alpha_1}/r_{\alpha_1})^{(0.5)}. \tag{6.12}$$

r_{α_1} is another dimensionless grid parameter, this time for a plate, which in the present work is taken to be the same as r_{β_2}.

The finite difference analysis is carried out using nondimensional variables, the concentrations x and distances w being normalised with respect to average concentration in the alloy and the thickness of matrix respectively (Crank, 1975). The normalised variables are defined as follows:

$$w' = w/w_{\beta_2} \tag{6.13}$$

$$x' = x/\overline{x} \tag{6.14}$$

$$t' = Dt/(w_{\beta_2})^2 \tag{6.15}$$

where D is the diffusion coefficient. Since the α_1–plate occupies the space $0 \leq w' \leq (w_{\alpha_1}/2w_{\beta_2})$, the region is covered by a grid of rectangles of sides $\delta w'$ and $\delta t'$. The coordinates of a grid point (w', t') can be written $(i\delta w', j\delta t')$, where i and j are integers. The normalised concentration at that point (for α_1–plate) is written $x_{i,j}'^{\alpha_1}$.

The explicit finite difference formula is then given by (Crank, 1975):

$$x_{1,j+1}'^{\alpha_1} = x_{i,j}'^{\alpha_1} + r_{\alpha_1}(x_{i-1,j}'^{\alpha_1} - 2x_{i,j}'^{\alpha_1} + x_{i+1,j}'^{\alpha_1}) \tag{6.16}$$

where the $r_{\alpha_1} = \delta t'/(\delta w')^2$ is grid parameter for the finite difference parameter. The normalised concentration $x_s'^{\alpha_1}$ in the α_1 at the α_1/β_2 interface has been taken as $x^{\alpha_1\beta_2}/\overline{x}$. The relationship (6.16) has been used to calculate the value of x at all points along successive time rows of the grid, for the initial conditions that $x_{0,0}'^{\alpha_1} = x^{\alpha_1\beta_2}/\overline{x}$, and $x_{i,0}'^{\alpha_1} = 1$ for all $i > 0$.

A similar analysis was carried out for the matrix, and the diffusion processes in the plate and matrix were related by using the mass conservation condition which ensures that the amount of cadmium leaving the plate at any instant is identical to that entering the matrix (*i.e.* the fluxes to and from the interface must be equal):

$$D_{Cd}^{\beta_2}(x_{0,j}'^{\beta_2} - x_{i,j}'^{\beta_2}) = D_{Cd}^{\alpha_1}(x_{1,j}'^{\alpha_1} - x_{0,j}'^{\alpha_1}) \tag{6.17}$$

77

where $x'^{\beta_2}_{i,0} = 1$ for all $i > 0$. Thus the value of $x'^{\beta_2}_{0,j} = 1$ can be obtained by using the above equation.

The concentrations in the slices with $i = i_{max}$ are not significantly affected during the early stages of diffusion, but soft–impingement must eventually occur in both phases, the ferrite first since $D^{\alpha_1}_{Cd} \gg D^{\beta_2}_{Cd}$. When soft–impingement does occur, the concentrations in these limiting slices can be calculated by reflecting the concentration profile across an imaginary boundary located at i_{max}; the finite difference formula is then given by:

$$x'^{\beta_2}_{i_{max},j+1} = x'^{\beta_2}_{i_{max},j} + 2r_{\beta_2}(x'^{\beta_2}_{i_{max}-1,j} - x'^{\beta_2}_{i_{max},j}) \qquad (6.18)$$

6.4 Results and Discussion

The calculations were carried out at Ag–44.9Cd at.% alloys for 240 °C for different plate sizes (in the range 60–300 nm) with different aging time. The equilibrium values of concentration were taken from Wu *et al.*, (1988). The calculations for the concentration profile were repeated with different values of grid parameter (taking $r_{\alpha_1} = r_{\beta_2}$) in order to find the value of the grid parameter where a reduction in r makes a little difference to the results. Figure 6.5 shows that the results begin to converge when the value of r gets smaller. Thus, a value of grid parameter r of 0.05 was found to be a good compromise between numerical accuracy and computer time.

The finite difference model takes into account the coupling of fluxes in the β_2 matrix and α_1 plate through equation 6.17. Typical concentration gradients that develop during the partitioning process for freshly formed bainite plate of 160 nm projected length and aged for 30 s, are illustrated in Figure 6.6. This figure compares the calculated profile with the earlier experimental results obtained by Wu *et al.*, (1988). This comparison shows that, in the case of the matrix, there is a very good agreement between theoretical and earlier experimental results but there is a difference in the case of the plates. Both theoretical and experimental results show that the cadmium concentration in β_2 matrix increases gradually as the interface is approached. For the α_1–plate, the calculated concentration decreases gradually from the middle of the plate when it approaches the interface whereas there is no significant increase in composition in the experimental data. A uniform plate composition is only predicted at long times. The diffusion profiles in the matrix (both observed and calculated) are, however, significant and show a composition difference after as little as 30 seconds of ageing time when transformed at 240 °C .

Figure 6.7 compares the concentration of cadmium as a function of specimen ageing time, due to the partitioning of cadmium from the α_1 bainite plate, between calculated and experimentally measured values for plates of different sizes. The comparison of calculated results with the observed values (Wu *et al.* 1988) is encourging. It strengthens the idea that there is some degree of supersaturation inspite of the fact that there is little difference in the equilibrium compositions of both phases. In Figure 6.8 the time taken to diffuse all of the excess cadmium versus different transformation temperatures is illustrated. The comparison of the values calculated from using finite difference method with that calculated by analytical method (Bhadeshia, 1988) shows that the analytical method underestimates the diffusion time because it does not take into account the coupling of fluxes at the interface.

6.4.1 Soft–impingement in the β_2 Matrix

In all of the cases discussed above, the concentration in the matrix phase far from the α_1/β_2 interface never rose significantly above $\overline{x}$. This is because there is a very small difference in the equilibrium cadmium composition in both phases. For the purposes of the partitioning of cadmium, the matrix therefore remained essentially semi–infinite in extent in the direction of the diffusion flux. The thickness of the matrix has been taken to be sufficiently large (400 nm) to avoid soft–impingement but averaging of cadmium concentration has been done at 20 nm from the interface in order to compare the results with the earlier experimental results.

There are, in practice, many circumstances where plates of bainite grow in close proximity, with only small regions of matrix trapped between the plates. This is particularly the case for transformations where platelets of supersaturated plate grow in parallel formations, adjacent platelets being separated by rather thin films of matrix. The intervening matrix phase films tend to become thinner as the undercooling below the equilibrium transformation temperature increases, probably because the α_1–plate nucleation rate then rises. In such circumstances, the composition of the matrix in all regions is likely to rise beyond $\overline{x}$ during the partitioning process, even in the furthest regions from the plate/matrix interface. Thus, soft–impingement in the matrix phase is likely to occur before the plate has lost all of its excess cadmium.

The soft–impingement phenomenon was investigated by progressively reducing the thickness of the matrix slabs adjacent to the plate (Figure 6.9). For a plate of thickness 300 nm, the thickness of the two matrix slabs in contact with the plate were progressively reduced from 400 nm towards zero, and the time taken for diffusion within the plate to

cease was computed. For the particular case considered, as the thickness is reduced below 400 nm, the time for diffusion to stop in the matrix goes through a maximum, because the matrix is no longer able to accommodate all the excess cadmium within the plate (it saturates at the concentration $x^{\beta_2 \alpha_1}$). This can be concluded from the fact that the cadmium concentration in the plate when diffusion in the plate stops, rises towards $\bar{x}$ as w_{β_2} decreases. The maximum in the time occurs because initially, soft–impingement in the matrix leads to a reduction in the diffusion flux from the plate. As the matrix thickness is decreased, it becomes impossible to accommodate all the cadmium that is rejected from the plate; the matrix achieves its paraequilibrium carbon concentration before the plate has lost all the excess cadmium, and diffusion ceases even though $\bar{x}^{\alpha_1} > x^{\alpha_1 \beta_2}$. The time required to saturate the matrix decreases with w_γ, giving the maximum observed in Figure 6.9.

The results prove that if the plates of supersaturated plate form sufficiently rapidly, and leave very limited regions of matrix untransformed, then it becomes impossible to partition all of the excess cadmium into the residual matrix phase. The cadmium must remain in solution or precipitate as in the case of steels carbides remain within the ferrite.

The work therefore suggests an interesting experiment introducing the examination of the chemical composition of plates which are in close proximity, in which case any supersaturation should be more readily detectable. This would give conclusive results as far as the mechanism of transformation is concerned.

It is clear from Figures 6.5 – 6.7 that there is a large variation in the calculated results as a function of choice of diffusion coefficient. The variation is large enough to render the interpretation of transformation mechanism impossible. Reliable low temperature diffusion data for the parent and product phases are essential in order to facilitate the present work.

6.5 Conclusions

The kinetics of the partitioning of excess cadmium from a supersaturated bainite plate of Ag–44.9Cd at.% alloy have been examined using a finite difference method. The results have been compared with an earlier experimental results. The experimental results in general underestimate the composition of cadmium in plate (Figure 6.6), otherwise for all the other results there is a good agreement between calculated and measured values (Figures 6.6; 6.7). The basic trends of both experimental and calculated results are, however, found to be similar. Soft–impingement in the matrix is found to reduce the rate at which cadmium is partitioned from supersaturated plate. With the reduction of the matrix thickness,

the amount of matrix available is inadequate to fully absorb the excess cadmium in the plate, in which case diffusion stops even though the plate is supersaturated with cadmium. Unfortunately, the analysis shows that accurate diffusion data are essential before any firm conclusions can be drawn about the mechanism of transformation.
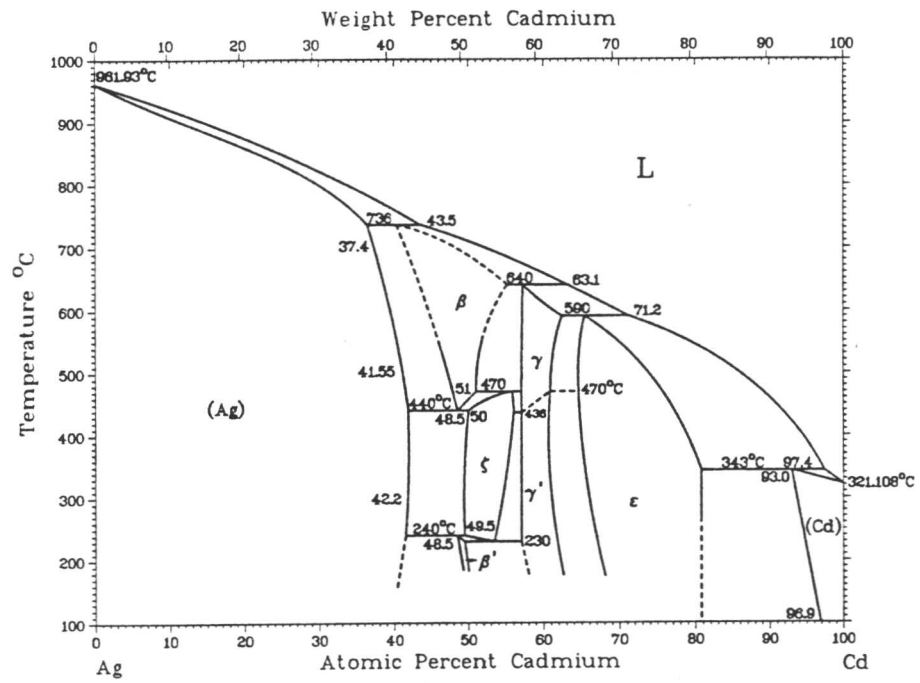
Figure 6.1: Ag–Cd phase diagram (Hansen, 1958).
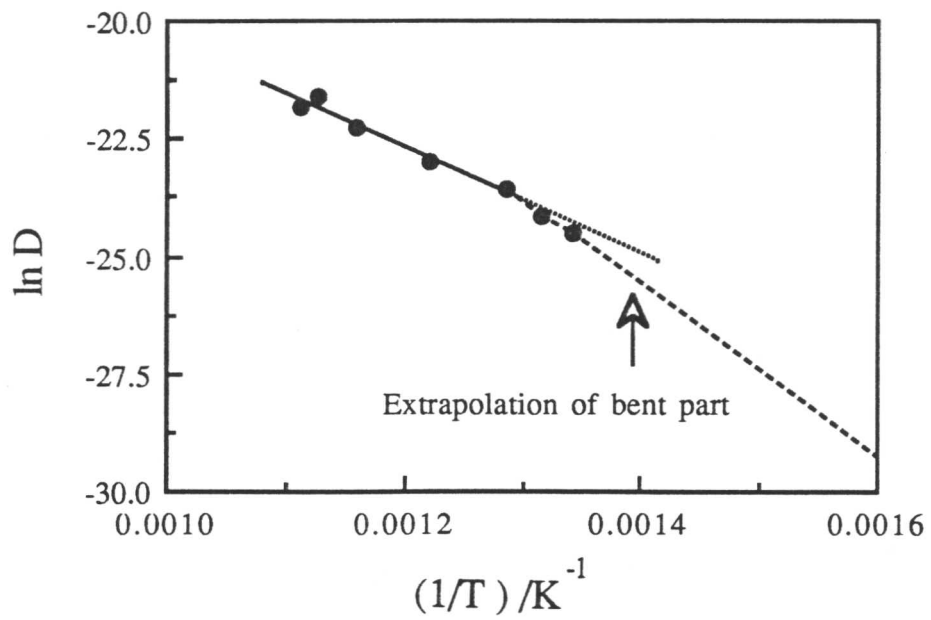
Figure 6.2: Graph of diffusion coefficient $D_{Cd}^{\beta_2}$ versus tempeature in β_2 Ag–Cd with the extrapolation of the bent part of curve (Lexcellent *et al.*, 1989).
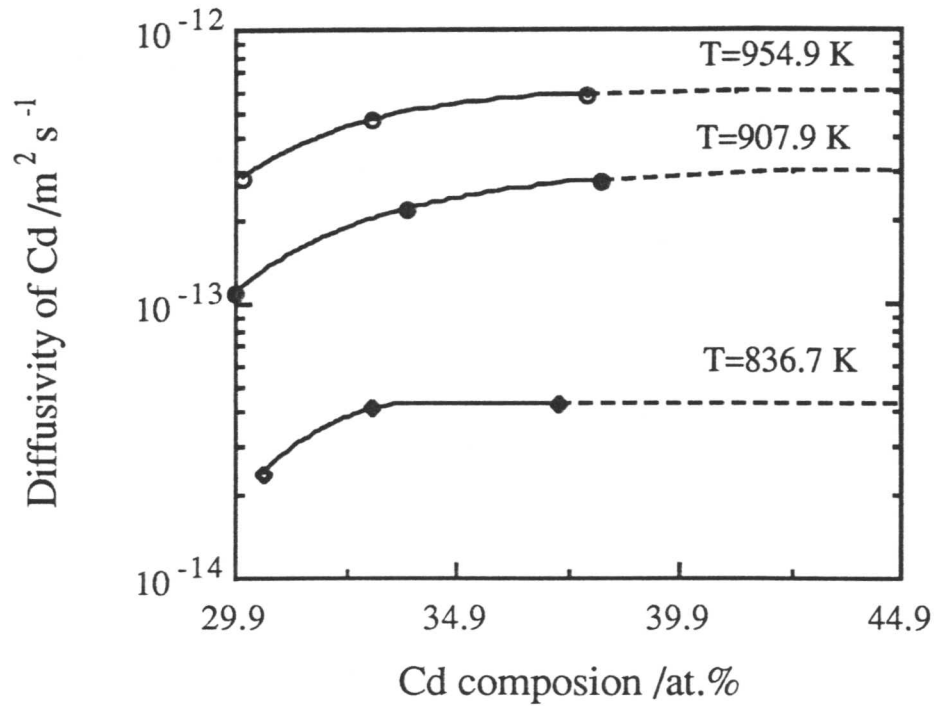
Figure 6.3a: Graph of composition versus diffusivity at three different temperatures for Ag–Cd alloy.
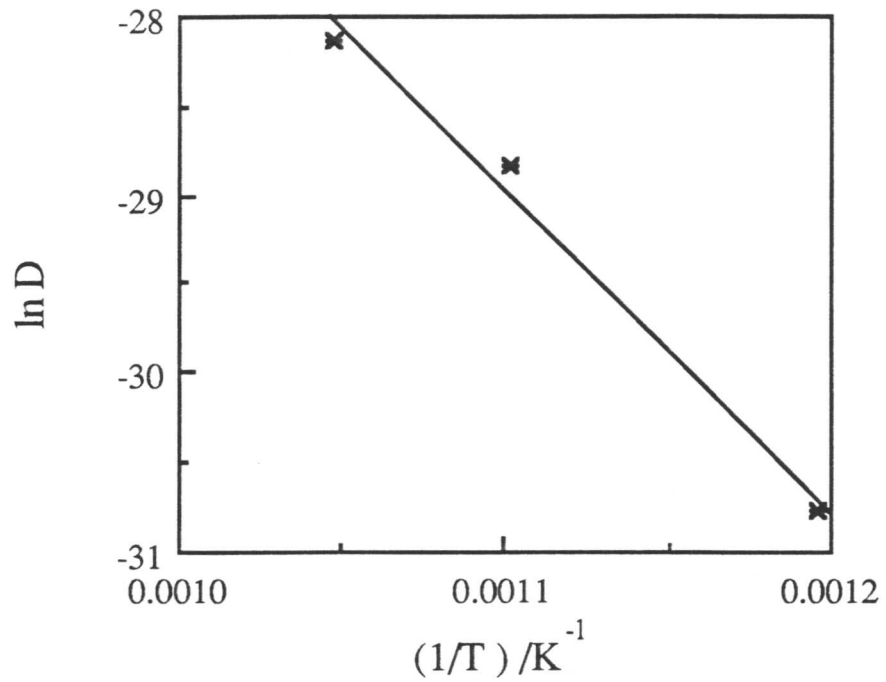
Figure 6.3b: Graph of reciprocal of temperature (1/T) versus ln (diffusivity) at 44.9 at.% of Cd (estimated value from figure 6.3a). Straight line has been obtained by curve fitting.
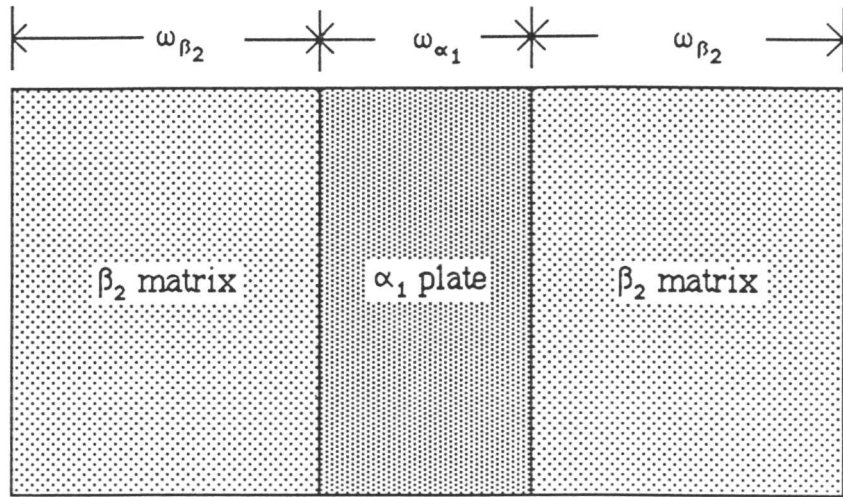
Figure 6.4: Schematic illustration of the plate/matrix diffusion couple.
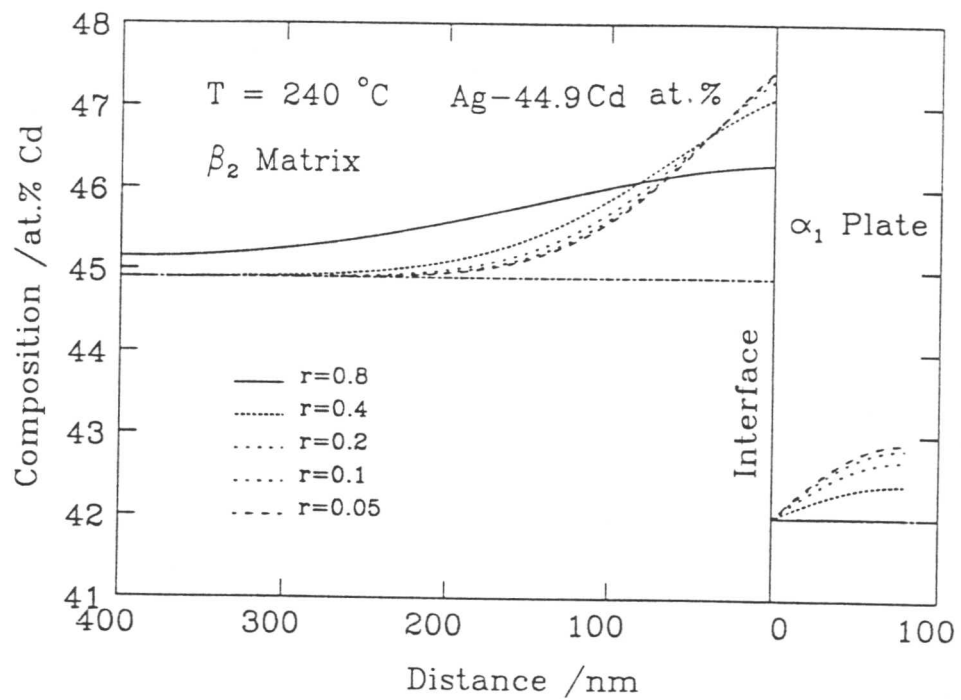
Figure 6.5: Calculated concentration profile for a freshly formed α_1 plate of 160 nm width at the ageing time of 30 s for different values of grid parameter.
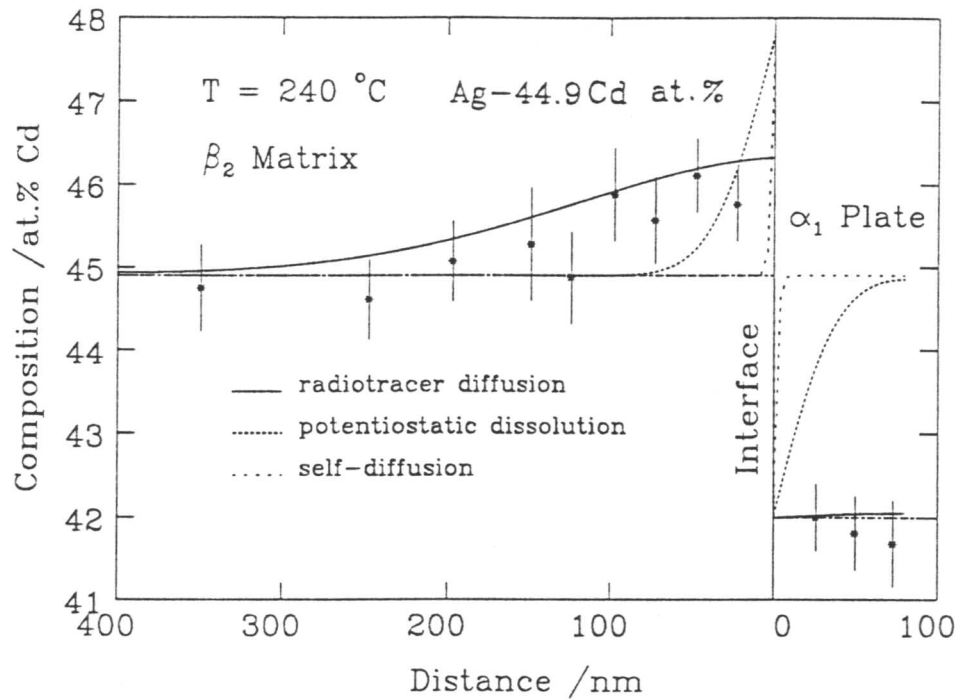
Figure 6.6: Comparison between calculated and measured profile normal to the α_1/β_2 interface for a freshly formed α_1 plate of 160 nm projected width for the specimen aged for 30 s at 240 °C . Measured composition data were taken from Wu *et al.* 1988.
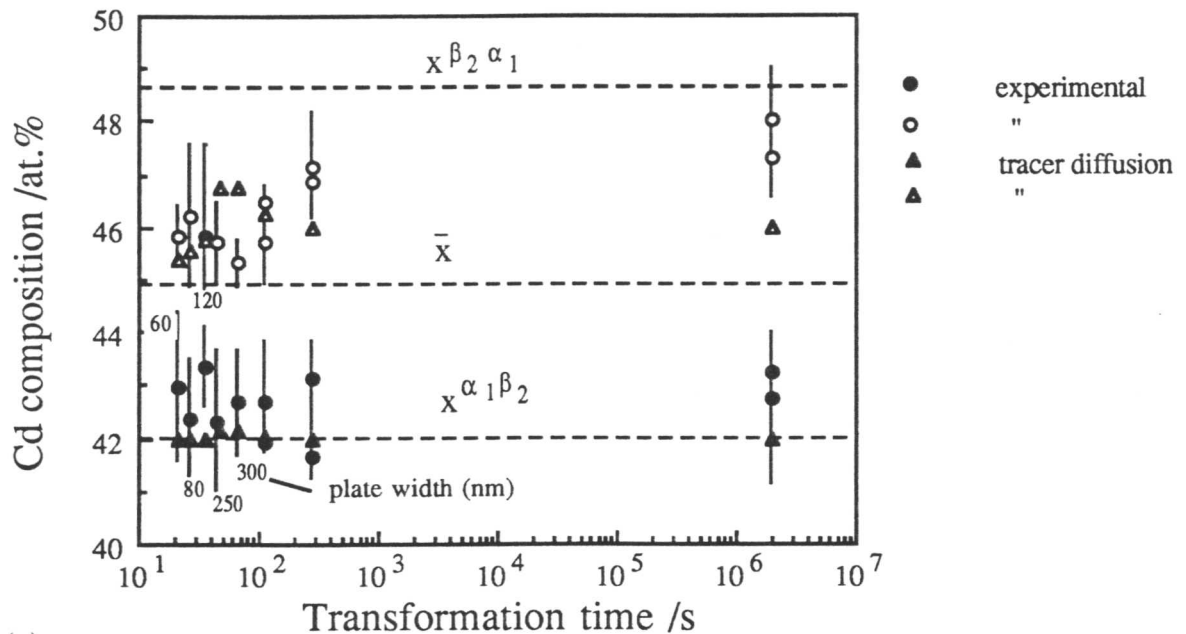
(a)

Figure 6.7: Comparison of calculated (solid points) with measured (empty points) composition for different ageing times for various size of plates. Triangular and circular points represent matrix and plate respectively. Diffusion data are taken from tracer diffusion.
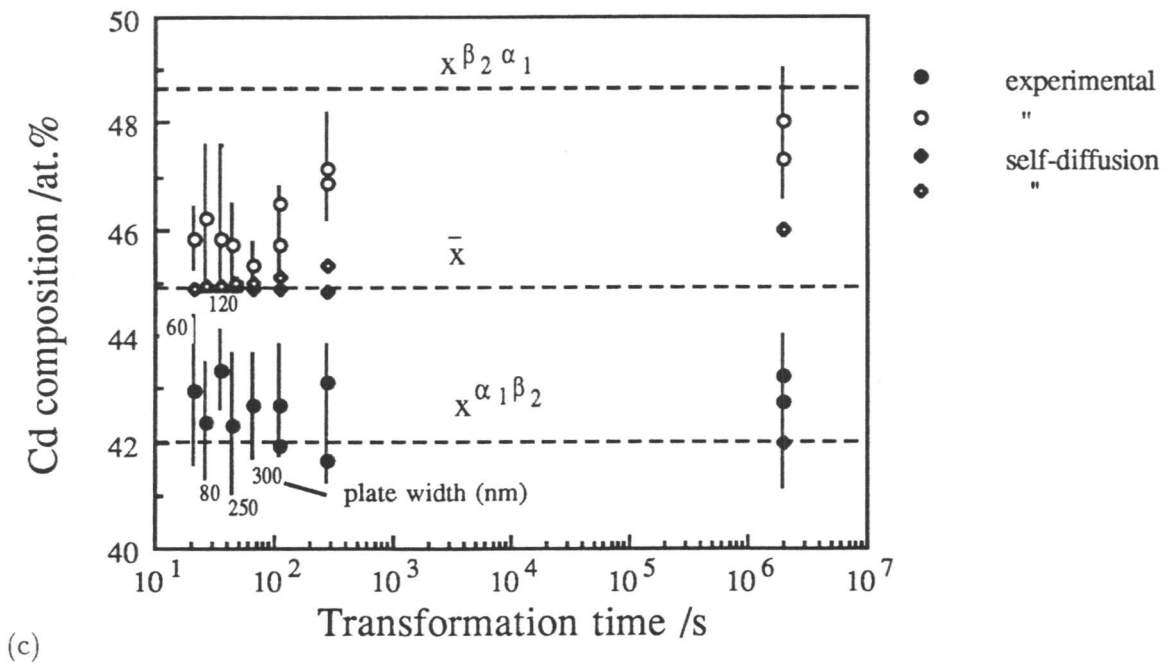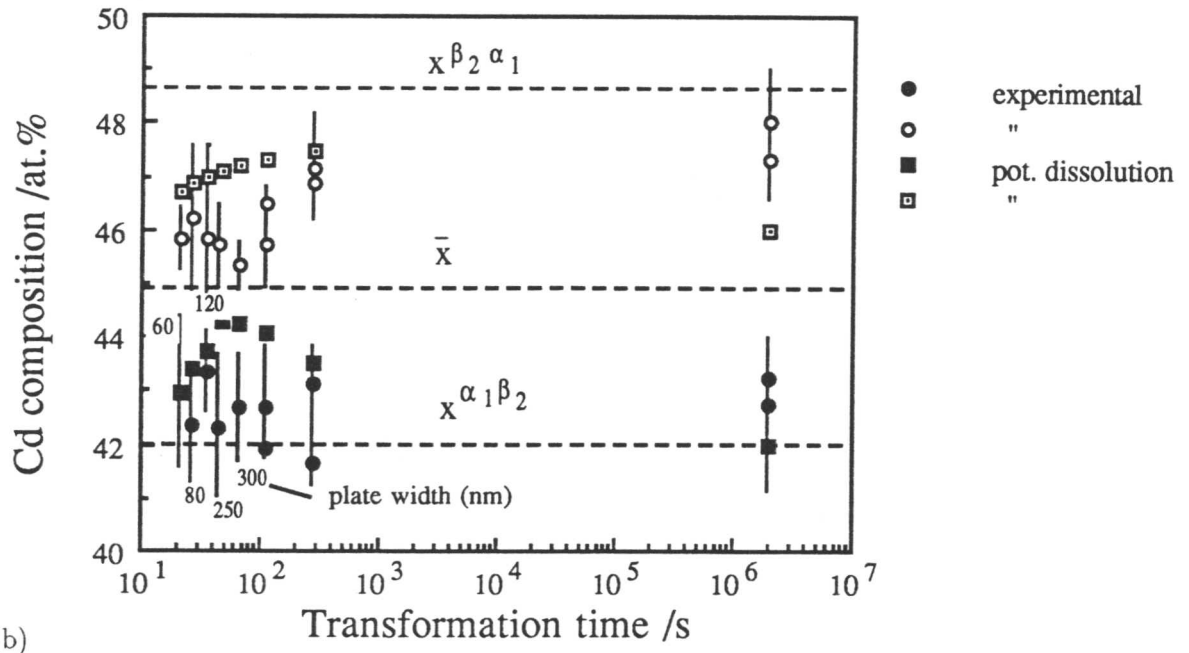
(b)

(c)

Figure 6.7: Comparison of calculated (solid points) with measured (empty points) composition for different ageing times for various size of plates. Triangular and circular points represent matrix and plate respectively. Diffusion data are taken from (b) potentiostatic dissolution (c) self–diffusion.

86
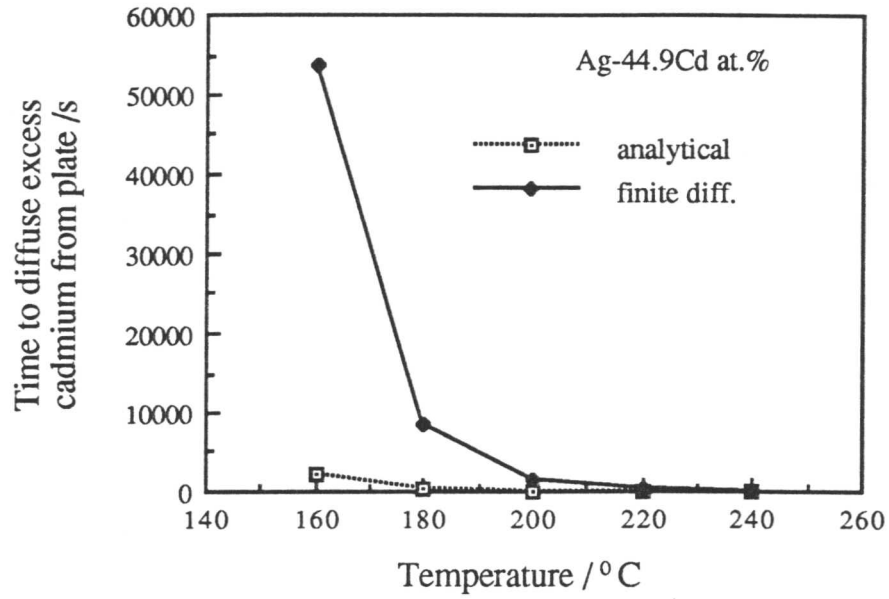
Figure 6.8: Time taken to diffuse excess cadmium as a function of temperature. The dashed curve represent calculations carried out using approximate analytical solution, whereas the continuous curves were calculated using finite difference method.
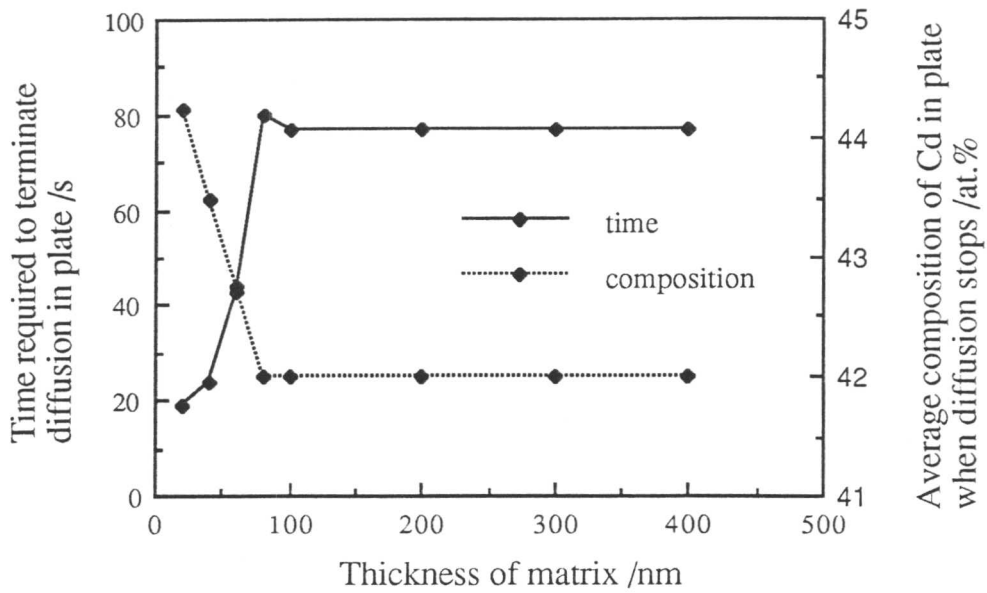
Figure 6.9: Plot of the time required to terminate the diffusion process within the α_1–plate, versus the thickness of the adjacent austenite slab. Note that there are two such slabs of β_2 matrix per α_1–plate, one on each side of the α_1–plate. The discontinuous curve represents the cadmium concentration in the α_1–plate at the point where diffusion stops.

87

Chapter 7

Suggestions for Future Work

A mathematical model for coupled diffusional and displacive transformations has been applied to a series of alloys to examine the growth of partially carbon supersaturated ferrite plates. This is the only method capable of predicting the transformation temperatures without making any assumptions about the magnitude of the driving force necessary to induce martensitic transformation. All the parameters used in implementing the interface response functions were obtained from independent data. This model is informative in the sense that it directly reveals the growth velocities and compositions of the phases at the transformation interface. All of the previous methods have been based on the empirical regression analysis and the assumption of a constant value of driving force at M_s. On the basis of the calculations for low alloy steels, the following specific conclusions can be reached:

(a) It is in principle possible to envisage displacive growth involving a partial supersaturation of interstitial carbon.

(b) The level of supersaturation increases steadily as the transformation temperature is decreased. It is therefore possible to imagine the growth of ferrite plates with an equilibrium carbon concentration at high temperatures, and diffusionless martensitic transformation at low temperatures.

(c) Because during nucleation the surface to volume ratio of the nucleus is rather large, extra free energy is required to account for the corresponding surface energy. Thus, the level of carbon supersaturation that can be sustained in the nucleus tends in general to be less than during growth at the same temperature.

The variation in the B_s temperature as a function of carbon concentration can be satisfactorily estimated if it is assumed that:

(1) the bainite–start temperature can be identified with the highest temperature at which diffusionless growth becomes possible, and

(2) the stored energy of the growing ferrite varies with temperature.

However, the absolute values of calculated B_s temperatures show relatively poor agreement

with published experimental data. For a number of alloyed steels, good agreement is found between calculated and experimental M_s data. For these alloys, the B_s temperatures reveal clear discrepancies, the reasons for which are not understood. The calculations consistently underestimate the eperimental data. The trend in B_s temperatures nevertheless appears to be roughly predicted. On the basis of all these results it can be concluded the model appears to be physically reasonable.

On the basis of the work done to date, it would be fruitful to examine the following phenomena:

(i) The current models fail to take full account of the effect of substitutional solutes on influancing interfacial motion via a solid solution strengthening effect, it is unlikely to be reasonable at larger solute concentrations. The interface consists of dislocations and hence its mobility must depend to some extent on solid solution effects.

(ii) It would be worthwhile measuring the predicted variation in stored energy as a function of transformation temperature, possibly with the help of differential scanning calorimetery.

(iii) The model can in principle be coupled to deal with the transition between local equilibrium growth and paraequilibrium growth in substitutionally alloyed steels. The interface response functions would of course be different and account would have to be taken of the time dependence of interfacial velocities.

(iv) The work needs to be extended to nonferrous systems where substitutional atoms may or may not diffuse during transformation, to establish the character of so–called "nonferrous bainites". However, any theoretical study must be complimented by a parallel study of basic parameters such as diffusion coefficients in such alloys. There is a derth of such data.

References

Aaronson, H. I., Domian, H. A. and Pound G. M. (1966)

Thermodynamics of austenite $\rightarrow$ proeutectoid ferrite transformation II, F–C–X alloys, *TMS-AIME,* **236,** 768–780.

Aaronson, H. I., Hall, M. G., Barnett, D. M. and Kinsman, K. R. (1975)

The Watson–McDougall Shear: Proof that Widmanstätten ferrite cannot grow martensitically, *Scripta Metallurgica,* **9,** 705–712.

Agren, J. (1989)

A simplified treatment of the transition from diffusion controlled to diffusionless growth, *Acta Metallurgica,* **37,** 181–189.

Ali, A. and Bhadeshia, H. K. D. H. (1989)

Growth rate data on bainite in alloys, *Materials Science and Technology,* **5,** 398–402.

Ayers, J. D. and Massalski, T. B. (1972)

Influence of completing reactions on the extent of β–to–α massive transformation in Ag–Cd, Ag–Zn, and Cu–Zn alloys, *Metallurgical Transactions,* **3,** 261–271.

Aziz, M. J. (1982)

Model for solute redistribution during rapid solidification, *Journal of Applied Physics,* **53,** 1158–1168.

Aziz, M. J. (1983)

Dissipation–theory treatment of the transition from diffusion–controlled to diffusionless solidification, *Applied Physics Letters,* **43,** 552–554.

Baker, J. C. and Cahn, J. W. (1969)

Solute trapping by rapid solidification, *Acta Metallurgica,* **17,** 575–578.

Baker, J. C. and Cahn, J. W. (1971)

Thermodynamics of solidification, *Solidification,* **23,** pp. 23–58, ASM Metals Park, Ohio.

Bhadeshia, H. K. D. H. (1981a)

A rationalisation of shear transformations in steels, *Acta Metallurgica,* **29,** 1117–1130.

Bhadeshia, H. K. D. H. (1981b)

Driving force for martensitic transformation in steels, *Metal Science,* **15,** 175–177.

Bhadeshia, H. K. D. H. (1981c)

Thermodynamic extrapolation and martensite–start temperature of substitutionally alloyed

steels, *Metal Science,* **15,** 178–180.

Bhadeshia, H. K. D. H. (1981d)

Diffusion of carbon in austenite, *Metal Science,* **15,** 477–479.

Bhadeshia, H. K. D. H. (1982)

Application of first–order quasichemical theory to transformations in steels, *Metal Science,* **16,** 167–169.

Bhadeshia, H. K. D. H. (1984)

Solute–drag, kinetics and the mechanism of the bainite reaction in steels, Proc. International Conference on *Phase Transformations in Ferrous Alloys,* eds. A. R. Marder and J. R. Goldstein, TMS–AIME, pp. 335–340, Cleveland, Ohio, USA.

Bhadeshia, H. K. D. H. (1985a)

Diffusion–controlled growth of ferrite plates in plain–carbon steels, *Materials Science and Technology,* **1,** 497–504.

Bhadeshia, H. K. D. H. (1985b)

Diffusional formation of ferrite in iron and its alloys, *Progress in Materials Science,* **29,** 321–386.

Bhadeshia, H. K. D. H. (1988)

Bainite in steels, *Proceedings of an International Conference: Phase Transformations '87,* ed. Lorimer, G. W., pp. 309–314, Institute of Metals, London.

Bhadeshia, H. K. D. H. (1989)

Theoretical analysis of changes in cementite composition during tempering of bainite, *Materials Science and Technology,* **5,** 131–137.

Bhadeshia, H. K. D. H. and Christian, J. W. (1990)

Bainite in steels, *Metallurgical Transactions A,* **21A,** 767–797.

Bhadeshia, H. K. D. H. and Edmonds, D. V. (1980)

The mechanism of bainite formation in steels, *Acta Metallurgica,* **28,** 1265–1273.

Bhadeshia, H. K. D. H. and Waugh, A. R. (1981), *Proc. Int. Conf. on Solid $\rightarrow$ Solid Phase Transformations,* pp. 993–998, Pittsburgh, PA, ASM, Metals Park, OH.

Bhadeshia, H. K. D. H. and Waugh, A. R. (1982)

Bainite: An atom–probe study of the incomplete reaction phenomenon, *Acta Metallurgica,* **30,** 775–784.

Binary Alloy Phase Diagrams (1990)

Materials Information Society.

Burger, M. J. (1951)

Phase Transformations in Solids, p. 183, Wiley, New York.

Cahn, R. W. and Haasen, P. (1983)

Physical metallurgy, North–Holland Physics Publishing Company, Amsterdam, Oxford, New York, Tokyo.

Christian, J. W. (1965a)

Physical properties of martensite and bainite, Iron and Steel Institute Spec. Rep. **93**, 1.

Christian, J. W. (1965b)

The Theory of Transformations in Metals and Alloys, Pergamon Press, Oxford.

Christian, J. W. (1975)

Theory of transformations in Metals and Alloys, **II**, 2nd edn., Pergamon press, Oxford.

Christian, J. W. (1979)

Thermodynamics of martensite transformations, Proc. International Conference on Martensitic Transformations, ICOMAT '79, pp. 220–234, Massachusetts Institute of Technology, Cambridge, Massachusetts, USA.

Christian, J. W. (1981)

The theory of transformations in metals and alloys, Pergamon Press Ltd., Oxford.

Christian, J. W. and Edmonds, D. V. (1984)

The bainite transformation, Proc. International Conference on *Phase Transformations in Ferrous Alloys*, eds. Marder, A. R. and Goldstein, J. R., TMS–AIME, pp. 293–326, Cleveland, Ohio, USA.

Cornelis, I. and Wayman, C. M. (1973)

Composition changes during the isothermal transformation of β' CuZn, *Scripta Metallurgica,* **7,** 579–590.

Cornelis, I. and Wayman, C. M. (1974)

Phase transformations in metastable β' CuZn alloys–II: Isothermal transformations, *Acta Metallurgica,* **22,** 301–311.

Crank, J. (1975)

The Mathematics of Diffusion, 2nd edition, Clarendon Press, Oxford.

Diffusion Data (1969)

Diffusion Information Center, Cleveland, Ohio, USA.

Diffusion and Defect Data – Solid State Data (1986)

Trans. Tech. Publications, ed. Wohlbier, F. H., **46,** pp. 93–94, Swizerland–Germany–UK–USA.

Flewitt, P. E. J. and Towner, J. M. (1967)

The decomposition of beta prime in copper–zinic alloys, *Journal of the Institute of Metals,* **95,** 273–280.

Frank, F. C. (1950)

Radially symmetric phase growth controlled by diffusion, *Proceedings of the Royal Society,* **A201,** 586–599.

Frank, F. C. (1953)

Martensite, *Acta Metallurgica,* **1,** 15–21.

Frank, F. C. (1963)

Relation between Structure and Strength in Metals & Alloys, 248, HMSO, London.

Gardner, A. B., Sanders, R. L. and Slifkin, L. M. (1968)

Self–diffusion in alpha Ag–Cd (In English), *Phy. Stat. Sol.,* **30,** 96–106.

Garwood, R. D. (1954–55)

The bainitic transformation of beta phase in copper–zinic alloys, *Journal of the Institute of Metals,* **83,** 64–68.

Garwood, R. D. and Hull, D. (1958)

The orientation relationship of the low temperature martensite transformation in metastable β–brass, *Acta Metallurgica,* **6,** 98–102.

Grujicic, M., Olson, G. B. and Owen, W. S. (1985a)

Mobility of martensitic interfaces, *Metallurgical Transaction A,* **16A,** 1713–1722.

Grujicic, M., Olson, G. B. and Owen, W. S. (1985b)

Mobility of the β_1–γ_1' martensitic interface in Cu–Al–Ni: Part I. Experimental measurements, *Metallurgical Transaction A,* **16A,** 1723–1734.

Grujicic, M., Olson, G. B. and Owen, W. S. (1985c)

Mobility of the β_1–γ_1' martensitic interface in Cu–Al–Ni: Part II. Experimental measurements, *Metallurgical Transaction A,* **16A,** 1735–1744.

Hansen, M. (1958)

Constitution of Binary Alloys, pp. 13–14, McGraw–Hill Book Company, Inc. New York.

93

Hehemann, R. F. (1970)

The bainite transformation, *Phase Transformations*, ASM, 397–432.

Hillert, M. (1951)

The use of isoactivity lines in ternary phase diagrams, *Jernkontorets Annaler*, **136**, 25–37.

Hillert, M (1960)

The Growth of Ferrite, Bainite and Martensite, *Internal Report*, Swedish Institute of Metals Research, Stockholm, Sweden.

Hornbogen, E. and Warlimont, H. (1967)

Die bainitische umwandlung des β–messings, *Acta Metallurgica*, **15**, 943–951.

Hultgren, A. (1951)

Jernkontorets Ann., **135**, 403.

Ivantsov, G. P. (1947)

Dokl. Akad. Nauk. SSSR, **58**, 567–569.

Josefsson, B. and Andren, H. O. (1988)

Microstructure of granular bainite, *Proceedings of the 35th International Field Emission Symposium*, Oak Ridge, TN, Journal de Physique.

Kaufman, L and Cohen, M. (1956)

Martensite transformation in the iron–nickel system, *J. Metals*, , 1393–1401.

Kaufman, L and Cohen, M. (1958)

Thermodynamics and kinetics of martensitic transformations, *Progress in Metal Phys.*, **7**, 165–246.

Kaufman, L., Clougherty, E. V. and Weiss, R. J. (1963)

The lattice stability of metals – III Iron, *Acta Metallurgica*, **11**, 323–335.

Kinsman K. E. and Aronson, H. I. (1967)

Discussion to Oblak and Hehemann, *Transformation and Hardenability in Steels*, Climax Molybdenum, pp. 33–38, Ann Arbor, Michigan, USA.

Kocks, U. F., Argon, A. S. and Ashby, M. F. (1975)

Progress in Materials Science, 19, 1.

Kostic, M. M., Hawbolt (1979)

Morphology and structure of bainite plates in the β' phase of an Ag–45 At. Pct Cd alloy, *Metallurgical Transactions A*, **10A**, 165–176.

Kostic, M. M., Hawbolt, E. B. and Brown, L. C. (1976)

Growth kinetics of bainite plates and Widmanstätten needles in the β' phase of a Ag–45

At. Pct Cd alloy, *Metallurgical Transactions A,* **7A,** 1643–53.

Lexcellent, Ch., Benlemlih, Moya, G. and Bernardini (1989)

Creep and bulk diffusion in equiatomic beta Ag–Zn and beta Ag–Cd, *Defect and Diffusion Forum,* **66–69,** 1365–1370.

Lorimer, G. W. Cliff, G., Aaronson, H. I. and Kinsman, K. R. (1975)

Analysis of the composition of α_1 plates precipitated from β' Cu–Zn using analytical electron microscopy, *Scripta Metallurgica,* **9,** 271–279.

McLellan, R. B., Rudee, M. L. and Ishibachi, T. (1965)

The thermodynamics of dilute interstitial solid solutions with dual site occupancy and its application to the diffusion of carbon in alpha iron, *TMS–AIME,* **233,** 1938–1943.

Massalski, T. B., Perkin, A. J. and Jaklovsky, J. (1972)

Extension of solid solubility during massive transformations, *Metallurgical Transactions,* **3,** 687–694.

Masson, D. B. and Barrett, C. S. (1958)

Effect of deformation and low temperatures on the structures of AgCd and AuZn, *Transactions of the American Institute of Mining and Petroleum Engineers – AIME,* **212,** 260–265.

Matas, S. J. and Hehemann, R. F. (1961)

The structure of bainite in hypoeutectoid steels, *Trans. TMS–AIME,* **221,** 179–185.

Mujahid, S. A. and Bhadeshia, H. K. D. H. (1992)

Partitioning of carbon from supersaturated ferrite plares, *Acta Metallurgica,* **40,** 389–396.

Nabarro, F. R. N. (1982)

Stress equivalence in the theory of solution hardening, *Proceedings of the Royal Society,* **A381,** 285–292.

Olson, G. B. (1981)

Fine structure of interphase boundaries, *Acta Metallurgica,* **29,** 1475–1484.

Olson, G. B. (1989)

Unpublished research, Northwestern University, Chicago.

Olson, G. B., Bhadeshia, H. K. D. H. and Cohen, M. (1989)

Coupled diffusional/displacive transformations, *Acta Metallurgica,* **37,** 381–390.

Olson, G. B, Bhadeshia, H. K. D. H. and Cohen, M. (1990)

Coupled diffusional/displacive transformations: Part II. Solute trapping *Metallurgical Transactions A,* **21A,** 805–809.

Olson, G. B. and Cohen M. (1976)

A general mechanism for martensitic nucleation: Part III. Kinetics of martensitic nucleation, *Metallurgical Transactions A*, **7A**, 1915–1923.

Olson, G. B. and Cohen, M. (1982)

Dislocation structure of martensitic interfaces, Proc. International Conference on *Solid-State Phase Transformations*, Carnegie–Mellon Univ., AIME, 1209–1213.

Olson, G. B. and Cohen, M. (1986)

Dislocation theory of martensitic transformations, *"Dislocations in Solids" Chapter 37*, (edited by Nabarro, F. R. N.), **7**, pp. 297–408, Elsevier Science Publishers, B.V.

Pchelnikov, A. P., Marshakov, A. I. and Losev, V. V. (1985)

Elektrokhimiya, 21[7], 949–953 [Soviet Electrochemistry, 1985, 21[7], 891–894]).

Rudberg, E. (1952)

Jernkontorets Ann., **136**, 91.

Sarikaya, M., Steinberg, B. G. and Thomas, G. (1982)

Optimisation of Fe/Cr/C base structural steels for improved strength and toughness, *Metallurgical Transactions A*, **13A**, 2227–2237.

Schrader, A. and Wever, F. (1952)

Zur Frage der Eignung des Elektronenmikroskops fur die Gefugeuntersuchung von Stahlen, *Arch. Eisenhüttenwes*, **23**, 489–495.

Siller, R. H. and Mclellan, R. B. (1970)

The application of first order mixing statistics to the variation of the diffusivity of carbon in austenite, *Metallurgical Transactions*, **1**, 985–988.

Smith, R. P. (1953)

The diffusivity of carbon in iron by the steady state method, *Acta Metallurgica*, **1**, 578–587.

Srinivasan, G. R. and Hepworth, M. T. (1971)

The crystallography of the bainite transformation in beta brass, *Acta Metallurgica*, **19**, 1121–1131.

Stark, I. Smith, G. D. W. and Bhadeshia, H. K. D. H. (1988)

The element distribution associated with the incomplete reaction phenomenon in bainitic steels: an atom probe investigation, *Phase Transformations '87*, Lorimer, G . W. ed., pp. 211–215, Institute of Metals, London.

Stark, I., Smith, G. D. W. and Bhadeshia, H. K. D. H. (1990)

The distribution of substitutional alloying elements during the bainite transformation, *Met-*

allurgical Transactions A, **21A,** 837–844.

Steven, W, and Haynes, A. G. (1956)

The temperature of formation of martensite and bainite in low alloy steels, *Journal of the Iron and Steel Institute,* **183,** 449–359.

Takahashi, M. and Bhadeshia, H. K. D. H. (1990)

Model for transition from upper to lower bainite, *Materials Science and Technology,* **6,** 592–603.

Trivedi, R. (1970a)

Growth of dendritic needles from a supercooled melt, *Acta Metallurgica,* **18,** 287–296.

Trivedi, R. (1970b)

The role of interfacial free energy and interface kinetics during the growth of precipitate plates and needles, *Metallurgical Transactions,* **1,** 921–927.

Trivedi, R. and Pound, G. M. (1967)

Effect of concentration dependent diffusion coefficient on the migration of interphase boundaries, *Journal of Applied Physics,* **38,** 3569–3576.

Wells, C., Batz, W. and Mehl, R. F. (1950)

Diffusion coefficient in austenite, *Trans. of the American Institute of Mining and Metallurgical Engineers – AIME,* **188,** 553–560.

Wu, M. H., muddle, B. C. and Wayman, C. M. (1988)

Analytical electron microscopy studies of the $\beta \to \alpha$ ("bainite") transformation in an Ag–45 at.% Cd alloy, *Acta Metallurgica,* **36,** 2095–2106.

Zener, C. (1949)

Theory of growth of spherical precipitation from solid solution, *Journal of Applied Physics,* **20,** 950–953.

Appendix I

Computer Program for CDDT Model

```
C FTVSCLR PROGRAM =.PP DATA =.DD OUTPUT =.OUT PLOT =.GRAPH NAG CAMPLOT
C
C PROGRAM FOR THE ANALYSIS OF GROWTH INVOLVING PARTIAL SUPERSATURATION
C FOR ALLOY STEELS, ON THE BASIS OF LFG THERMODYNAMICS.
C
C TYPICAL INPUT DATASET
C     400                    10
C Temperature in deg C     Increment
C 0.4      0      0      0      0      0      0
C  C      Si     Mn     Ni     Mo     Cr     V
C
        COMMON XI(50,50,16),GID(50,50,16),FE(50,50,16),
       &VR(50,50,16),CTEMP,MUM,XAL(50,50,16),XALP(12,16),FN1(12,16),
       &FN2(12,16),PT1(12,16),PT2(12,16),PTF1(12,16),PTF2(12,16),
       &ANS1(50,50,16),ANS11(100),VKR1(12,16),VKR2(12,16),
       &XI11(12,16),XI22(12,16),XBAR
        COMMON /ONE/ G(10)
        COMMON /TWO/ TDSE
        COMMON /THREE/ CC(8),T10,T20
        COMMON /FOUR/ W
        DIMENSION XMAX2(100),GDD(50,50,16),
       &XALPHA1(50,50,16),XMAX1(50,50,16),C(10),
       &ERROR1(50,50,16),PECLET1(50,50,16),MOLVOL1(50,50,16),
       &RADIUS1(50,50,16),CAPCON1(50,50,16),EPSI1(50,50,16),
       &OMEGA1(50,50,16),VMAX1(50,50,16),XMAXR1(50,50,16)
        INTEGER T1,DUMMY,DUMMY3,ST,
       &C96,Z,II,II2,II3,II22,I2,I3,I4,I5,CCK3FN
        DOUBLE PRECISION XM,W1,T,T7,H1,S1,R,F,Q3,
       &XAS,XGS,FEA2,FEG2,CA2,CG2,G2,DG2,DFEG2,DCG2,T4,STRAIN,
       &J1,FEA1,FEG1,CA1,CG1,G1,DG1,DFEA1,DCA1,FEA3,CA3,G3,G4,
       &ACTIV,THETA,X,DACTIV,PSI,SIGMA,D1,M1,A5,D,YMAX,YMIN
       &,M2,DASH,HH,KK,DUMMY1,DUMMY2,XALPHA,ANS,XMAX,DIFF(1000)
       &,RADIUS,VMAX,XMAXR,ERROR,CARB(1000),SIG,OMEG,XINTER
        WRITE(6,901)
901     FORMAT(/' XAS = Xalp = TOTAL AMOUNT OF CARBON IN FERRITE'/
       &' XAG  = Xi  = COMPATIBLE CARBON CONTENT IN THE AUSTENITE'/
       &'               AT THE TRANSFORMATION INTERFACE'/
       &' G3  = Gdd = JOULES/MOL. FREE ENERGY CHANGE ACCOMPANYING THE'/
       &'               MOVEMENT OF THE INTERFACE WHEN THE INT.'/
       &'               COMPOSITIONS ARE GIVEN BY Xalp,Xi'/
       &'        CTEMP = TEMPERATURE IN DEGREES CENTIGRADE')
        WRITE(6,902)
902     FORMAT('**************************************************')
```

```
      READ (5,*) CTEMP,TINC
      READ (5,*) CC(1),CC(2),CC(3),CC(4),CC(5),CC(6),CC(7)
      CALL OMEGA(W,XBAR)
1006  FORMAT(' CARBON-CARBON INTERACTION ENERGY IN GAMMA, J/MOL=',F7.0,
     &5X,'CARBON CONTENT=',F10.5,5X,'T10=',F10.6,5X,'T20=',F10.6)
      XINTER=(XBAR-0.0001D0)/20.0D0
C
      DO 114 L=1,1
      CTEMP = CTEMP + TINC
C
C TDSE = TEMPERATURE DEPENDENT STORED ENERGY
C STRAIN = STORED ENERGY OF FERRITE, J/mol
C
      I=0
      TDSE= 10404303.9978638154D0+(-106411.999671455444D0*CTEMP)+
     *(452.296738118523649D0*(CTEMP**2))+
     &(-1.02257891654823418D0*(CTEMP**3))
     &+(0.129694991884510345D-02*(CTEMP**4))+
     &(-0.874920033684982458D-06*(CTEMP**5))+
     &(0.245252701547428680D-09*(CTEMP**6))
      IF(CTEMP.LT.465.8) TDSE=700.0
      IF(CTEMP.GT.500.0) TDSE=325.0
      IJ=TDSE
      IK=IJ+950
      DO 6000 ST=IJ,IK,25
      STRAIN=ST
      I=I+1
      IF(ST.EQ.IK)N=I
      R=8.31432
      W1=48570.0
      T4=CTEMP
      T=T4+273
      IF (T .LE. 1000) GOTO 20
      H1=105525
      S1=45.34521
      GOTO 19
20    H1=111918
      S1=51.44
19    T7=T-100*T20
      IF (T7 .LT. 300) GOTO 1
      IF (T7 .LT. 700) GOTO 2
      IF (T7 .LT. 940) GOTO 3
      F=-8.88909+0.26557*(T7-1140)-1.04923D-3*((T7-1140)**2)
      F=F+2.70013D-6*((T7-1140)**3)-3.58434D-9*((T7-1140)**4)
      GOTO 4
1     F=1.38*T7-1499
      GOTO 4
2     F=1.65786*T7-1581
      GOTO 4
3     F=1.30089*T7-1331
4     Q3=141*T10
      F=F+Q3
      F=F*4.187+STRAIN
```

```
        XM=0.25*XBAR
        FEG1=FEG(XBAR,T,W,R)
        CG1=CG(XBAR,T,W,R)
31      FEA1=FEA(XM)
        CA1=CA(XM,T,W1,H1,S1,R)
        G1=(1-XM)*(F+R*T*(FEA1-FEG1))+XM*R*T*(CA1-CG1)
        IF (DABS(G1) .GE. 2.0) GOTO 32
        GOTO 33
32      DFEA1=DFEA(XM)
        DCA1=DCA(XM,T,W1,R)
        DG1=-F-(R*T*(-FEG1+FEA1))+(1-XM)*(R*T*DFEA1)+XM*R*T*(
        1DCA1)+R*T*(CA1-CG1)
        XM=XM-G1/DG1
        IF (XM .LE. 0.0) GOTO 6000
        GOTO 31
33      XMAX2(I)=XM
        J=0
40      DO 41 DUMMY=1,20
        J=J+1
        XAS=DUMMY*XINTER
        XGS=2*XAS
        FEA2=FEA(XAS)
        CA2=CA(XAS,T,W1,H1,S1,R)
38      FEG2=FEG(XGS,T,W,R)
        CG2=CG(XGS,T,W,R)
        G2=(1-XAS)*(F+R*T*(FEA2-FEG2))+XAS*R*T*(CA2-CG2)
        IF (DABS(G2) .GE. 2.0) GOTO 36
        GOTO 37
36      DFEG2=DFEG(XGS,T,W,R)
        DCG2=DCG(XGS,T,W,R)
        DG2=(1-XAS)*R*T*(-DFEG2)+XAS*R*T*(-DCG2)
        XGS=XGS-G2/DG2
        IF (XGS .LE. 0.0.OR.XGS.GE.0.5) GOTO 41
        GOTO 38
37      FEA3=FEA(XAS)
        CA3=CA(XAS,T,W1,H1,S1,R)
        G3=(1-XAS)*(F+R*T*(FEA3-FEG1))+XAS*R*T*(CA3-CG1)
        XAL(I,J,L)=XAS
        XI(I,J,L)=XGS
        GDD(I,J,L)=G3
41      CONTINUE
6000    CONTINUE
        M=20
        DO 5 J=1,M
        WRITE(6,42) XBAR
42      FORMAT (/' Xbar = ALLOY CARBON CONTENT=',F8.4,'  mole fraction')
        WRITE(6,34)XMAX2(J),T
34      FORMAT (/' Xm = MAX. PERMITTED CARBON CONTENT IN FERRITE=' ,F8.4,
        &2X,'mole fraction'/
        &/' DEGREES KELVIN=',F5.0)
        WRITE(6,8)XAL(1,J,L)
        WRITE(6,6)
8       FORMAT(/' Xalph = ',F10.4,2X,'mole fraction'/)
```

100

```
       DO 5 I=1,N
       GID(I,J,L)=GDD(I,J,L)-GDD(1,J,L)
5      IF(XI(I,J,L).NE.0) WRITE(6,*)XI(I,J,L),GDD(I,J,L),GID(I,J,L)
6      FORMAT (/'       Xi             Gdd             Gid'/
      &'  (mole fraction)   (J/mol/m**3)   (J/mol/m**3)'/)
17     FORMAT (F10.4,9X,F10.4,1X,F12.4,F10.4)
C
C ** IVANTSOV ANALYSIS OF PLATE GROWTH CALCULATION FROM MASTER CURVE **
C
C CAPCON = Capillarity constant (normally capital gamma)
C XMAXR  = Equilibrium conc at plate tip of radius R, in gamma
C HH     = Plancks const. Joules/sec
C KK     = Boltzmanns const. Joules/degree kelvin
C D      = Diffudsibvity of carbon in austenite
C Z      = Coordination of interstial site
C PSI    = Composition dependence of diffusion coefficient
C THETA  = No. C atoms/ No. Fe atoms
C Activ  = Activity of carbon in austenite
C R      = Gas constant
C X      = Mole Fraction of carbon
C T      = Absolute temperature
C SIGMA  = Site exclusion probability
C W      = Carbon Carbon Interaction Energy in austenite
C
       HH=6.6262D-34
       KK=1.38062D-23
       T=CTEMP+273.0D+00
       CALL OMEGA(W,XBAR)
       Z=12
       A5=1.0D+00
       R=8.31432D+00
       RADIUS=0.0
       VMAX=0.0
       M1=0.00
       DO 12 J=1,20
       DO 1008 II22=1,N
       WRITE(6,1009)
1009   FORMAT('**************************'/5H       )
       I=II22
       XALPHA1(1,J,L)=XAL(1,J,L)
       XALPHA=XALPHA1(1,J,L)
       XMAX1(I,J,L)=XI(I,J,L)
       IF(XMAX1(I,J,L).EQ.0)GOTO 12
       XMAX=XMAX1(I,J,L)
       FE(I,J,L) = (TDSE) + GID(I,J,L)
       II2=0
       WRITE(6,1005)T,CTEMP,XBAR,XMAX,XALPHA,FE(I,J,L)
       CALL RRAD(RADIUS,XMAX,XALPHA,XBAR,T,R,XMAXR,W,SIG,MOLVOL,
      &CAPCON,EPSI)
       XMAXR1(I,J,L)=XMAXR
       MOLVOL1(I,J,L)=MOLVOL
       RADIUS1(I,J,L)=RADIUS
       CAPCON1(I,J,L)=CAPCON
```

```fortran
      EPSI1(I,J,L)=EPSI
1005  FORMAT(' DEGREES KELVIN =',F8.1,
     &'       DEGREES CENTIGRADE =',F8.1/
     &' MOL FRAC CARBON IN ALLOY = ',F8.4,/
     &'      MOL FRAC CARBON IN AUSTENITE =',F8.4/
     &' MOL FRAC OF C IN FERRITE=',D12.4/
     &' (Gel+Gsu+Gid) = ',D15.6)
      DASH=(KK*T/HH)*DEXP(-(21230.0D+00/T))*DEXP(-31.84D+00)
      DO 999 II=1,1000
      CARB(1)=XBAR
      IF (II .GT. 1)GOTO 1000
      GOTO 1001
1000  CARB(II)=CARB(II-1)+0.0001D+00
      IF (CARB(II) .GT. XMAX) GOTO 1002
1001  X=CARB(II)
      II2=II2+1
      THETA=X/(A5-X)
      ACTIV=CG(X,T,W,R)
      ACTIV=DEXP(ACTIV)
      DACTIV=DCG(X,T,W,R)
      DACTIV=DACTIV*ACTIV
      DACTIV=DACTIV*A5/((A5+THETA)**2)
      SIGMA=A5-DEXP((-(W))/(R*T))
      PSI=ACTIV*(A5+Z*((A5+THETA)/(A5-(A5+Z/2)*THETA+(Z/2)*(A5+Z/2)*
     &(A5-SIGMA)*THETA*THETA)))+(A5+THETA)*DACTIV
      DIFF(II)=DASH*PSI
999   CONTINUE
1002  IF(II2.LT.4) GOTO 1008
      II3=-1
      CALL D01GAF(CARB,DIFF,II2,ANS,ERROR,II3)
      ANS=ANS/(XMAX-XBAR)
      ANS1(I,J,L)=1.0D-04*ANS
      ERROR1(I,J,L)=ERROR
      WRITE(6,1004)ANS1(I,J,L),ERROR1(I,J,L)
1004  FORMAT(12H INTEGRAL = ,D12.4, '  M**2/SEC  '/
     &' ERROR = ', D12.4)
      IF(XMAX .LT. XBAR)GOTO 990
      CALL VEL5(XMAX,XBAR,XALPHA,ANS,VMAX,PECLET,OMEG,RAD)
      PECLET1(I,J,L)=PECLET
      VMAX1(I,J,L)=VMAX
      OMEGA1(I,J,L)=OMEG
      VR(I,J,L) = 2*PECLET1(I,J,L)*ANS1(I,J,L)
77    FORMAT(' PECLET NUMBER = ',D12.4)
      WRITE (6,119) VR(I,J,L)
119   FORMAT (' Velocity * Radius = ',D15.6)
990   CONTINUE
1008  CONTINUE
12    CONTINUE
      WRITE(6,7) T,CTEMP,XBAR,RAD
      WRITE(6,13) SIG
7     FORMAT('  Following data is at the the following values of:'//
     &'T = ',F8.1,' Degree Kelvin'//'    ',F8.1,' Degree Centidrade'//
     &' Carbon in alloy = ',F8.4,' Mole fraction'//' Rad = ',D15.5//)
```

```fortran
13      FORMAT(' Interfacial Energy = ',F8.4,'  Joules / m**2'//)
        DO 110 J =1,20
        WRITE(6,10) XALPHA1(1,J,L)
        WRITE(6,9)
        DO 110 I =1,N
        IF(VR(I,J,L).LE.0.0) GOTO 110
        WRITE(6,55) FE(I,J,L),XMAX1(I,J,L),MOLVOL1(I,J,L),RADIUS1(I,J,L),
       &XMAXR1(I,J,L),CAPCON1(I,J,L),EPSI1(I,J,L),ANS1(I,J,L),
       &ERROR1(I,J,L),OMEGA1(I,J,L),VMAX1(I,J,L),PECLET1(I,J,L),VR(I,J,L)
110     CONTINUE
10      FORMAT(//' Carbon in ferrite = ',D15.5,' Mole fraction'//)
9       FORMAT(' (Gel+Gsu+Gid) Xi  MOLVOL     G.T.C.R     XMAXR      CAPCON
       &     EPSI      Int.       Err.   Omega     Vmax       p
       &V*rho'//'(J/mole) (mole fr.) (m**3/mole) (m)    (mole fr.)',
       &5x,'          (m**2/sec)                  (m/sec)',12x,
       &'     (m**2/sec)'///)
55      FORMAT(D11.3,F6.3,D11.3,6D11.3,F6.3,3D11.3/)
        IF(L.EQ.1) CALL GRST3D (1.0,400.0)
        IF(L.GT.1) GOTO 115
        CALL PLOT1 (N,L)
        CALL PLOT2 (N,L)
115     CALL INSEC (N,FNMAX1,FNMAX2,L)
        CALL TRAP (N,L)
        CALL PLOT3 (L)
114     CONTINUE
        CALL GRST9D
        STOP
        END
C *******************************************************************
C     Function giving the activity of carbon in gamma
C *******************************************************************
        DOUBLE PRECISION FUNCTION CG(X,T,W,R)
        DOUBLE PRECISION J,DG,DUMMY,T,R,W,X,A,U,V,SS,TT
        J=1-DEXP(-W/(R*T))
        SS=2*(1+2*J)*X+(1+8*J)*X*X
        IF(SS.GT.1.0D+30) GOTO 11
        DG=DSQRT(1-2*(1+2*J)*X+(1+8*J)*X*X)
        U= (1-2*X)/X
        IF(U.LE.0) GOTO 11
        DUMMY=5*DLOG((1-2*X)/X)+6*W/(R*T)+((38575)-(
        113.48)*T)/(R*T)
        V= ((DG-1+3*X)/(DG+1-3*X))**6
        TT=DUMMY+DLOG(((DG-1+3*X)/(DG+1-3*X))**6)
        IF(TT.GT.1.0D+30) GOTO 11
        IF(SS.GT.1.0D+30) GOTO 11
        CG=DUMMY+DLOG(((DG-1+3*X)/(DG+1-3*X))**6)
11      RETURN
        END
C *******************************************************************
C     Function giving the activity of iron in gamma
C *******************************************************************
        DOUBLE PRECISION FUNCTION FEG(X,T,W,R)
        DOUBLE PRECISION J,DG,X,T,W,R
```

103

```
        J=1-DEXP(-W/(R*T))
        DG=DSQRT(1-2*(1+2*J)*X+(1+8*J)*X*X)
        FEG=5*DLOG((1-X)/(1-2*X))+DLOG(((1-2*J+(4*J-1)*X-DG
      1)/(2*J*(2*X-1)))**6)
        RETURN
        END
C ************************************************************************
C       subroutine giving the carbon carbon interaction energy in
C       austenite (J/mol), as a function of alloy composition
C ************************************************************************
        SUBROUTINE OMEGA(W,XBAR)
        COMMON /THREE/ CC(8),T10,T20
        DOUBLE PRECISION C(8),W,P(8),B1,B2,Y(8),B3,XBAR
        INTEGER B5,I,U,B4
        DO 1 I=1,7
1       C(I)=CC(I)
        B3=0.0D+00
        C(8)=C(1)+C(2)+C(3)+C(4)+C(5)+C(6)+C(7)
        C(8)=100.0D+00-C(8)
        C(8)=C(8)/55.84D+00
        C(1)=C(1)/12.0115D+00
        C(2)=C(2)/28.09D+00
        C(3)=C(3)/54.94D+00
        C(4)=C(4)/58.71D+00
        C(5)=C(5)/95.94D+00
        C(6)=C(6)/52.0D+00
        C(7)=C(7)/50.94D+00
        B1=C(1)+C(2)+C(3)+C(4)+C(5)+C(6)+C(7)+C(8)
        DO 107 U=2,7
        Y(U)=C(U)/C(8)
107     CONTINUE
        DO 106 U=1,8
        C(U)=C(U)/B1
106     CONTINUE
        XBAR=C(1)
        XBAR=DINT(10000.0D+00*XBAR)
        XBAR=XBAR/10000
        B2=0.0D+00
        T10=Y(2)*(-3)+Y(3)*2+Y(4)*12+Y(5)*(-9)+Y(6)*(-1)+Y(7)*(-12)
        T20=-3*Y(2)-37.5*Y(3)-6*Y(4)-26*Y(5)-19*Y(6)-44*Y(7)
        P(2)=2013.0341+763.8167*C(2)+45802.87*C(2)**2-280061.63*C(2)**3
      &+3.864D+06*C(2)**4-2.4233D+07*C(2)**5+6.9547D+07*C(2)**6
        P(3)=2012.067-1764.095*C(3)+6287.52*C(3)**2-21647.96*C(3)**3-
      &2.0119D+06*C(3)**4+3.1716D+07*C(3)**5-1.3885D+08*C(3)**6
        P(4)=2006.8017+2330.2424*C(4)-54915.32*C(4)**2+1.6216D+06*C(4)**3
      &-2.4968D+07*C(4)**4+1.8838D+08*C(4)**5-5.5531D+08*C(4)**6
        P(5)=2006.834-2997.314*C(5)-37906.61*C(5)**2+1.0328D+06*C(5)**3
      &-1.3306D+07*C(5)**4+8.411D+07*C(5)**5-2.0826D+08*C(5)**6
        P(6)=2012.367-9224.2655*C(6)+33657.8*C(6)**2-566827.83*C(6)**3
      &+8.5676D+06*C(6)**4-6.7482D+07*C(6)**5 +2.0837D+08*C(6)**6
        P(7)=2011.9996-6247.9118*C(7)+5411.7566*C(7)**2
      &+250118.1085*C(7)**3-4.1676D+06*C(7)**4
        DO 108 U=2,7
```

```fortran
      B3=B3+P(U)*Y(U)
      B2=B2+Y(U)
108   CONTINUE
      IF (B2 .EQ. 0.0D+00) GOTO 455
      W=(B3/B2)*4.187
      GOTO 456
455   W=8054.0
      WRITE (6,261)(C(J),J=1,7)
261   FORMAT (//6H    C=,F8.4,6H   SI=,F8.4,6H    MN=,F8.4,
     &6H    NI=,F8.4,6H    MO=,F8.4,6H    CR=,F8.4,6H     V=,F8.4)
456   RETURN
      END
C *********************************************************************
C     Function giving the differential of activity of carbon in gamma
C *********************************************************************
      DOUBLE PRECISION FUNCTION DCG(X,T,W,R)
      DOUBLE PRECISION J,DG,DDG,X,T,W,R
      J=1-DEXP(-W/(R*T))
      DG=DSQRT(1-2*(1+2*J)*X+(1+8*J)*X*X)
      DDG=(0.5/DG)*(-2-4*J+2*X+16*J*X)
      DCG=-((10/(1-2*X))+(5/X))+6*((DDG+3)/(DG-1+3*X
     1)-(DDG-3)/(DG+1-3*X))
      RETURN
      END
C *********************************************************************
C     Function giving the differential of activity of iron in gamma
C *********************************************************************
      DOUBLE PRECISION FUNCTION DFEG(X,T,W,R)
      DOUBLE PRECISION J,DG,DDG,X,T,W,R
      J=1-DEXP(-W/(R*T))
      DG=DSQRT(1-2*(1+2*J)*X+(1+8*J)*X*X)
      DDG=(0.5/DG)*(-2-4*J+2*X+16*J*X)
      DFEG=10/(1-2*X)-5/(1-X)+6*((4*J-1-DDG)/(1-2*J+(4*
     1J-1)*X-DG)-2/(2*J*(2*X-1)))
      RETURN
      END
C *********************************************************************
C     Function giving the activity of carbon in alpha
C *********************************************************************
      DOUBLE PRECISION FUNCTION CA(X1,T,W1,H1,S1,R)
      DOUBLE PRECISION J1,DA,X1,T,W1,H1,S1,R
      J1=1-DEXP(-W1/(R*T))
      DA=DSQRT(9-6*X1*(2*J1+3)+(9+16*J1)*X1*X1)
      CA=3*DLOG((3-4*X1)/X1)+(4*W1)/(R*T)+
     1DLOG(((DA-3+5*X1)/(DA+3-5*X1))**4)+(H1-S1*T)/(R*T)
      RETURN
      END
C *********************************************************************
C     Function giving the activity of iron in alpha
C *********************************************************************
      DOUBLE PRECISION FUNCTION FEA(X1)
      DOUBLE PRECISION X1
      FEA=DLOG(1-X1)
```

```
      RETURN
      END
C ********************************************************************
C     Function giving the differential of activity of carbon in alpha
C ********************************************************************
      DOUBLE PRECISION FUNCTION DCA(X1,T,W1,R)
      DOUBLE PRECISION J1,DA,DUMMY,DUMMY3,X1,T,W1,R
      J1=1-DEXP(-W1/(R*T))
      DA=DSQRT(9-6*X1*(2*J1+3)+(9+16*J1)*X1*X1)
      DUMMY3=(3*X1/(3-4*X1))*((4*X1-3)/(X1**2)-4/X1)
      DUMMY=(0.5/DA)*(-12*J1-18+18*X1+32*J1*X1)
      DUMMY=4*(((DUMMY+5)/(DA-3+5*X1))-((DUMMY-5)/(DA+3-5*X1)))
      DCA=DUMMY3+DUMMY
      RETURN
      END
C ********************************************************************
C     Function giving the differential of activity of iron in alpha
C ********************************************************************
      DOUBLE PRECISION FUNCTION DFEA(X1)
      DOUBLE PRECISION X1
      DFEA=1/(X1-1)
      RETURN
      END
C ********************************************************************
C
      SUBROUTINE RRAD(RADIUS,XMAX,XALPHA,XBAR,T,R,XMAXR,W,SIG,MOLVOL,
     &CAPCON,EPSI)
      DOUBLE PRECISION RADIUS,XMAX,XBAR,T,R,SIG,MOLVOL,XMAXR
     &,XALPHA,RAD,OMEGA,CAPCON,EPSI
C SIG    = Interfacial energy, Joules per metre squared
C MOLVOL = Molar volume of ferrite
C RADIUS = Critical radius for zero growth
C RAD    = Ratio of the actual radius to the critical radius
      SIG=0.2
      MOLVOL=7.0894317D-06*(1.0D+00+3.549D-05*(T-298.0D+00))
      EPSI=XMAX*DCG(XMAX,T,W,R)
      CAPCON=(SIG*MOLVOL/(R*T))*((1.0D+00-XMAX)/(XALPHA-XMAX))
     &/EPSI
      RADIUS=CAPCON*XMAX/(XBAR-XMAX)
      OMEGA=(XMAX-XBAR)/(XMAX-XALPHA)
      RAD=1.5D-09
      XMAXR=XMAX*(1.0D+00+(CAPCON/RAD))
      WRITE(6,1)SIG,MOLVOL,RADIUS,XMAXR,CAPCON,EPSI
1     FORMAT(' INTERFACIAL ENERGY=',F8.4,' JOULES/METERS SQUARED',/
     &' MOLAR VOLUME OF FERRITE(METERS CUBED PER MOL)=',D15.6/
     &' GIBBS THOMPSON CRITICAL RADIUS(METERS)=',D15.6/
     &' EQUILIBRIUM CONC AT PLATE TIP, MOL FRAC, XMAXR=',D15.6/
     &' CAPILLARITY CONSTANT CAPCON,=',D15.6,/
     &' NON-IDEALITY PARAMETER EPSI=',D15.6)
      RETURN
      END
C ********************************************************************
C
```

```fortran
      SUBROUTINE DUMM(DUMMY,PECLET,OMEGA,RAD)
      DOUBLE PRECISION DUMMY,PECLET,OMEGA,RADIUS,RAD,S2,PI
      PI=3.14159D+00
      DUMMY=(DSQRT(PI*PECLET))*(DEXP(PECLET))*(DERFC(DSQRT(PECLET)))
      RETURN
      END
C *******************************************************************
C
      SUBROUTINE VEL5(XMAX,XBAR,XALPHA,ANS,VMAX,PECLET,OMEGA,RAD)
      DOUBLE PRECISION OMEGA,PECLET,LOGPEC,A1,A2,A3,A4,A5,A6,A7
     &,RAD,ANS
      ANS2=ANS*(XMAX-XBAR)
      OMEGA=(XMAX-XBAR)/(XMAX-XALPHA)
      RAD=1.5D-09
      A1=-0.10312623D+02
      A2=0.10088194D+03
      A3=-0.43377705D+03
      A4=0.88436018D+03
      A5=-0.83962224D+03
      A6=0.30048670D+03
      A7=0.9969D+00
      LOGPEC=A1+A2*OMEGA/A7+A3*OMEGA*OMEGA/(A7*A7)+
     &A4*OMEGA*OMEGA*OMEGA/(A7*A7*A7)+A5*OMEGA*OMEGA*OMEGA
     &*OMEGA/(A7*A7*A7*A7)+A6*OMEGA*OMEGA*OMEGA*OMEGA*OMEGA
     &/(A7*A7*A7*A7*A7)
      IF(LOGPEC.GT.50.0) GOTO 30
      PECLET=10.00**LOGPEC
      ANS=ANS*1.0D-04
      VMAX=ANS*PECLET*2.0D+00/RAD
      WRITE(6,2)OMEGA,VMAX,PECLET,RAD
2     FORMAT(' OMEGA=',F10.4,/' VMAX,M/S=',D12.4,/
     &' PECLET=',D12.4,/' RAD,METERS=',D12.4)
30    RETURN
      END
C *******************************************************************
C     Subroutine plotting Gid versus Xi
C *******************************************************************
      SUBROUTINE PLOT1 (N,K)
      COMMON XI(50,50,16),GID(50,50,16),FE(50,50,16),
     &VR(50,50,16),CTEMP,MUM
      COMMON /TWO/ TDSE
      DIMENSION XI1(100),GID1(100),GID2(100),XI2(100),XI3(100),
     &GID3(100),XI4(100),GID4(100),XI5(100),GID5(100)
      DOUBLE PRECISION CMAX,CMIN
C     ***** Initialise and spesify aspect ratio *****
C     CALL GRST3D (1.0,400.0)
C     ***** Make both plots on the same page ******
      CALL GRLM2D (0.15,0.45,0.12,0.42)
C     ***** Set user limits *****
      CALL GRLM3S (0.0D0, 1200.0D0, 0.02D0, 0.12D0)
C     ***** Scale lines inside *****
      CALL GRFT6S (-1.0,0.0)
C     ***** Select line style for graph *****
```

107

```
        CALL GRTY5S (1,3)
C       ***** Draw graph *****
        I1=0
        DO 14 I=1,N
        IF(XI(I,1,K) .LE. 0.02D0)GOTO 25
        GID1(I)=GID(I,1,K)
        I1=I1+1
14      XI1(I) = XI(I,1,K)
25      IF(I1.LT.2)GOTO 34
        CALL GRGR6S (GID1, XI1, I1)
C       ***** Draw point for curve identification *****
        CALL GRGR6S (760.0, 0.11,1)
C       ***** Reduce text size *****
C        CALL GRTX3S (1, 2.2, 0.0, 0.0, 2.2)
C       ***** Defining character for annotation *****
        CALL GRTX4S (1, '!')
C       ***** Write string *****
        CALL GRAN5S (800.0,0.11,'X!F3!!SB!a!NL!!F1!=0.0003',25,0.0)
34      I2=0
        DO 18 I=1,N
        IF(XI(I,5,K).LE.0.02D+0)GOTO 19
        XI2(I)=XI(I,5,K)
        I2=I2+1
18      GID2(I)=GID(I,5,K)
C       ***** Select line style for graph *****
19      CALL GRTY5S (1,5)
        IF(I2.LT.2)GOTO 33
C       ***** Draw curve *****
        CALL GRGR6S (GID2, XI2, I2)
C       ***** Draw point for curve identification *****
        CALL GRGR6S (760.0,0.105,1)
C       ***** Write string *****
        CALL GRAN5S(800.00,0.105,'X!F3!!SB!a!NL!!F1!=0.0043',25,0.0)
33      I3=0
        DO 15 I=1,N
        IF(XI(I,9,K).LE.0.02D+0)GOTO 20
        XI3(I)=XI(I,9,K)
        I3=I3+1
15      GID3(I)=GID(I,9,K)
C       ***** Select line style for graph *****
20      CALL GRTY5S(1,7,K)
        IF(I3.LT.2)GOTO 32
C       ***** Draw curve *****
        CALL GRGR6S (GID3, XI3, I3)
C       ***** Draw point for curve identification *****
        CALL GRGR6S (760.0,0.10,1)
C       ***** Write string *****
        CALL GRAN5S (800.0,0.10,'X!F3!!SB!a!NL!!F1!=0.0083',25,0.0)
32      I4=0
        DO 16 I=1,N
        IF(XI(I,13,K).LE.0.02D+0)GOTO 21
        XI4(I)=XI(I,13,K)
        I4=I4+1
```

```
16      GID4(I)=GID(I,13,K)
C       ***** Select line style for graph *****
21      CALL GRTY5S(1,9)
        IF(I4.LT.2)GOTO 31
C       ***** Draw curve *****
        CALL GRGR6S (GID4,XI4,I4)
C       ***** Draw point for curve identification *****
        CALL GRGR6S (760.0,0.095,1)
C       ***** Write string *****
        CALL GRAN5S (800.0,0.095,'X!F3!!SB!a!NL!!F1!=0.0123',25,0.0)
31      I5=0
        DO 17 I=1,N
        IF(XI(I,17,K).LE.0.02D+0)GOTO 22
        XI5(I)=XI(I,17,K)
        I5=I5+1
17      GID5(I)=GID(I,17,K)
C       ***** Select line style for graph *****
22      CALL GRTY5S(1,11)
C       ***** Draw curve *****
        IF(I5.LT.2)GOTO 30
        CALL GRGR6S (GID5,XI5,I5)
C       ***** Draw point for curve identification *****
        CALL GRGR6S (760.0,0.09,1)
C       ***** Write string *****
        CALL GRAN5S (800.0,0.09,'X!F3!!SB!a!NL!!F1!=0.0163',25,0.0)
C       ***** Select normal text size *****
C       ***** Write heading and title *****
30      CALL GRAN6S (' ',1,
     &'G!SB!id!NL!',11,'x!SB!i!NL!',10)
C       ***** Close package *****
        RETURN
        END
C ********************************************************************
C       Subroutine plotting free energy versus Velocity
C ********************************************************************
        SUBROUTINE PLOT2 (N,K)
        COMMON XI(50,50,16),GID(50,50,16),FE(50,50,16),
     &VR(50,50,16),CTEMP,MUM
        COMMON /TWO/ TDSE
        DIMENSION X1(100),X2(100),Y1(100),Y2(5),X11(100),Y11(100),
     &X22(100),Y22(5),FE1(100),FE2(100),FE3(100),FE4(100),FE5(100),
     &FE6(100),FE7(100),FE8(100),FE9(100),FE10(100),FE11(100),
     &VR1(100),VR2(100),VR3(100),VR4(100),VR5(100),VR6(100),
     &VR7(100),VR8(100),VR9(100),VR10(100),VR11(100),
     &VI(100),X(100)
        DOUBLE PRECISION X1,Y2,Y1,X2,FE1,FE2,FE3,FE4,FE5,FE6,FE7,
     &FE8,FE9,FE10,FE11,VR1,VR2,VR3,VR4,VR5,VR6,VR7,VR8,VR9,VR10,VR11,
     &YMAX,YMIN,YQ,YW,X11,Y11,X22,Y22,DD,DD1,DD2,DD3,YY11,YY22,
     &KK,V0,T,EE,V,MU,OMEGA,A,TK,GIH,Q0,RAD,GI,VI,Q,XX
        YMIN=1.0D+60
        YMAX=1.0D-60
        T = CTEMP
        DO 1 J=1,17,2
```

```
      DO 1 I=1,N
      IF(VR(I,J,K).LT.1.0D-16)GOTO 1
      IF(VR(I,J,K).GT.1.0D-0) GOTO 1
      IF(VR(I,J,K).LT.YMIN) YMIN=VR(I,J,K)
      IF(VR(I,J,K).GT.YMAX) YMAX=VR(I,J,K)
1     CONTINUE
      DO 2 I=1,N
      IF(VR(I,18,K).LT.1.0D-16)GOTO 2
      IF(VR(I,18,K).GT.1.0D-0) GOTO 2
      IF(VR(I,18,K).LT.YMIN) YMIN=VR(I,18,K)
      IF(VR(I,18,K).GT.YMAX) YMAX=VR(I,18,K)
2     CONTINUE
      YMAX=YMAX/1.5D-9
      YMAX=YMAX*10.0D0
      YMIN=YMIN/1.5D-9
      YY11=DLOG10(YMIN)
      YY22=DLOG10(YMAX)
      DD=(YY22-YY11)/10.0
      DD1=YY22-DD
      DD2=DD1-DD
      DD3=YY11+DD
      V0=30.0D0
      RAD=1.5D-09
      KK=1.38062D-23
      TK=T+273.0
      OMEGA=6.679D-6*(1+7.89D-5*TK)/6.0225D+23
      IF(T.GE.25.AND.T.LE.540) EE=(-18.8D0*T+52400)*4.18E+6
      IF(T.GE.540.AND.T.LE.705) EE=(-37.6D0*T+62300)*4.18E+6
      IF(T.GE.260.AND.T.LE.595) V=(3.6D-5)*T+0.284
      IF(T.GE.595.AND.T.LE.705) V=(9.9D-5)*T+0.246
      MU=0.5D0*EE/(1+V)
      MUM= MU*OMEGA*6.0225D+23
      GIH=1.22D-3*MUM
      Q0=0.31*MU*OMEGA
      DO 11 I=1,100
      X(I)=X(I-1)+10
      Q=Q0*(1-(X(I)/GIH )**0.5)
      VI(I)=V0*EXP(-Q/(KK*TK))
      Y1(I)=VI(I)
      X1(I)=(TDSE)+X(I)
11    X2(I)=2.0D-3*MUM+X(I)
      CALL GRTX2D(2,9)
      CALL GRTX2D(1,9)
C     ***** Initialise and spesify aspect ratio and width *****
      CALL GRLM2D (0.15,0.45,0.52,0.97)
      XX=TDSE
C     ***** Set user limits *****
      CALL GRLM3D (XX,1800.0,YY11,YY22)
      CALL GRFR6D(1)
C     ***** Select line style for graph *****
      CALL GRTY5D (0,3)
C     ***** Define annotation *****
      CALL GRTX4D (1,'!')
```

110

```fortran
C         ***** Write string at any point *****
          CALL GRAN5D (1000.0,DD1,'Fe-0.4C wt.%',12,0.0)
C         ***** Write string at defined point *****
          IF(K.EQ.1) CALL GRAN5D(1000.0,DD2,'T=410!SP!o!NL!C',15,0.0)
C         ***** Draw graph *****
          J1=0
          DO 28 I=1,N
          IF(VR(I,1,K).LT.1.0D-16)GOTO 28
          IF(VR(I,1,K).GT.1.0D-0) GOTO 28
          IF(VR(I,1,K).LE.0)GOTO 28
          J1=J1+1
          VR1(J1)=VR(I,1,K)/1.5D-9
          FE1(J1)=FE(I,1,K)
28        CONTINUE
          IF(J1.LE.1) GOTO 49
          CALL GRGR7D (FE1,VR1,J1)
49        J2=0
          DO 19 I=1,N
          IF(VR(I,3,K).LT.1.0D-16)GOTO 19
          IF(VR(I,3,K).GT.1.0D-0) GOTO 19
          IF(VR(I,3,K).LE.0)GOTO 19
          J2=J2+1
          VR2(J2)=VR(I,3,K)/1.5D-9
          FE2(J2)=FE(I,3,K)
19        CONTINUE
          IF(J2.LE.1)GOTO 48
          CALL GRGR7D (FE2,VR2,J2)
48        J3=0
          DO 20 I=1,N
          IF(VR(I,5,K).LT.1.0D-16)GOTO 20
          IF(VR(I,5,K).GT.1.0D-0) GOTO 20
          IF(VR(I,5,K).LE.0)GOTO 20
          J3=J3+1
          VR3(J3)=VR(I,5,K)/1.5D-9
          FE3(J3)=FE(I,5,K)
20        CONTINUE
          IF(J3.LE.1)GOTO 47
          CALL GRGR7D (FE3,VR3,J3)
47        J4=0
          DO 21 I=1,N
          IF(VR(I,7,K).LT.1.0D-16)GOTO 21
          IF(VR(I,7,K).GT.1.0D-0) GOTO 21
          IF(VR(I,7,K).LE.0)GOTO 21
          J4=J4+1
          VR4(J4)=VR(I,7,K)/1.5D-9
          FE4(J4)=FE(I,7,K)
21        CONTINUE
          IF(J4.LE.1)GOTO 46
          CALL GRGR7D (FE4,VR4,J4)
46        J5=0
          DO 22 I=1,N
          IF(VR(I,9,K).LT.1.0D-16)GOTO 22
          IF(VR(I,9,K).GT.1.0D-0) GOTO 22
```

```
        IF(VR(I,9,K).LE.0)GOTO 22
        J5=J5+1
        VR5(J5)=VR(I,9,K)/1.5D-9
        FE5(J5)=FE(I,9,K)
22      CONTINUE
        IF(J5.LE.1)GOTO 45
        CALL GRGR7D (FE5,VR5,J5)
45      J6=0
        DO 23 I=1,N
        IF(VR(I,11,K).LT.1.0D-16)GOTO 23
        IF(VR(I,11,K).GT.1.0D-0) GOTO 23
        IF(VR(I,11,K).LE.0)GOTO 23
        J6=J6+1
        VR6(J6)=VR(I,11,K)/1.5D-9
        FE6(J6)=FE(I,11,K)
23      CONTINUE
        IF(J6.LE.1)GOTO 44
        CALL GRGR7D (FE6,VR6,J6)
44      J7=0
        DO 24 I=1,N
        IF(VR(I,13,K).LT.1.0D-16)GOTO 24
        IF(VR(I,13,K).GT.1.0D-0) GOTO 24
        IF(VR(I,13,K).LE.0)GOTO 24
        J7=J7+1
        VR7(J7)=VR(I,13,K)/1.5D-9
        FE7(J7)=FE(I,13,K)
24      CONTINUE
        IF(J7.LE.1)GOTO 43
        CALL GRGR7D (FE7,VR7,J7)
43      J8=0
        DO 25 I=1,N
        IF(VR(I,15,K).LT.1.0D-16)GOTO 25
        IF(VR(I,15,K).GT.1.0D-0) GOTO 25
        IF(VR(I,15,K).LE.0)GOTO 25
        J8=J8+1
        VR8(J8)=VR(I,15,K)/1.5D-9
        FE8(J8)=FE(I,15,K)
25      CONTINUE
        IF(J8.LE.1)GO TO 42
        CALL GRGR7D (FE8,VR8,J8)
42      J9=0
        DO 26 I=1,N
        IF(VR(I,17,K).LT.1.0D-16)GOTO 26
        IF(VR(I,17,K).GT.1.0D-0) GOTO 26
        IF(VR(I,17,K).LE.0)GOTO 26
        J9=J9+1
        VR9(J9)=VR(I,17,K)/1.5D-9
        FE9(J9)=FE(I,17,K)
26      CONTINUE
        IF(J9.LE.1)GOTO 40
        CALL GRGR7D (FE9,VR9,J9)
40      J10=0
        DO 27 I=1,N
```

```
        IF(VR(I,18,K).LT.1.0D-16)GOTO 27
        IF(VR(I,18,K).GT.1.0D-0) GOTO 27
        IF(VR(I,18,K).LE.0)GOTO 27
        J10=J10+1
        VR10(J10)=VR(I,18,K)/1.5D-9
        FE10(J10)=FE(I,18,K)
27      CONTINUE
        IF(J10.LE.1)GOTO 41
        CALL GRGR7D (FE10,VR10,J10)
C       ***** Select line for graph *****
41      CALL GRLS3D (7)
        II=0
        DO 4 I=1,100
        IF(Y1(I).GT.YMAX.OR.Y1(I).LT.YMIN) GOTO 4
        IF(X1(I).GT.1800.0.OR.X2(I).GT.1800.0) GOTO 4
        II=II+1
        X11(II)=X1(I)
        X22(II)=X2(I)
        Y11(II)=Y1(I)
4       CONTINUE
C
        CALL GRGR7D (X11, Y11, II)
C       ***** Select line for graph *****
32      CALL GRLS3D (5)
C       ***** Draw line *****
        CALL GRGR7D (X22, Y11, II)
C       ***** Write heading and axis title *****
34      CALL GRAN6D (' ',1,
      &'(G!SB!el!NL!+G!SB!su!NL!+G!SB!id!NL!) /J mole!SP!-1!NL!',55,
      &'Velocity /ms!SP!-1!NL!',22)
        RETURN
        END
C *********************************************************************
C Subroutine for the curve fitting and for the calculation of point of
C intersection
C *********************************************************************
        SUBROUTINE INSEC (N,FNMAX1,FNMAX2,K)
        COMMON XI(50,50,16),GID(50,50,16),FE(50,50,16),
      &VR(50,50,16),CTEMP,MUM,XAL(50,50,16),XALP(12,16),FN1(12,16),
      &FN2(12,16),PT1(12,16),PT2(12,16),PTF1(12,16),PTF2(12,16),
      &ANS1(50,50,16),ANS11(100),VKR1(12,16),VKR2(12,16),
      &XI11(12,16),XI22(12,16)
        COMMON /ONE/ G(10)
        COMMON /TWO/ TDSE
        DIMENSION FE1(100),FE2(100),FE3(100),FE4(100),FE5(100),FE6(100),
      &FE7(100),FE8(100),FE9(100),FE10(100),FE11(100),FE12(100),XX1(5),
      &XX2(5),YY1(5),YY2(5),VR1(100),VR2(100),VR3(100),VR4(100),VR5(100),
      &VR6(100),VR7(100),VR8(100),VR9(100),VR10(100),VR11(100),
      &VR12(100),Y(12,16),D(10),PT(12,16)
        DOUBLE PRECISION X1,Y2,Y1,X2,FE1,FE2,FE3,FE4,FE5,FE6,FE7,
      &FE8,FE9,FE10,FE11,FE12,VR1,VR2,VR3,VR4,VR5,VR6,VR7,VR8,VR9,VR10,
      &VR11,VR12,Y,P1,P2,REZ,IMZ,MU1,MU2,Z1,Z2,XX1,XX2,YY1,YY2,D
        INTEGER M1,I,J
```

113

```fortran
        DOUBLE PRECISION A,B,U,EPS, ETA, X
        INTEGER         IFAIL
        DOUBLE PRECISION FN
        DOUBLE PRECISION FFN
        EXTERNAL        FN
        EXTERNAL        FFN
        EXTERNAL        C05ADF
        A = TDSE
        U =2.0D-3*MUM
        B = 4600.0D0
        EPS = 1.0D-5
        ETA = 0.0D0
        IFAIL = 1
        M1=2
C ******** Point of intersection of 1st curve ********
        J1=0
        DO 28 I=1,N
        IF(VR(I,1,K).GT.1.0D-0)GOTO 28
        IF(VR(I,1,K).EQ.0)GOTO 28
        J1=J1+1
        VR1(J1)=VR(I,1,K)
        FE1(J1)=FE(I,1,K)
28      CONTINUE
        IF(M1.GE.J1) GOTO 49
        CALL E02ACF(FE1,VR1,J1,D,M1,REF)
        DO 1 I=1,10
1       G(I)=D(I)
        IF(FN(A)*FN(B).GT.0)GO TO 49
        CALL C05ADF(A,B,EPS,ETA,FN,X,IFAIL)
        IF (IFAIL.EQ.0) THEN
           WRITE (6,FMT=99997) X
        ELSE
           WRITE (6,FMT=99998) IFAIL
           IF (IFAIL.EQ.2 .OR. IFAIL.EQ.3) WRITE (6,FMT=99996) X
        END IF
        PT1(1,K)=X
        FN1(1,K)=D(1)+D(2)*PT1(1,K)+D(3)*(PT1(1,K)**2)+D(4)*(PT1(1,K)**3)+
     &D(5)*(PT1(1,K)**4)+D(6)*(PT1(1,K)**5)+D(7)*(PT1(1,K)**6)+
     &D(8)*(PT1(1,K)**7)+D(9)*(PT1(1,K)**8)+D(10)*(PT1(1,K)**9)
        IF(FFN(U)*FFN(B).GT.0)GO TO 49
         CALL C05ADF(U,B,EPS,ETA,FFN,X,IFAIL)
         IF (IFAIL.EQ.0) THEN
            WRITE (6,FMT=99997) X
         ELSE
            WRITE (6,FMT=99998) IFAIL
            IF (IFAIL.EQ.2 .OR. IFAIL.EQ.3) WRITE (6,FMT=99996) X
         END IF
        PT2(1,K)=X
        FN2(1,K)=D(1)+D(2)*PT2(1,K)+D(3)*(PT2(1,K)**2)+D(4)*(PT2(1,K)**3)+
     &D(5)*(PT2(1,K)**4)+D(6)*(PT2(1,K)**5)+D(7)*(PT2(1,K)**6)+
     &D(8)*(PT2(1,K)**7)+D(9)*(PT2(1,K)**8)+D(10)*(PT2(1,K)**9)
C ******** Point of intersection of 2nd curve ********
49      J2=0
```

114

```fortran
        DO 19 I=1,N
        IF(VR(I,3,K).GT.1.0D-0)GOTO 19
        IF(VR(I,3,K).EQ.0)GOTO 19
        J2=J2+1
        VR2(J2)=VR(I,3,K)
        FE2(J2)=FE(I,3,K)
C        WRITE(6,*) J2,FE2(J2),VR2(J2)
19      CONTINUE
        IF(M1.GE.J2)GOTO 48
C        IF(M1.GE.J2) M1=J2-2
        CALL E02ACF(FE2,VR2,J2,D,M1,REF)
        DO 2 I=1,10
2       G(I)=D(I)
C
        IF(FN(A)*FN(B).GT.0)GO TO 48
        CALL C05ADF(A,B,EPS,ETA,FN,X,IFAIL)
        IF (IFAIL.EQ.0) THEN
           WRITE (6,FMT=99997) X
        ELSE
           WRITE (6,FMT=99998) IFAIL
           IF (IFAIL.EQ.2 .OR. IFAIL.EQ.3) WRITE (6,FMT=99996) X
        END IF
        PT1(2,K)=X
        FN1(2,K)=D(1)+D(2)*PT1(2,K)+D(3)*(PT1(2,K)**2)+D(4)*(PT1(2,K)**3)+
     &D(5)*(PT1(2,K)**4)+D(6)*(PT1(2,K)**5)+D(7)*(PT1(2,K)**6)+
     &D(8)*(PT1(2,K)**7)+D(9)*(PT1(2,K)**8)+D(10)*(PT1(2,K)**9)
C
        IF(FFN(U)*FFN(B).GT.0)GO TO 48
         CALL C05ADF(U,B,EPS,ETA,FFN,X,IFAIL)
         IF (IFAIL.EQ.0) THEN
            WRITE (6,FMT=99997) X
         ELSE
            WRITE (6,FMT=99998) IFAIL
            IF (IFAIL.EQ.2 .OR. IFAIL.EQ.3) WRITE (6,FMT=99996) X
         END IF
        PT2(2,K)=X
        FN2(2,K)=D(1)+D(2)*PT2(2,K)+D(3)*(PT2(2,K)**2)+D(4)*(PT2(2,K)**3)+
     &D(5)*(PT2(2,K)**4)+D(6)*(PT2(2,K)**5)+D(7)*(PT2(2,K)**6)+
     &D(8)*(PT2(2,K)**7)+D(9)*(PT2(2,K)**8)+D(10)*(PT2(2,K)**9)
C ******** Point of intersection of 3rd curve ********
48      J3=0
        DO 20 I=1,N
C        IF(VR(I,5,K).LT.1.0D-16)GOTO 20
        IF(VR(I,5,K).GT.1.0D-0)GOTO 20
        IF(VR(I,5,K).EQ.0)GOTO 20
        J3=J3+1
        VR3(J3)=VR(I,5,K)
        FE3(J3)=FE(I,5,K)
C        WRITE(6,*) J3,FE3(J3),VR3(J3)
20      CONTINUE
        IF(M1.GE.J3)GOTO 47
        CALL E02ACF(FE3,VR3,J3,D,M1,REF)
        DO 3 I=1,10
```

```
3         G(I)=D(I)
C
          IF(FN(A)*FN(B).GT.0)GO TO 47
          CALL C05ADF(A,B,EPS,ETA,FN,X,IFAIL)
          IF (IFAIL.EQ.0) THEN
             WRITE (6,FMT=99997) X
          ELSE
             WRITE (6,FMT=99998) IFAIL
             IF (IFAIL.EQ.2 .OR. IFAIL.EQ.3) WRITE (6,FMT=99996) X
          END IF
          PT1(3,K)=X
          FN1(3,K)=D(1)+D(2)*PT1(3,K)+D(3)*(PT1(3,K)**2)+D(4)*(PT1(3,K)**3)+
         &D(5)*(PT1(3,K)**4)+D(6)*(PT1(3,K)**5)+D(7)*(PT1(3,K)**6)+
         &D(8)*(PT1(3,K)**7)+D(9)*(PT1(3,K)**8)+D(10)*(PT1(3,K)**9)
C
          IF(FFN(U)*FFN(B).GT.0)GO TO 47
           CALL C05ADF(U,B,EPS,ETA,FFN,X,IFAIL)
           IF (IFAIL.EQ.0) THEN
              WRITE (6,FMT=99997) X
           ELSE
              WRITE (6,FMT=99998) IFAIL
              IF (IFAIL.EQ.2 .OR. IFAIL.EQ.3) WRITE (6,FMT=99996) X
           END IF
          PT2(3,K)=X
          FN2(3,K)=D(1)+D(2)*PT2(3,K)+D(3)*(PT2(3,K)**2)+D(4)*(PT2(3,K)**3)+
         &D(5)*(PT2(3,K)**4)+D(6)*(PT2(3,K)**5)+D(7)*(PT2(3,K)**6)+
         &D(8)*(PT2(3,K)**7)+D(9)*(PT2(3,K)**8)+D(10)*(PT2(3,K)**9)
C ******** Point of intersection of 4th curve ********
47        J4=0
          DO 21 I=1,N
          IF(VR(I,7,K).GT.1.0D-0)GOTO 21
          IF(VR(I,7,K).EQ.0)GOTO 21
          J4=J4+1
          VR4(J4)=VR(I,7,K)
          FE4(J4)=FE(I,7,K)
21        CONTINUE
          IF(M1.GE.J4)GOTO 46
          CALL E02ACF(FE4,VR4,J4,D,M1,REF)
          DO 4 I=1,10
4         G(I)=D(I)
C
          IF(FN(A)*FN(B).GT.0)GO TO 46
          CALL C05ADF(A,B,EPS,ETA,FN,X,IFAIL)
          IF (IFAIL.EQ.0) THEN
             WRITE (6,FMT=99997) X
          ELSE
             WRITE (6,FMT=99998) IFAIL
             IF (IFAIL.EQ.2 .OR. IFAIL.EQ.3) WRITE (6,FMT=99996) X
          END IF
          PT1(4,K)=X
          FN1(4,K)=D(1)+D(2)*PT1(4,K)+D(3)*(PT1(4,K)**2)+D(4)*(PT1(4,K)**3)+
         &D(5)*(PT1(4,K)**4)+D(6)*(PT1(4,K)**5)+D(7)*(PT1(4,K)**6)+
         &D(8)*(PT1(4,K)**7)+D(9)*(PT1(4,K)**8)+D(10)*(PT1(4,K)**9)
```

```
C
      IF(FFN(U)*FFN(B).GT.0)GO TO 46
       CALL C05ADF(U,B,EPS,ETA,FFN,X,IFAIL)
       IF (IFAIL.EQ.0) THEN
          WRITE (6,FMT=99997) X
       ELSE
          WRITE (6,FMT=99998) IFAIL
          IF (IFAIL.EQ.2 .OR. IFAIL.EQ.3) WRITE (6,FMT=99996) X
       END IF
      PT2(4,K)=X
      FN2(4,K)=D(1)+D(2)*PT2(4,K)+D(3)*(PT2(4,K)**2)+D(4)*(PT2(4,K)**3)+
     &D(5)*(PT2(4,K)**4)+D(6)*(PT2(4,K)**5)+D(7)*(PT2(4,K)**6)+
     &D(8)*(PT2(4,K)**7)+D(9)*(PT2(4,K)**8)+D(10)*(PT2(4,K)**9)
C ******** Point of intersection of 5th curve ********
46    J5=0
      DO 22 I=1,N
      IF(VR(I,9,K).GT.1.0D-0)GOTO 22
      IF(VR(I,9,K).EQ.0)GOTO 22
      J5=J5+1
      VR5(J5)=VR(I,9,K)
      FE5(J5)=FE(I,9,K)
C     WRITE(6,*) J5,FE5(J5),VR5(J5)
22    CONTINUE
      IF(M1.GE.J5)GOTO 45
      CALL E02ACF(FE5,VR5,J5,D,M1,REF)
      DO 5 I=1,10
5     G(I)=D(I)
C
      IF(FN(A)*FN(B).GT.0)GO TO 45
      CALL C05ADF(A,B,EPS,ETA,FN,X,IFAIL)
      IF (IFAIL.EQ.0) THEN
         WRITE (6,FMT=99997) X
      ELSE
         WRITE (6,FMT=99998) IFAIL
         IF (IFAIL.EQ.2 .OR. IFAIL.EQ.3) WRITE (6,FMT=99996) X
      END IF
      PT1(5,K)=X
      FN1(5,K)=D(1)+D(2)*PT1(5,K)+D(3)*(PT1(5,K)**2)+D(4)*(PT1(5,K)**3)+
     &D(5)*(PT1(5,K)**4)+D(6)*(PT1(5,K)**5)+D(7)*(PT1(5,K)**6)+
     &D(8)*(PT1(5,K)**7)+D(9)*(PT1(5,K)**8)+D(10)*(PT1(5,K)**9)
C
      IF(FFN(U)*FFN(B).GT.0)GO TO 45
       CALL C05ADF(U,B,EPS,ETA,FFN,X,IFAIL)
       IF (IFAIL.EQ.0) THEN
          WRITE (6,FMT=99997) X
       ELSE
          WRITE (6,FMT=99998) IFAIL
          IF (IFAIL.EQ.2 .OR. IFAIL.EQ.3) WRITE (6,FMT=99996) X
       END IF
      PT2(5,K)=X
      FN2(5,K)=D(1)+D(2)*PT2(5,K)+D(3)*(PT2(5,K)**2)+D(4)*(PT2(5,K)**3)+
     &D(5)*(PT2(5,K)**4)+D(6)*(PT2(5,K)**5)+D(7)*(PT2(5,K)**6)+
     &D(8)*(PT2(5,K)**7)+D(9)*(PT2(5,K)**8)+D(10)*(PT2(5,K)**9)
```

117

```
C ******** Point of intersection of 6th curve ********
45      J6=0
        DO 23 I=1,N
        IF(VR(I,11,K).GT.1.0D-0)GOTO 23
        IF(VR(I,11,K).EQ.0)GOTO 23
        J6=J6+1
        VR6(J6)=VR(I,11,K)
        FE6(J6)=FE(I,11,K)
23      CONTINUE
        IF(M1.GE.J6)GOTO 44
        CALL E02ACF(FE6,VR6,J6,D,M1,REF)
        DO 6 I=1,10
6       G(I)=D(I)
C
        IF(FN(A)*FN(B).GT.0)GO TO 44
        CALL C05ADF(A,B,EPS,ETA,FN,X,IFAIL)
        IF (IFAIL.EQ.0) THEN
           WRITE (6,FMT=99997) X
        ELSE
           WRITE (6,FMT=99998) IFAIL
           IF (IFAIL.EQ.2 .OR. IFAIL.EQ.3) WRITE (6,FMT=99996) X
        END IF
        PT1(6,K)=X
        FN1(6,K)=D(1)+D(2)*PT1(6,K)+D(3)*(PT1(6,K)**2)+D(4)*(PT1(6,K)**3)+
       &D(5)*(PT1(6,K)**4)+D(6)*(PT1(6,K)**5)+D(7)*(PT1(6,K)**6)+
       &D(8)*(PT1(6,K)**7)+D(9)*(PT1(6,K)**8)+D(10)*(PT1(6,K)**9)
C
        IF(FFN(U)*FFN(B).GT.0)GO TO 44
         CALL C05ADF(U,B,EPS,ETA,FFN,X,IFAIL)
         IF (IFAIL.EQ.0) THEN
            WRITE (6,FMT=99997) X
         ELSE
            WRITE (6,FMT=99998) IFAIL
            IF (IFAIL.EQ.2 .OR. IFAIL.EQ.3) WRITE (6,FMT=99996) X
         END IF
        PT2(6,K)=X
        FN2(6,K)=D(1)+D(2)*PT2(6,K)+D(3)*(PT2(6,K)**2)+D(4)*(PT2(6,K)**3)+
       &D(5)*(PT2(6,K)**4)+D(6)*(PT2(6,K)**5)+D(7)*(PT2(6,K)**6)+
       &D(8)*(PT2(6,K)**7)+D(9)*(PT2(6,K)**8)+D(10)*(PT2(6,K)**9)
C ******** Point of intersection of 7th curve ********
44      J7=0
        DO 24 I=1,N
        IF(VR(I,13,K).GT.1.0D-0)GOTO 24
        IF(VR(I,13,K).EQ.0)GOTO 24
        J7=J7+1
        VR7(J7)=VR(I,13,K)
        FE7(J7)=FE(I,13,K)
24      CONTINUE
        IF(M1.GE.J7)GOTO 43
        CALL E02ACF(FE7,VR7,J7,D,M1,REF)
        DO 7 I=1,10
7       G(I)=D(I)
C
```

```fortran
      IF(FN(A)*FN(B).GT.0)GO TO 43
      CALL C05ADF(A,B,EPS,ETA,FN,X,IFAIL)
      IF (IFAIL.EQ.0) THEN
         WRITE (6,FMT=99997) X
      ELSE
         WRITE (6,FMT=99998) IFAIL
         IF (IFAIL.EQ.2 .OR. IFAIL.EQ.3) WRITE (6,FMT=99996) X
      END IF
      PT1(7,K)=X
      FN1(7,K)=D(1)+D(2)*PT1(7,K)+D(3)*(PT1(7,K)**2)+D(4)*(PT1(7,K)**3)+
     &D(5)*(PT1(7,K)**4)+D(6)*(PT1(7,K)**5)+D(7)*(PT1(7,K)**6)+
     &D(8)*(PT1(7,K)**7)+D(9)*(PT1(7,K)**8)+D(10)*(PT1(7,K)**9)
C
      IF(FFN(U)*FFN(B).GT.0) GOTO 43
       CALL C05ADF(U,B,EPS,ETA,FFN,X,IFAIL)
       IF (IFAIL.EQ.0) THEN
          WRITE (6,FMT=99997) X
       ELSE
          WRITE (6,FMT=99998) IFAIL
          IF (IFAIL.EQ.2 .OR. IFAIL.EQ.3) WRITE (6,FMT=99996) X
       END IF
       PT2(7,K)=X
      FN2(7,K)=D(1)+D(2)*PT2(7,K)+D(3)*(PT2(7,K)**2)+D(4)*(PT2(7,K)**3)+
     &D(5)*(PT2(7,K)**4)+D(6)*(PT2(7,K)**5)+D(7)*(PT2(7,K)**6)+
     &D(8)*(PT2(7,K)**7)+D(9)*(PT2(7,K)**8)+D(10)*(PT2(7,K)**9)
C ******** Point of intersection of 8th curve ********
43    J8=0
      DO 25 I=1,N
      IF(VR(I,15,K).GT.1.0D-0)GOTO 25
      IF(VR(I,15,K).EQ.0)GOTO 25
      J8=J8+1
      VR8(J8)=VR(I,15,K)
      FE8(J8)=FE(I,15,K)
25    CONTINUE
      IF(M1.GE.J8)GO TO 42
      CALL E02ACF(FE8,VR8,J8,D,M1,REF)
      DO 8 I=1,10
8      G(I)=D(I)
C
      IF(FN(A)*FN(B).GT.0)GO TO 42
      CALL C05ADF(A,B,EPS,ETA,FN,X,IFAIL)
      IF (IFAIL.EQ.0) THEN
         WRITE (6,FMT=99997) X
      ELSE
         WRITE (6,FMT=99998) IFAIL
         IF (IFAIL.EQ.2 .OR. IFAIL.EQ.3) WRITE (6,FMT=99996) X
      END IF
      PT1(8,K)=X
      FN1(8,K)=D(1)+D(2)*PT1(8,K)+D(3)*(PT1(8,K)**2)+D(4)*(PT1(8,K)**3)+
     &D(5)*(PT1(8,K)**4)+D(6)*(PT1(8,K)**5)+D(7)*(PT1(8,K)**6)+
     &D(8)*(PT1(8,K)**7)+D(9)*(PT1(8,K)**8)+D(10)*(PT1(8,K)**9)
C
      IF(FFN(U)*FFN(B).GT.0) GOTO 42
```

```fortran
      CALL C05ADF(U,B,EPS,ETA,FFN,X,IFAIL)
      IF (IFAIL.EQ.0) THEN
         WRITE (6,FMT=99997) X
      ELSE
         WRITE (6,FMT=99998) IFAIL
         IF (IFAIL.EQ.2 .OR. IFAIL.EQ.3) WRITE (6,FMT=99996) X
      END IF
      PT2(8,K)=X
      FN2(8,K)=D(1)+D(2)*PT2(8,K)+D(3)*(PT2(8,K)**2)+D(4)*(PT2(8,K)**3)+
     &D(5)*(PT2(8,K)**4)+D(6)*(PT2(8,K)**5)+D(7)*(PT2(8,K)**6)+
     &D(8)*(PT2(8,K)**7)+D(9)*(PT2(8,K)**8)+D(10)*(PT2(8,K)**9)
C ******** Point of intersection of 9th curve ********
42    J9=0
      DO 26 I=1,N
      IF(VR(I,17,K).GT.1.0D-0)GOTO 26
      IF(VR(I,17,K).EQ.0)GOTO 26
      J9=J9+1
      VR9(J9)=VR(I,17,K)
      FE9(J9)=FE(I,17,K)
26    CONTINUE
      IF(M1.GE.J9) GOTO 40
      CALL E02ACF(FE9,VR9,J9,D,M1,REF)
      DO 9 I=1,10
      G(I)=D(I)
9     WRITE(6,*)D(I)
C
      IF(FN(A)*FN(B).GT.0)GO TO 40
      CALL C05ADF(A,B,EPS,ETA,FN,X,IFAIL)
      IF (IFAIL.EQ.0) THEN
         WRITE (6,FMT=99997) X
      ELSE
         WRITE (6,FMT=99998) IFAIL
         IF (IFAIL.EQ.2 .OR. IFAIL.EQ.3) WRITE (6,FMT=99996) X
      END IF
      PT1(9,K)=X
      FN1(9,K)=D(1)+D(2)*PT1(9,K)+D(3)*(PT1(9,K)**2)+D(4)*(PT1(9,K)**3)+
     &D(5)*(PT1(9,K)**4)+D(6)*(PT1(9,K)**5)+D(7)*(PT1(9,K)**6)+
     &D(8)*(PT1(9,K)**7)+D(9)*(PT1(9,K)**8)+D(10)*(PT1(9,K)**9)
C
      IF(FFN(U)*FFN(B).GT.0) GOTO 40
      CALL C05ADF(U,B,EPS,ETA,FFN,X,IFAIL)
      IF (IFAIL.EQ.0) THEN
         WRITE (6,FMT=99997) X
      ELSE
         WRITE (6,FMT=99998) IFAIL
         IF (IFAIL.EQ.2 .OR. IFAIL.EQ.3) WRITE (6,FMT=99996) X
      END IF
      PT2(9,K)=X
      FN2(9,K)=D(1)+D(2)*PT2(9,K)+D(3)*(PT2(9,K)**2)+D(4)*(PT2(9,K)**3)+
     &D(5)*(PT2(9,K)**4)+D(6)*(PT2(9,K)**5)+D(7)*(PT2(9,K)**6)+
     &D(8)*(PT2(9,K)**7)+D(9)*(PT2(9,K)**8)+D(10)*(PT2(9,K)**9)
C ******** Point of intersection of 10th curve ********
40    J10=0
```

120

```fortran
        DO 27 I=1,N
        IF(VR(I,18,K).GT.1.0D-0)GOTO 27
        IF(VR(I,18,K).EQ.0.D+0)GOTO 27
        J10=J10+1
        VR10(J10)=VR(I,18,K)
        FE10(J10)=FE(I,18,K)
27      CONTINUE
        IF(M1.GE.J10) GOTO 38
        CALL E02ACF(FE10,VR10,J10,D,M1,REF)
        DO 10 I=1,10
10      G(I)=D(I)
C
        IF(FN(A)*FN(B).GT.0)GO TO 38
        CALL C05ADF(A,B,EPS,ETA,FN,X,IFAIL)
        IF (IFAIL.EQ.0) THEN
           WRITE (6,FMT=99997) X
        ELSE
           WRITE (6,FMT=99998) IFAIL
           IF (IFAIL.EQ.2 .OR. IFAIL.EQ.3) WRITE (6,FMT=99996) X
        END IF
        PT1(10,K)=X
        FN1(10,K)=D(1)+D(2)*PT1(10,K)+D(3)*(PT1(10,K)**2)+
       &D(4)*(PT1(10,K)**3)+
       &D(5)*(PT1(10,K)**4)+D(6)*(PT1(10,K)**5)+D(7)*(PT1(10,K)**6)+
       &D(8)*(PT1(10,K)**7)+D(9)*(PT1(10,K)**8)+D(10)*(PT1(10,K)**9)
C
        IF( FFN(U)*FFN(B).GT.0) GOTO 38
         CALL C05ADF(U,B,EPS,ETA,FFN,X,IFAIL)
         IF (IFAIL.EQ.0) THEN
            WRITE (6,FMT=99997) X
         ELSE
            WRITE (6,FMT=99998) IFAIL
            IF (IFAIL.EQ.2 .OR. IFAIL.EQ.3) WRITE (6,FMT=99996) X
         END IF
         PT2(10,K)=X
         FN2(10,K)=D(1)+D(2)*PT2(10,K)+D(3)*(PT2(10,K)**2)+
       &D(4)*(PT2(10,K)**3)+
       &D(5)*(PT2(10,K)**4)+D(6)*(PT2(10,K)**5)+D(7)*(PT2(10,K)**6)+
       &D(8)*(PT2(10,K)**7)+D(9)*(PT2(10,K)**8)+D(10)*(PT2(10,K)**9)
C ******** Point of intersection of 11th curve ********
38      J11=0
        DO 37 I=1,N
        IF(VR(I,19,K).GT.1.0D-0)GOTO 37
        IF(VR(I,19,K).EQ.0)GOTO 37
        J11=J11+1
        VR11(J11)=VR(I,19,K)
        FE11(J11)=FE(I,19,K)
        WRITE(6,*) J11,FE11(J11),VR11(J11)
37      CONTINUE
C       M1=10
        IF(M1.GE.J11)GOTO 41
C       IF(M1.GE.J11) M1=J11-2
        CALL E02ACF(FE11,VR11,J11,D,M1,REF)
```

121

```
         DO 36 I=1,10
36       G(I)=D(I)
C
         IF(FN(A)*FN(B).GT.0)GO TO 41
         CALL C05ADF(A,B,EPS,ETA,FN,X,IFAIL)
         IF (IFAIL.EQ.0) THEN
            WRITE (6,FMT=99997) X
         ELSE
            WRITE (6,FMT=99998) IFAIL
            IF (IFAIL.EQ.2 .OR. IFAIL.EQ.3) WRITE (6,FMT=99996) X
         END IF
         PT1(11,K)=X
         FN1(11,K)=D(1)+D(2)*PT1(11,K)+D(3)*(PT1(11,K)**2)+
        &D(4)*(PT1(11,K)**3)+
        &D(5)*(PT1(11,K)**4)+D(6)*(PT1(11,K)**5)+D(7)*(PT1(11,K)**6)+
        &D(8)*(PT1(11,K)**7)+D(9)*(PT1(11,K)**8)+D(10)*(PT1(11,K)**9)
C
         IF(FFN(U)*FFN(B).GT.0)GO TO 41
          CALL C05ADF(U,B,EPS,ETA,FFN,X,IFAIL)
          IF (IFAIL.EQ.0) THEN
             WRITE (6,FMT=99997) X
          ELSE
             WRITE (6,FMT=99998) IFAIL
             IF (IFAIL.EQ.2 .OR. IFAIL.EQ.3) WRITE (6,FMT=99996) X
          END IF
         PT2(11,K)=X
         FN2(11,K)=D(1)+D(2)*PT2(11,K)+D(3)*(PT2(11,K)**2)+
        &D(4)*(PT2(11,K)**3)+
        &D(5)*(PT2(11,K)**4)+D(6)*(PT2(11,K)**5)+D(7)*(PT2(11,K)**6)+
        &D(8)*(PT2(11,K)**7)+D(9)*(PT2(11,K)**8)+D(10)*(PT2(11,K)**9)
C ******** Point of intersection of 12th curve ********
41       J12=0
         DO 137 I=1,N
         IF(VR(I,20,K).GT.1.0D-0)GOTO 137
         IF(VR(I,20,K).EQ.0)GOTO 137
         J12=J12+1
         VR12(J12)=VR(I,20,K)
         FE12(J12)=FE(I,20,K)
137        CONTINUE
         IF(M1.GE.J12)GOTO 141
         CALL E02ACF(FE12,VR12,J12,D,M1,REF)
         DO 336 I=1,10
336       G(I)=D(I)
C
         IF(FN(A)*FN(B).GT.0)GO TO 141
         CALL C05ADF(A,B,EPS,ETA,FN,X,IFAIL)
         IF (IFAIL.EQ.0) THEN
            WRITE (6,FMT=99997) X
         ELSE
            WRITE (6,FMT=99998) IFAIL
            IF (IFAIL.EQ.2 .OR. IFAIL.EQ.3) WRITE (6,FMT=99996) X
         END IF
         PT1(12,K)=X
```

```fortran
      FN1(12,K)=D(1)+D(2)*PT1(12,K)+D(3)*(PT1(12,K)**2)+
     &D(4)*(PT1(12,K)**3)+
     &D(5)*(PT1(12,K)**4)+D(6)*(PT1(12,K)**5)+D(7)*(PT1(12,K)**6)+
     &D(8)*(PT1(12,K)**7)+D(9)*(PT1(12,K)**8)+D(10)*(PT1(12,K)**9)
C
      IF(FFN(U)*FFN(B).GT.0)GO TO 141
       CALL C05ADF(U,B,EPS,ETA,FFN,X,IFAIL)
       IF (IFAIL.EQ.0) THEN
          WRITE (6,FMT=99997) X
       ELSE
          WRITE (6,FMT=99998) IFAIL
          IF (IFAIL.EQ.2 .OR. IFAIL.EQ.3) WRITE (6,FMT=99996) X
       END IF
      PT2(12,K)=X
      FN2(12,K)=D(1)+D(2)*PT2(12,K)+D(3)*(PT2(12,K)**2)+
     &D(4)*(PT2(12,K)**3)+
     &D(5)*(PT2(12,K)**4)+D(6)*(PT2(12,K)**5)+D(7)*(PT2(12,K)**6)+
     &D(8)*(PT2(12,K)**7)+D(9)*(PT2(12,K)**8)+D(10)*(PT2(12,K)**9)
141   XALP(1,K)=XAL(1,1,K)
      I=1
      DO 77 J=3,17,2
      I=I+1
77    XALP(I,K)=XAL(1,J,K)
      XALP(10,K)=XAL(1,18,K)
      XALP(11,K)=XAL(1,19,K)
      XALP(12,K)=XAL(1,20,K)
      WRITE(6,97)
      DO 73 I=1,12
      IF(FN1(I,K).EQ.0.0) GOTO 74
      PTF1(I,K)=PT1(I,K)-(TDSE)
73    WRITE(6,*) XALP(I,K),PTF1(I,K),PT1(I,K),FN1(I,K)
74    WRITE(6,95)
      DO 75 J=1,12
      IF(FN2(J,K).EQ.0)GOTO 76
      PTF2(J,K)=PT2(J,K)-(TDSE)
75    WRITE(6,*) XALP(J,K),PTF2(J,K),PT2(J,K),FN2(J,K)
76    RETURN
99998 FORMAT (' IFAIL =',I3)
99997 FORMAT (' ZERO =',F12.5)
99996 FORMAT (' FINAL POINT = ',F12.5)
100   FORMAT(5X,'POINT OF INTERSECTION OF FIRST CURVE = ',D15.6)
97    FORMAT (/' POINT OF INTERSECTION OF THE CURVES WITH THE GROWTH
     & LINE'/' STARTING FROM THE FIRST CURVE ARE FOLLOWING'/
     &'      (Xalpha)          (Gid)          (Gid+Gel+Gsurf)         (
     &Vrho)',/)
96    FORMAT ('      ',F8.4, 3(5X,D15.6))
95    FORMAT (/' POINT OF INTERSECTION OF CURVES WITH THE LINE OF NUCLEA
     &TION'/'      (Xalpha)          (Gid)          (Gid+Gel+Gsurf)
     & (Vrho)',/)
      END
C ********************************************************************
C     Subroutine plotting Xalpha versus velocity
C ********************************************************************
```

```fortran
      SUBROUTINE PLOT3 (K)
      COMMON XI(50,50,16),GID(50,50,16),FE(50,50,16),
     &VR(50,50,16),CTEMP,MUM,XAL(50,50,16),XALP(12,16),FN1(12,16),
     &FN2(12,16),PT1(12,16),PT2(12,16),PTF1(12,16),PTF2(12,16),
     &ANS1(50,50,16),ANS11(100),VKR1(12,16),VKR2(12,16),
     &XI11(12,16),XI22(12,16)
      COMMON /TWO/ TDSE
      DIMENSION FN11(12),FN22(12),VKR11(12),VKR22(12),
     &XALP1(12),XALP2(12),XX1(2),YY1(2),YY2(2),YY3(2),YY4(2)
      DOUBLE PRECISION Y1,Y2,YLA,FNMAX,FNMIN,DD,DD1,DD2,DD3,DD4,
     &XX1,YY1,YY2,YY3,YY4,A
      N=12
      T=CTEMP
      CALL GRMS3S(1.5)
      FNMAX=1.0D-30
      FNMIN=1.0D+30
      DO 123 I=1,N
      IF(FN1(I,K).LE.0.0) GOTO 124
      IF(FN1(I,K).LT.FNMIN) FNMIN=FN1(I,K)
      IF(FN1(I,K).GT.FNMAX) FNMAX=FN1(I,K)
124   IF(FN2(I,K).LE.0.0) GOTO 123
      IF(FN2(I,K).LT.FNMIN) FNMIN=FN2(I,K)
      IF(FN2(I,K).GT.FNMAX) FNMAX=FN2(I,K)
123   CONTINUE
      A=FNMAX*1.0D+1
      DO 150 I=1,N
      IF(VKR1(I,K).LE.0.0) GOTO 151
      IF(VKR1(I,K).GT.A) GOTO 150
      IF(VKR1(I,K).LT.FNMIN) FNMIN=VKR1(I,K)
      IF(VKR1(I,K).GT.FNMAX) FNMAX=VKR1(I,K)
151   IF(VKR2(I,K).LE.0.0) GOTO 150
      IF(VKR2(I,K).LT.FNMIN) FNMIN=VKR2(I,K)
      IF(VKR2(I,K).GT.FNMAX) FNMAX=VKR2(I,K)
150   CONTINUE
      IF(A.GT.FNMAX) FNMAX=A
      FNMAX=FNMAX/1.5D-09
      FNMIN=FNMIN/1.5D-09
      Y1=DLOG10(FNMIN)
      Y2=DLOG10(FNMAX)
      DD=(Y2-Y1)/25.0
      DD1=Y2-2*DD
      DD2=DD1-DD
      DD3=DD2-DD
      DD4=DD3-DD
      DD5=DD4-DD
      DD6=DD5-DD
      DD7=DD6-DD
      XX1(1)=0.0015D0
      XX1(2)=0.003D0
      YY1(1)=10**DD4
      YY1(2)=YY1(1)
      YY2(1)=10**DD5
      YY2(2)=YY2(1)
```

```
          YY3(1)=10**DD6
          YY3(2)=YY3(1)
          YY4(1)=10**DD7
          YY4(2)=YY4(1)
          CALL GRTX3D (1, 3.7, 0.0, 0.0, 3.7)
          CALL GRTX3D (2, 4.2, 0.0, 0.0, 4.2)
          CALL GRTX2D(2,9)
          CALL GRTX2D(1,9)
          CALL GRLM2S(0.15,0.45,0.52,0.97)
          CALL GRLM3S (0.00,0.015,Y1,Y2)
C         ***** Define annotation *****
          CALL GRTX4S (1,'!')
          CALL GRLS3S (1)
C         ***** Select line style for graph *****
          CALL GRTY5S (0,1)
          XALP(1,K)=0.0003D0
          J1=0
          DO 1 I=1,12
          IF(PT1(I,K).LE.0)GOTO 3
          IF(FN1(I,K).LE.0)GOTO 3
          J1=J1+1
          FN11(J1)=FN1(I,K)/1.5D-09
1         CONTINUE
3         IF(J1.LT.2) GOTO 101
          CALL GRGR7S (XALP,FN11,J1)
C         ***** Draw point for the curve identification *****
          CALL GRGR7D (XX1,YY1,2)
          CALL GRAN5S (0.0035,DD4,'growth',6,0.0)
C         ***** Select line style for graph *****
101       CALL GRTY5S (0,2)
          J2=0
          DO 2 I=1,12
          IF(PT2(I,K).LE.0)GOTO 4
          IF(FN2(I,K).LE.0)GOTO 4
          J2=J2+1
          FN22(J2)=FN2(I,K)/1.5D-09
2         CONTINUE
4         IF(J2.LT.2)GOTO 5
          CALL GRLS3S (2)
C         ***** Select line style for graph *****
          CALL GRGR7S (XALP,FN22,J2)
C         ***** Draw point for the curve identification *****
          CALL GRGR7D (XX1,YY2,2)
          CALL GRAN5S (0.0035,DD5,'nucleation',10,0.0)
5         I1=0
          DO 9 I=1,N
C          IF(I.LE.4) GOTO 9
          IF(XI11(I,K).LE.0) GOTO 9
          IF(VKR1(I,K).LE.0)GOTO 9
          IF(VKR1(I,K).GT.A) GOTO 9
          I1=I1+1
          VKR11(I1)=VKR1(I,K)/1.5D-09
          XALP1(I1)=XALP(I,K)
```

```
9       CONTINUE
        IF(I1.LT.2)GOTO 102
        CALL GRLS3S (4)
C       ***** Select line style for graph *****
        CALL GRTY5S (0,3)
        CALL GRGR7S (XALP1,VKR11,I1)
C       ***** Draw point for the curve identification *****
        CALL GRGR7D (XX1,YY3,2)
        CALL GRAN5S (0.0035,DD6,'solute trap (growth)',20,0.0)
102     I2=0
        DO 7 I=1,12
        IF(XI22(I,K).LE.0) GOTO 7
        IF(VKR2(I,K).LE.0)GOTO 7
        I2=I2+1
        VKR22(I2)=VKR2(I,K)/1.5D-09
        IF(VKR22(I2).GT.1.0D-03)VKR22(I2)=1.0D-04
        XALP2(I2)= XALP(I,K)
7       CONTINUE
        IF(I2.LT.2) GOTO 555
        CALL GRLS3S (3)
C       ***** Select line style for graph *****
        CALL GRTY5S (0,4)
        CALL GRGR7S (XALP2,VKR22,I2)
C       ***** Draw point for the curve identification *****
        CALL GRGR7D (XX1,YY4,2)
        CALL GRAN5S (0.0035,DD7,'solute trap (nucleation)',24,0.0)
555     CALL GRLS3S (1)
C       ***** Write string at any point *****
        CALL GRAN5D (0.0035,DD1,'Fe-0.4C wt.%',12,0.0)
        IF(K.EQ.1) CALL GRAN5S(0.0035,DD2,'T=410!SP!o!NL!C',15,0.0)
C       ***** Write heading and axis title *****
        CALL GRAN6S (' ',1,
       &'x!F3!!SB!a!NL!!RE! /mole fraction',33,
       &'Velocity /ms!SP!-1!NL!',22)
        RETURN
11      FORMAT(F6.4,2X,D15.5)
        END
C    ****************************************************************
C
        DOUBLE PRECISION FUNCTION FN(X)
        COMMON XI(50,50,16),GID(50,50,16),FE(50,50,16),
       &VR(50,50,16),CTEMP,MUM,XAL(50,50,16),XALP(12,16),FN1(12,16),
       &FN2(12,16),PT1(12,16),PT2(12,16),PTF1(12,16),PTF2(12,16),
       &ANS1(50,50,16),ANS11(100),VKR1(12,16),VKR2(12,16),
       &XI11(12,16),XI22(12,16)
        COMMON /ONE/ G(10)
        COMMON /TWO/ TDSE
        DOUBLE PRECISION X,W1,W2,W3,W4,W5,W6,K,V0,CTEMP,EE,V,MU,OMEGA,
       &A,T,GIH,Q0,RAD,GI,VI,Q
        V0=30.0D0
        RAD=1.5D-09
        K=1.38062D-23
        T=CTEMP+273.0
```

```fortran
      OMEGA=6.679D-6*(1+7.89D-5*T)/6.0225D+23
      IF(CTEMP.GE.25.AND.CTEMP.LE.540) EE=(-18.8D0*CTEMP+52400)*4.18E+6
      IF(CTEMP.GE.540.AND.CTEMP.LE.705) EE=(-37.6D0*CTEMP+62300)*4.18E+6
      IF(CTEMP.GE.260.AND.CTEMP.LE.595) V=(3.6D-5)*CTEMP+0.284
      IF(CTEMP.GE.595.AND.CTEMP.LE.705) V=(9.9D-5)*CTEMP+0.246
      MU=0.5D0*EE/(1+V)
      MUM= MU*OMEGA*6.0225D+23
      GIH=1.22D-3*MUM
      Q0=0.31*MU*OMEGA
       W1 =  V0*RAD
       W2 =        ( 1.0-DSQRT ( (X-(TDSE)) / GIH)    )
       W3 =      (K*T)
       W4 =       G(1) + G(2)*X + G(3)*(X*X)+G(4)*(X**3)+G(5)*(X**4)+
     &G(6)*(X**5)+G(7)*(X**6)+G(8)*(X**7)+G(9)*(X**8)+G(10)*(X**9)
       W5 =       -0.31 * OMEGA * MU * W2
       W6 = W5 / W3
      FN=  W1 * DEXP ( W6 ) -  W4
      RETURN
      END
C    *******************************************************************
C
      DOUBLE PRECISION FUNCTION FFN(X)
      COMMON XI(50,50,16),GID(50,50,16),FE(50,50,16),
     &VR(50,50,16),CTEMP,MUM,XAL(50,50,16),XALP(12,16),FN1(12,16),
     &FN2(12,16),PT1(12,16),PT2(12,16),PTF1(12,16),PTF2(12,16),
     &ANS1(50,50,16),ANS11(100),VKR1(12,16),VKR2(12,16),
     &XI11(12,16),XI22(12,16)
      COMMON /ONE/ G(10)
      COMMON /TWO/ TDSE
      DOUBLE PRECISION X,W1,W2,W3,W4,W5,W6,K,V0,EE,V,MU,OMEGA,
     &A,T,GIH,Q0,RAD,GI,VI,Q,W0,U,WW
      V0=30.0D0
      RAD=1.5D-09
      K=1.38062D-23
      T=CTEMP+273.0
      OMEGA=6.679D-6*(1+7.89D-5*T)/6.0225D+23
      IF(CTEMP.GE.25.AND.CTEMP.LE.540) EE=(-18.8D0*CTEMP+52400)*4.18E+6
      IF(CTEMP.GE.540.AND.CTEMP.LE.705) EE=(-37.6D0*CTEMP+62300)*4.18E+6
      IF(CTEMP.GE.260.AND.CTEMP.LE.595) V=(3.6D-5)*CTEMP+0.284
      IF(CTEMP.GE.595.AND.CTEMP.LE.705) V=(9.9D-5)*CTEMP+0.246
      MU=0.5D0*EE/(1+V)
      MUM= MU*OMEGA*6.0225D+23
      GIH=1.22D-3*MUM
      Q0=0.31*MU*OMEGA
      W7 =2.0D-3*MUM
       W1 =  V0*RAD
       IF(X.LT.W7) GOTO 1
       W2 =        ( 1.0-DSQRT ( (X-W7) / GIH)    )
       W3 =      (K*T)
       W4 =       G(1) + G(2)*X + G(3)*(X*X)+G(4)*(X**3)+G(5)*(X**4)+
     &G(6)*(X**5)+G(7)*(X**6)+G(8)*(X**7)+G(9)*(X**8)+G(10)*(X**9)
       W5 =       -0.31 * OMEGA * MU * W2
       W6 = W5 / W3
```

```
        FFN=  W1 * DEXP ( W6 )  -   W4
1       RETURN
        END
C ********************************************************************
C
        SUBROUTINE TRAP (N,K)
        COMMON XI(50,50,16),GID(50,50,16),FE(50,50,16),
       &VR(50,50,16),CTEMP,MUM,XAL(50,50,16),XALP(12,16),FN1(12,16),
       &FN2(12,16),PT1(12,16),PT2(12,16),PTF1(12,16),PTF2(12,16),
       &ANS1(50,50,16),ANS11(100),VKR1(12,16),VKR2(12,16),
       &XI11(12,16),XI22(12,16),XBAR
        COMMON /ONE/ G(10)
        COMMON /TWO/ TDSE
        DIMENSION FE1(100),FE2(100),FE3(100),FE4(100),FE5(100),
       &FE6(100),FE7(100),FE8(100),FE9(100),FE10(100),FE11(100),
       &XX1(5),XX2(5),YY1(5),YY2(5),
       &VR1(100),VR2(100),VR3(100),VR4(100),VR5(100),VR6(100),
       &VR7(100),VR8(100),VR9(100),VR10(100),VR11(100),Y(12),
       &VK1(12),VK2(12),DCT1(12),DCT2(12),
       &PT(12),C(3),KP1(12),KP2(12),E(12),F(12),
       &GID1(100),XI1(100),GID2(100),XI2(100),GID3(100),XI3(100),
       &GID4(100),XI4(100),GID5(100),XI5(100),GID6(100),XI6(100),
       &GID7(100),XI7(100),GID8(100),XI8(100),GID9(100),XI9(100),
       &GID10(100),XI10(100),GID11(100),XI101(100),GID12(100),XI12(100),
       &VD1(12),VD2(12),XI111(12),XALP11(12),XI222(12),XALP2(12),
       &XXII1(15),XXII2(15)
        DOUBLE PRECISION X1,Y2,Y1,X2,FE1,FE2,FE3,FE4,FE5,FE6,FE7,
       &FE8,FE9,FE10,VR1,VR2,VR3,VR4,VR5,VR6,VR7,VR8,VR9,VR10,VR11,
       &Y,P1,P2,MU1,MU2,Z1,Z2,XX1,XX2,YY1,YY2,DC,DCT1,DCT2,
       &GID1,XI1,GID2,XI2,GID3,XI3,GID4,XI4,GID5,XI5,GID6,XI6,
       &GID7,XI7,GID8,XI8,GID9,XI9,GID10,XI10,XI101,GID11,GID12,XI12,
       &C,X,RAD,XI111,XALP11,XI222,XALP2,XXII1,XXII2
        DOUBLE PRECISION XALPH,KE,KP1,KP2,A,B,LAM,VD,VD1,VD2,E,F,
       &XXII11(15),XALP111(15),XXII22(15), XALP222(15),VDR1(12,16),XEQ
        INTEGER M1,I,J,N1,N2
        INTEGER M
        INTEGER         IFAIL
        EXTERNAL        E02ACF
        EXTERNAL        XALPH
        T=CTEMP+273.0
        PI=3.1415927
        CALL ECON(T,XEQ)
        XALPP=XALPH(T)
        KE=XALPP/XEQ
        I1=0
        DO 14 I=1,N
        IF(XI(I,1,K) .LE. 0.0D0)GOTO 15
        GID1(I)=GID(I,1,K)
        I1=I1+1
14      XI1(I) = XI(I,1,K)
15      M1=3
        IF(FN1(1,K).LE.0)GOTO 10
        IF(M1.GE.I1) GOTO 220
```

```
          CALL E02ACF (GID1,XI1,I1,C,M1,REF)
          XI11(1,K)=C(1)+C(2)*PTF1(1,K)+C(3)*(PTF1(1,K)**2)
          A=XI11(1,K)
          XALP(1,K)=0.0003D0
          B=XALP(1,K)
          CALL INTEG (RAD,B,A,DC)
          DCT1(1)=DC
10        IF(FN2(1,K).LE.0)GOTO 220
          XI22(1,K)=C(1)+C(2)*PTF2(1,K)+C(3)*(PTF2(1,K)**2)
          A=XI22(1,K)
          CALL INTEG(RAD,B,A,DC)
          DCT2(1)=DC
220       I2=0
          DO 16 I=1,N
          IF(XI(I,3,K) .LE. 0.0D0)GOTO 17
          GID2(I)=GID(I,3,K)
          I2=I2+1
16        XI2(I) = XI(I,3,K)
17        IF(FN1(2,K).LE.0)GOTO 330
          IF(M1.GE.I2) GOTO 40
          CALL E02ACF (GID2,XI2,I2,C,M1,REF)
          XI11(2,K)=C(1)+C(2)*PTF1(2,K)+C(3)*(PTF1(2,K)**2)
          A=XI11(2,K)
          B=XALP(2,K)
          CALL INTEG(RAD,B,A,DC)
          DCT1(2)=DC
330       IF(FN2(2,K).LE.0)GOTO 40
          XI22(2,K)=C(1)+C(2)*PTF2(2,K)+C(3)*(PTF2(2,K)**2)
          A=XI22(2,K)
          CALL INTEG(RAD,B,A,DC)
          DCT2(2)=DC
40        I3=0
          DO 18 I=1,N
          IF(XI(I,5,K) .LE. 0.0D0)GOTO 19
          GID3(I)=GID(I,5,K)
          I3=I3+1
18        XI3(I) = XI(I,5,K)
19        IF(FN1(3,K).LE.0)GOTO 50
          IF(M1.GE.I3) GOTO 60
          CALL E02ACF (GID3,XI3,I3,C,M1,REF)
          XI11(3,K)=C(1)+C(2)*PTF1(3,K)+C(3)*(PTF1(3,K)**2)
          A=XI11(3,K)
          B=XALP(3,K)
          CALL INTEG(RAD,B,A,DC)
          DCT1(3)=DC
50        IF(FN2(3,K).LE.0)GOTO 60
          XI22(3,K)=C(1)+C(2)*PTF2(3,K)+C(3)*(PTF2(3,K)**2)
          A=XI22(3,K)
          CALL INTEG(RAD,B,A,DC)
          DCT2(3)=DC
60        I4=0
          DO 20 I=1,N
          IF(XI(I,7,K) .LE. 0.0D0)GOTO 21
```

129

```
       GID4(I)=GID(I,7,K)
       I4=I4+1
20     XI4(I) = XI(I,7,K)
21     IF(FN1(4,K).LE.0)GOTO 70
       IF(M1.GE.I4) GOTO 80
       CALL E02ACF (GID4,XI4,I4,C,M1,REF)
       XI11(4,K)=C(1)+C(2)*PTF1(4,K)+C(3)*(PTF1(4,K)**2)
       A=XI11(4,K)
       B=XALP(4,K)
       CALL INTEG(RAD,B,A,DC)
       DCT1(4)=DC
70     IF(FN2(4,K).LE.0)GOTO 80
       XI22(4,K)=C(1)+C(2)*PTF2(4,K)+C(3)*(PTF2(4,K)**2)
       A=XI22(4,K)
       CALL INTEG(RAD,B,A,DC)
       DCT2(4)=DC
80     I5=0
       DO 22 I=1,N
       IF(XI(I,9,K) .LE. 0.0D0)GOTO 23
       GID5(I)=GID(I,9,K)
       I5=I5+1
22     XI5(I) = XI(I,9,K)
23     IF(FN1(5,K).LE.0)GOTO 90
       IF(M1.GE.I5) GOTO 100
       CALL E02ACF (GID5,XI5,I5,C,M1,REF)
       XI11(5,K)=C(1)+C(2)*PTF1(5,K)+C(3)*(PTF1(5,K)**2)
       A=XI11(5,K)
       B=XALP(5,K)
       CALL INTEG(RAD,B,A,DC)
       DCT1(5)=DC
90     IF(FN2(5,K).LE.0)GOTO 100
       XI22(5,K)=C(1)+C(2)*PTF2(5,K)+C(3)*(PTF2(5,K)**2)
       A=XI22(5,K)
       CALL INTEG(RAD,B,A,DC)
       DCT2(5)=DC
100    I6=0
       DO 24 I=1,N
       IF(XI(I,11,K) .LE. 0.0D0)GOTO 25
       GID6(I)=GID(I,11,K)
       I6=I6+1
24     XI6(I) = XI(I,11,K)
25     IF(FN1(6,K).LE.0)GOTO 110
       X = PTF1(6,K)
       IF(M1.GE.I6) GOTO 120
       CALL E02ACF (GID6,XI6,I6,C,M1,REF)
       XI11(6,K)=C(1)+C(2)*PTF1(6,K)+C(3)*(PTF1(6,K)**2)
       A=XI11(6,K)
       B=XALP(6,K)
       CALL INTEG(RAD,B,A,DC)
       DCT1(6)=DC
110    IF(FN2(6,K).LE.0)GOTO 120
       XI22(6,K)=C(1)+C(2)*PTF2(6,K)+C(3)*(PTF2(6,K)**2)
       A=XI22(6,K)
```

```
        CALL INTEG(RAD,B,A,DC)
        DCT2(6)=DC
120     I7=0
        DO 26 I=1,N
        IF(XI(I,13,K) .LE. 0.0D0)GOTO 27
        GID7(I)=GID(I,13,K)
        I7=I7+1
26      XI7(I) = XI(I,13,K)
27      IF(FN1(7,K).LE.0)GOTO 130
        IF(M1.GE.I7) GOTO 140
        CALL E02ACF (GID7,XI7,I7,C,M1,REF)
        XI11(7,K)=C(1)+C(2)*PTF1(7,K)+C(3)*(PTF1(7,K)**2)
        A=XI11(7,K)
        B=XALP(7,K)
        CALL INTEG(RAD,B,A,DC)
        DCT1(7)=DC
130     IF(FN2(7,K).LE.0)GOTO 140
        XI22(7,K)=C(1)+C(2)*PTF2(7,K)+C(3)*(PTF2(7,K)**2)
        A=XI22(7,K)
        CALL INTEG(RAD,B,A,DC)
        DCT2(7)=DC
140     I8=0
        DO 28 I=1,N
        IF(XI(I,15,K) .LE. 0.0D0)GOTO 29
        GID8(I)=GID(I,15,K)
        I8=I8+1
28      XI8(I) = XI(I,15,K)
29      IF(FN1(8,K).LE.0)GOTO 150
        IF(M1.GE.I8) GOTO 160
        CALL E02ACF (GID8,XI8,I8,C,M1,REF)
        XI11(8,K)=C(1)+C(2)*PTF1(8,K)+C(3)*(PTF1(8,K)**2)
        A=XI11(8,K)
        B=XALP(8,K)
        CALL INTEG(RAD,B,A,DC)
        DCT1(8)=DC
150     IF(FN2(8,K).LE.0)GOTO 160
        XI22(8,K)=C(1)+C(2)*PTF2(8,K)+C(3)*(PTF2(8,K)**2)
        A=XI22(8,K)
        CALL INTEG(RAD,B,A,DC)
        DCT2(8)=DC
160     I9=0
        DO 30 I=1,N
        IF(XI(I,17,K) .LE. 0.0D0)GOTO 31
        GID9(I)=GID(I,17,K)
        I9=I9+1
30      XI9(I) = XI(I,17,K)
31      IF(FN1(9,K).LE.0)GOTO 170
        IF(M1.GE.I9) GOTO 180
        CALL E02ACF (GID9,XI9,I9,C,M1,REF)
        XI11(9,K)=C(1)+C(2)*PTF1(9,K)+C(3)*(PTF1(9,K)**2)
        A=XI11(9,K)
        B=XALP(9,K)
        CALL INTEG(RAD,B,A,DC)
```

131

```fortran
          DCT1(9)=DC
170       IF(FN2(9,K).LE.0)GOTO 180
          XI22(9,K)=C(1)+C(2)*PTF2(9,K)+C(3)*(PTF2(9,K)**2)
          A=XI22(9,K)
          CALL INTEG(RAD,B,A,DC)
          DCT2(9)=DC
180       I10=0
          DO 32 I=1,N
          IF(XI(I,18,K) .LE. 0.0D0)GOTO 33
          GID10(I)=GID(I,18,K)
          I10=I10+1
32        XI10(I) = XI(I,18,K)
33        IF(FN1(10,K).LE.0)GOTO 190
          IF(M1.GE.I10) GOTO 200
          CALL E02ACF (GID10,XI10,I10,C,M1,REF)
          XI11(10,K)=C(1)+C(2)*PTF1(10,K)+C(3)*(PTF1(10,K)**2)
          A=XI11(10,K)
          B=XALP(10,K)
          CALL INTEG(RAD,B,A,DC)
          DCT1(10)=DC
190       IF(FN2(10,K).LE.0) GOTO 200
          XI22(10,K)=C(1)+C(2)*PTF2(10,K)+C(3)*(PTF2(10,K)**2)
          A=XI22(10,K)
          CALL INTEG(RAD,B,A,DC)
          DCT2(10)=DC
C ********** Data of Xal and Xi for curve fitting ************
200       DO 300 I=1,10
          XALP11(I)=XALP(I,K)
          XXII1(I)=XI11(I,K)
          XXII2(I)=XI22(I,K)
300       CONTINUE
          XALP11(11)=XBAR
          XXII1(11)=XBAR
          XXII2(11)=XBAR
          XALP(11,K)=XBAR-0.00018
          XALP(12,K)=XBAR-0.00003
          IFAIL = 1
C         .. Parameters ..
          M=10
          I1111=0
          DO 1111 I=1, 11
          IF(XXII1(I).LE.0) GOTO 1111
          I1111=I1111+1
          XXII11(I1111)=XXII1(I)
1111      XALP111(I1111)=XALP11(I)
          IF(I1111.LT.4) GOTO 1113
          M=I1111-1
          CALL E02ACF(XALP111,XXII11,I1111,F,M,REF)
          DO 2 I=11,12
          XI11(I,K)=F(1)+F(2)*XALP(I,K)+F(3)*(XALP(I,K)**2)+
         &F(4)*(XALP(I,K)**3)
         &+F(5)*(XALP(I,K)**4)+F(6)*(XALP(I,K)**5)+F(7)*(XALP(I,K)**6)+
         &F(8)*(XALP(I,K)**7)+F(9)*(XALP(I,K)**8)+F(10)*(XALP(I,K)**9)
```

```
2       CONTINUE
        KKK=1
        IF(KKK.EQ.1) GOTO 1113
        M=10
        I1112=0
        DO 1112 I=1, 11
        IF(XXII2(I).LE.0) GOTO 1112
        I1112=I1112+1
        XXII22(I1112)=XXII2(I)
1112    XALP222(I1112)=XALP11(I)
        IF(I1112.LT.4) GOTO 1113
        M=I1112-1
        CALL E02ACF(XALP222,XXII22,I1112,E,M,REF)
        DO 7 I=11,12
        XI22(I,K)=E(1)+E(2)*XALP(I,K)+E(3)*(XALP(I,K)**2)+
        &E(4)*(XALP(I,K)**3)
        &+E(5)*(XALP(I,K)**4)+E(6)*(XALP(I,K)**5)+E(7)*(XALP(I,K)**6)+
        &E(8)*(XALP(I,K)**7)+E(9)*(XALP(I,K)**8)+E(10)*(XALP(I,K)**9)
7       CONTINUE
1113    M=9
        A=XI11(11,K)
        B=XALP(11,K)
        CALL INTEG(RAD,B,A,DC)
        DCT1(11)=DC
        A=XI22(11,K)
        CALL INTEG(RAD,B,A,DC)
        DCT2(11)=DC
        A=XI11(12,K)
        B=XALP(12,K)
        CALL INTEG(RAD,B,A,DC)
        DCT1(12)=DC
        A=XI22(12,K)
        CALL INTEG(RAD,B,A,DC)
        DCT2(12)=DC
4200    RAD=1.5D-09
        LAM=0.25D-09
        DO 313 I=1,12
        IF(XI11(I,K).LE.0) GOTO 312
        KP1(I)=XALP(I,K)/XI11(I,K)
312     VD1(I)=DCT1(I)/LAM
        VDR1(I,K)=RAD*VD1(I)
313     CONTINUE
        DO 51 I=1,12
        VK1(I)=(DCT1(I)*(KP1(I)-KE))/(LAM *(1-KP1(I)))
51      VKR1(I,K)=RAD*VK1(I)
        WRITE(6,37)
37      FORMAT(/' For Growth'//'      D             T             XAG',9X,
        &'XGA        Xalp        Xi          Vk             Vd',10X,
        &'Kp          Ke          Vk*rho'/' (m**2/sec)  (Centigrade)',1X,
        &' (mole fr.)  (mole fr.)  (mole fr.)  (mole fr.) (m/sec)',8X,
        &' (m/sec)                       (m**2/sec)'//)
        DO 34 I=1,12
        WRITE(6,35) DCT1(I),CTEMP,XALPP,XEQ,XALP(I,K),XI11(I,K),
```

```fortran
      &VK1(I),VD1(I),KP1(I),KE,VKR1(I,K)
34    CONTINUE
      DO 59 I=1,12
59    KP2(I)=0
      DO 53 I=1,12
      IF(XI22(I,K).LE.0) GOTO 311
      KP2(I)=XALP(I,K)/XI22(I,K)
311   VD2(I)=DCT2(I)/LAM
53    CONTINUE
      WRITE(6,38)
38    FORMAT(/' For Nucleation'//'        D             T            XAG',9X,
     &'XGA        Xalp        Xi          Vk          Vd',10X,
     &'Kp         Ke         Vk*rho'/' (m**2/sec)  (Centigrade)',1X,
     &'(mole fr.)  (mole fr.)  (mole fr.)  (mole fr.)  (m/sec)',8X,
     &' (m/sec)                      (m**2/sec)'//)
      II2=0
      DO 36 I=1,12
      IF(FN2(I,K).LE.0) GOTO 36
      IF(XI22(I,K).LE.0) GOTO 36
      II2=II2+1
      VK2(II2)=(DCT2(II2)*(KP2(II2)-KE))/(LAM *(1-KP2(II2)))
      VKR2(II2,K)=RAD*VK2(II2)
      WRITE(6,35) DCT2(II2),CTEMP,XALPP,XEQ,XALP(II2,K),XI22(II2,K),
     &VK2(II2),VD2(II2),KP2(II2),KE,VKR2(II2,K)
36    CONTINUE
35    FORMAT(D12.4,F12.4,9D12.4/)
      RETURN
      END
C ******************************************************************
C
      SUBROUTINE INTEG (RAD,XA,X,DIF)
      COMMON XI(50,50,16),GID(50,50,16),FE(50,50,16),
     &VR(50,50,16),CTEMP,MUM,XAL(50,50,16),XALP(12,16),FN1(12,16),
     &FN2(12,16),PT1(12,16),PT2(12,16),PTF1(12,16),PTF2(12,16),
     &ANS1(50,50,16),ANS11(100),VKR1(12,16),VKR2(12,16),
     &XI11(12,16),XI22(12,16),XBAR
      COMMON /TWO/ TDSE
      INTEGER T1,DUMMY,DUMMY3,CZ,II,II2,II3,II22,I2,I3,I4,I5,Z
      DOUBLE PRECISION XM,W,W1,T,T7,H1,S1,R,F,Q3,
     &XAS,XGS,FEA2,FEG2,CA2,CG2,G2,DG2,DFEG2,DCG2,T4,STRAIN,
     &J1,FEA1,FEG1,CA1,CG1,G1,DG1,DFEA1,DCA1,FEA3,CA3,G3,G4,
     &ACTIV,THETA,X,DACTIV,PSI,SIGMA,D1,M1,A5,D,YMAX,YMIN,OMEG
     &,M2,DASH,HH,KK,DUMMY1,DUMMY2,XALPHA,XMAX,DIF
     &,XMAXR,ERROR,XA,PECLET
      HH=6.6262D-34
      KK=1.38062D-23
      T=CTEMP+273.0D+00
      Z=12
      W=8302D+00
      A5=1.0D+00
      R=8.31432D+00
      DASH=(KK*T/HH)*DEXP(-(21230.0D+00/T))*DEXP(-31.84D+00)
      IF(X.LE.0) GOTO 990
```

134

```fortran
      THETA=X/(A5-X)
      ACTIV=CG(X,T,W,R)
      IF (ACTIV.EQ.0)GOTO 990
      ACTIV=DEXP(ACTIV)
      DACTIV=DCG(X,T,W,R)
      DACTIV=DACTIV*ACTIV
      DACTIV=DACTIV*A5/((A5+THETA)**2)
      SIGMA=A5-DEXP((-(W))/(R*T))
      PSI=ACTIV*(A5+Z*((A5+THETA)/(A5-(A5+Z/2)*THETA+(Z/2)*(A5+Z/2)*
     &(A5-SIGMA)*THETA*THETA)))+(A5+THETA)*DACTIV
      DIF=DASH*PSI
      DIF=DIF*1.0D-04
990   RETURN
      END
C ********************************************************************
C     Function giving the equilibrium mol. frac. carbon in alpha
C     based on my paper on first order quasichemical theory
C ********************************************************************
      DOUBLE PRECISION FUNCTION XALPH(T)
      DOUBLE PRECISION T,CTEMP
      CTEMP=(T-273.0D+00)/900.0D+00
      XALPH=0.1528D-02-0.8816D-02*CTEMP+0.2450D-01*CTEMP*CTEMP
     &-0.2417D-01*CTEMP*CTEMP*CTEMP+
     &0.6966D-02*CTEMP*CTEMP*CTEMP*CTEMP
      RETURN
      END
C ********************************************************************
C     Subroutine giving the equilib. carbon conc. of gamma (XEQ)
C ********************************************************************
      SUBROUTINE ECON(TT,XEQ)
      IMPLICIT REAL*8 (A-H,K-Z), INTEGER (I,J)
      COMMON /THREE/ CC(8),T10,T20
      COMMON /FOUR/ W
      DOUBLE PRECISION DXQ(40),DT4(40),DDFTO(40),C(8),P(7),Y(7)
     &,TEC(10),ALP(10),TC(10),XQ(10),D(8),SHEARH(40),DIFFH(40),A
      R=8.31432
      XEQ=0.2
      T=TT*1.0D+00
19    F=ENERGY(T,T10,T20)
      AJ=1-DEXP(-W/(R*T))
51    TEQ=R*T*AFEG(XEQ,T,AJ)-F
      IF (DABS(TEQ) .LT. 1.0) GOTO 50
      ETEQ=DAFEG(XEQ,T,AJ)*R*T
      XEQ=XEQ-TEQ/ETEQ
      GOTO 51
50    RETURN
      END
C ********************************************************************
C     Function giving Ln activity of iron in gamma
C ********************************************************************
      DOUBLE PRECISION FUNCTION AFEG(XEQ,T,AJ)
      DOUBLE PRECISION XEQ,T,AJ,DEQ,TEQ
      DEQ=DSQRT(1-2*(1+2*AJ)*XEQ+(1+8*AJ)*XEQ*XEQ)
```

```fortran
      TEQ=5*DLOG((1-XEQ)/(1-2*XEQ))
      TEQ=TEQ+DLOG(((1-2*AJ+(4*AJ-1)*XEQ-DEQ)/(2*AJ*(2*XEQ-1)))**6)
      AFEG=TEQ
      RETURN
      END
C ********************************************************************
C     Function giving differential of Ln activity of iron in gamma
C ********************************************************************
      DOUBLE PRECISION FUNCTION DAFEG(XEQ,T,AJ)
      DOUBLE PRECISION ETEQ,ETEQ2,DEQ,XEQ,T,AJ
      DEQ=DSQRT(1-2*(1+2*AJ)*XEQ+(1+8*AJ)*XEQ*XEQ)
      ETEQ=5*((1/(XEQ-1))+2/(1-2*XEQ))
      ETEQ2=6*((4*AJ-1-(0.5/DEQ)*(-2-4*AJ+2*XEQ+16*XEQ*AJ))
     &/(1-2*AJ+(4*AJ-1)*XEQ-DEQ))+6*(4*AJ/(2*AJ*(2*XEQ-1)))
      DAFEG=ETEQ+ETEQ2
      RETURN
      END
C********************************************************************
C
      DOUBLE PRECISION FUNCTION ENERGY(T,T10,T20)
      DOUBLE PRECISION T,T10,T20,F,T7
      T7=T-100*T20
      IF (T7 .LT. 300) GOTO 1
      IF (T7 .LT. 700) GOTO 2
      IF (T7 .LT. 940) GOTO 3
      F=-8.88909+0.26557*(T7-1140)-1.04923D-3*((T7-1140)**2)
      F=F+2.70013D-6*((T7-1140)**3)-3.58434D-9*((T7-1140)**4)
      GOTO 4
1     F=1.38*T7-1499
      GOTO 4
2     F=1.65786*T7-1581
      GOTO 4
3     F=1.30089*T7-1331
4     ENERGY=(141*T10 + F)*4.187
      RETURN
      END
```

Appendix II

Computer Program for the Calculations of Partitioning of Carbon from Supersaturated Ferrite Plates

```
C FTVSCLR PROGRAM = .PRO DATA = .DATA OUTPUT = .OUT PLOT = .GRAPH NAG
C CAMPLOT
C
C Program using finite difference method for the solution of the problem
C of X enrichment of austenite during the ageing of bainitic steels
C
C W     = Carbon-carbon interaction energy in austenite
C EQFER = Equilibrium wt.% of X in ferrite at ageing temperature
C EQAUS = Equilibrium wt.% of X in austenite at ageing temperature
C EBAR  = Average X wt.% in alloy
C FERS  = normalised concentration of X at ferrite surface
C AUSS  = normalised concentration of X at austenite surface
C TIMH  = time in hours
C KTEMP = Absolute temperature
C TAUS  = Thickness of austenite in meters
C TFER  = (Half) thickness of ferrite in meters
C DFER  = Diffusivity of X in ferrite
C DAUS  = Diffusivity of X in austenite
C Concentrations normalized relative to average alloy concentration
C Dimension normalize relative to carbide particle thickness
C IAUS, IFER, J1 are the number of finite slices
C  for dimension and time respectively
C TIM   = Time, in seconds
C A3 controls the amount of information that is printed out
C IAUS2, IFER2 control the amount of information printed out
C SETIME controls the time in hours that the experiment runs.
C JTEST modifies the mass balance condition when the AUSS reaches
C        the equilibrium concentration. Hence mass conserved
C
C Typical data
C 838.15 0.5D-03 39.0D+00 2.5D+00 1.0D-07 2.0D-06 1000 5
C 1.0 1.0
C 8340
C End of data
C
      IMPLICIT REAL*8(A-H,K-Z), INTEGER(I,J)
      INTEGER L,NN,MM
     DOUBLE PRECISION XI(2500),CAUS1(2500),XJ(2500),
    &CFER1(2500),
    &CFER(2500,2), CAUS(2500,2),TIMS1(2500),FER4(2500),
    &TIMS2(2500),FER5(2500),DISG(2500),XG(2500),DISA(2500),XA(2500),
    &DISA1(2500),DISG1(2500),X(2500),DISA2(2500),DISG2(2500),
```

```
      &LENA1(2500),LENA2(2500),CON(2500),LENG1(2500),LENG2(2500),
      &TIMES(2500),TEMP(2500),LG1(5),LG2(5),XXA1(5), XXA2(5),
      &XXG1(2500),XXG2(2500),XA2(2500),XA22(2500),DISA11(2500),
      &XG1(2500),CONG(2500),CONA(2500),CAAUS(2500),
      &CAFER(2500),FER6(2500),AUS6(2500),XII
          J4=0
          J5=0
          JTEST=0
          IAUS2=20
          IFER2=1
          READ(5,*)KTEMP,EQFER,EQAUS,EBAR,TAUS,TFER,J1,IAUS
          READ(5,*)A3,SETIME
          READ(5,*)W
          RFER=0.04D+00
          RAUS=RFER
          WRITE(6,9998)RAUS,RFER
9998      FORMAT(' RAUS, RFER,(dimensionless) =', 2D12.4)
          CALL GRST3D(1.5,200.0)
          CALL GRFT6D(-1.0,0.0)
          N=1
          DO 10 JJ=1,N
          CTEMP=KTEMP-273.15D+00
          WRITE(6,13) CTEMP
13        FORMAT(//'  ************',F10.2,'***************')
          DFER=DIFF(KTEMP)
          DAUS=DIFFF(W,EBAR,EQAUS,CTEMP)
          STAUS=TAUS/IAUS
          TIME=RAUS*STAUS*STAUS/DAUS
          STFER=DSQRT(TIME*DFER/RFER)
          IFER=DINT(TFER/STFER)
        AUSS=EQAUS/EBAR
        DR=DAUS*STFER/(DFER*STAUS)
          CFER(1,1)=0.50D+00*AUSS*DR + EQFER/EBAR
          CAUS(1,1)=(EQFER/EBAR -CFER(1,1))/DR + AUSS
        WRITE(6,28)DFER,DAUS,TFER,TAUS,EQFER,EQAUS,KTEMP,IAUS,IFER
      &,STAUS,STFER,DR,W
         DO 6 I=2,IAUS
         CAUS(I,1)=1.0D+00
6         CONTINUE
         DO 26 I=2,IFER
         CFER(I,1)=1.0D+00
26        CONTINUE
        WRITE(6,12)CAUS(1,1),CFER(1,1)
C
C Finite difference analysis
C
        TIM=0.0D+00
        WRITE(6,34)
        II4=0
        DO 1 J=2,J1
         TIM=TIM+TIME
         TIMH=TIM/3600.0D+00
         IF(TIMH .GT. SETIME)GOTO 101
```

```
          AUS3=0.0D+00
          FER3=0.0D+00
C *************** Austenite  ******************
       DO 20 II=1,IAUS
       IF(II .EQ. 1)GOTO 21
C Ensure reflection at last slice
       IF(II .EQ. IAUS)GOTO 22
       CAUS(II,2)=CAUS(II,1)+RAUS*(CAUS(II-1,1)
      &-2.0D+00*CAUS(II,1)+CAUS(II+1,1))
       GOTO 23
21     IF(JTEST .EQ. 0) GOTO 30
       AUSS=((CFER(1,1)-FERS)/DR) + CAUS(1,1)
30     CAUS(1,2)=CAUS(1,1) + RAUS*(AUSS - 2.0D+00*CAUS(1,1)
      & + CAUS(2,1))
       GOTO 23
22     CAUS(IAUS,2)=CAUS(IAUS,1)+RAUS*(CAUS(IAUS-1,1)
      &-2.0D+00*CAUS(IAUS,1)+CAUS(IAUS-1,1))
       CALL SOFT(CAUS(IAUS,2),1,J4,TIMH)
23     AUS=CAUS(II,2)*EBAR
       XTAUS=STAUS*II
       AUS3=AUS+AUS3
       CAUS(II,1)=CAUS(II,2)
20        CONTINUE
C *************** Ferrite  ******************
       DO 2 I=1,IFER
       IF(I .EQ. 1)GOTO 3
C Reflect at position of symmetry
       IF(I .EQ. IFER) GOTO 4
       CFER(I,2)=CFER(I,1)+RFER*(CFER(I-1,1)
      &-2.0D+00*CFER(I,1)+CFER(I+1,1))
       IF(CFER(I,2).LT.0.1D-50) CFER(I,2)=0.0D0
       GOTO 5
C CALCULATE SURFACE CONCENTRATION IN FERRITE APPROPRIATE FOR MASS BALA
3      FERS=DR*(CAUS(1,1)-AUSS)+CFER(1,1)
       IF(FERS .LT. (EQFER/EBAR))GOTO 90
       GOTO 91
90     FERS=EQFER/EBAR
       JTEST=1
91     CFER(1,2)=CFER(1,1) + RFER*(FERS-2.0D+00*CFER(1,1)
      & + CFER(2,1))
       IF(CFER(I,2).LT.0.1D-50) CFER(I,2)=0.0D0
       GOTO 5
4      CFER(IFER,2)=CFER(IFER,1)+RFER*(CFER(IFER-1,1)
      &-2.0D+00*CFER(IFER,1)+CFER(IFER-1,1))
       IF(CFER(IFER,2).LT.0.1D-50) CFER(I,2)=0.0D0
       CALL SOFT(CFER(IFER,2),2,J5,TIMH)
5      FER=CFER(I,2)*EBAR
       XTFER=I*STFER
       FER3=FER+FER3
       CFER(I,1)=CFER(I,2)
2      CONTINUE
       AUS3=AUS3/IAUS
       FER3=FER3/IFER
```

```
      DUMMY=J/A3
      DUMMY=DINT(DUMMY)-DUMMY
      IF(DUMMY .NE. 0.0)GOTO 1
      AVER=(FER3*0.5D+00*TFER + AUS3*TAUS)/(0.5D+00*TFER+TAUS)
      II4=II4+1
      TIMS=TIMH*3600.0D+00
      TIMS1(II4)=TIMS
      FER4(II4)=FER3
      AUS6(II4)=AUSS*EBAR
      FER6(II4)=FERS*EBAR
      WRITE(6,27)TIMH,TIMS1(II4),AUS3,FER4(II4),AVER,FER6(II4),
     &AUSS*EBAR
      JJ1=0
      JJ2=0
      DO 201 II=1,IAUS,IAUS2
      IF(CAUS(II,2) .LT. 1.0001) GOTO 203
      JJ1=JJ1+1
      XI(JJ1)=II
      CAUS1(JJ1)=CAUS(II,2)*EBAR
201   CONTINUE
203   DO 202 I=1,IFER,IFER2
      IF(CFER(I,2) .GT. 0.9999) GOTO 204
      JJ2=JJ2+1
      XJ(JJ2)=I
      CFER1(JJ2)=CFER(I,2)*EBAR
202   CONTINUE
204      WRITE(6,7) XJ(JJ2),CFER1(JJ2)
      IF(FER4(II4) .LE. FER6(II4) )GOTO 101
      IF(II4.EQ.1) GOTO 210
      K=II4/201
      XX=II4/201.0
      IF(K.NE.XX)GOTO 1
210   NN=JJ1+1
      NN=JJ1+1
      MM=JJ2+1
      NFER=IFER
      DISG(1)=0
      XG(1)=AUSS*EBAR
      DO 15 I=2,NN
      DISG(I)=XI(I-1)
      XG(I)=CAUS1(I-1)
15    CONTINUE
      DO 16 I=1,JJ2
      DISA(I)=XJ(I)
      XA(I)=CFER1(I)
      IF(XA(I).LT.0.1D-50)XA(I)=0.0D0
16    CONTINUE
      DO 17 I=1,JJ2
      DISA1(I)=DISA(I)*STFER
      XA22(I)=XA(I)
17    CONTINUE
      DO 170 I=2,MM
      DISA11(I)=TFER-DISA1(I-1)
```

```
      XA2(I)=XA22(I-1)
170   CONTINUE
      DISA11(1)=TFER
      XA2(1)=FERS*EBAR
      IF(XA2(1).LT.0.1D-10) XA2(1)=0.0D0
      L=MM+NN
      DO 18 I=1,NN
      DISG1(I)=(DISG(I)*STAUS)+TFER
      XG1(I)=XG(I)
18    CONTINUE
      DO 19 I=1,NN
      DISG2(I)=-DISG1(I)
19    CONTINUE
      DO 119 I=1,MM
      DISA2(I)=-DISA11(I)
119   CONTINUE
      DO 116 I=1,NN
      LENG1(I)=DISG1(I)/(TAUS+TFER)
      LENG2(I)=DISG2(I)/(TAUS+TFER)
116   CONG(I)=XG1(I)
C...................... For boundary lines ...............
                      LG1(1)=-TFER/(TAUS+TFER)
                      XXG1(1)=0
                      LG1(2)=LG1(1)
                      XXG1(2)=EQAUS
                 LG2(1)=TFER/(TAUS+TFER)
                 XXG2(1)=0
                 LG2(2)=LG2(1)
                 XXG2(2)=EQAUS


                              CALL GRFT5D (4,2,1,2)
C CALL GRFT5S(ILEFT,IRIGHT,ILO,IHI)
C 0  nothing      3  annotations
C 1  line         4  marks and annotations C
C 2  marks

      CALL GRTX3D (1, 4.0, 0.0, 0.0, 4.0)
      CALL GRTX3D (2, 4.0, 0.0, 0.0, 4.0)
      CALL GRLM3D (0.0D0,1.0D0,0.0D0,0.20D0)
      CALL GRLM2S (0.3, 0.8, 0.45, 0.75)
      CALL GRTX2S(2,9)
C     ***** Define annotation *****
      CALL GRTX4S (1,'!')
       CALL GRGR6D (LG2,XXG2,2)
       CALL GRGR6D (LENG1,CONG,NN)
      IF(II4.EQ.1) CALL GRAN5S ( 0.6,0.1,'!F3!g!F1!',9,0.0)
      IF(II4.EQ.1) CALL GRAN5S ( 0.05,0.18,'T = 450 !SP!o!NL!C',18,0.0)
      IF(II4.EQ.1) CALL GRAN5S( 0.4,0.18,'Fe-0.4C wt. %',13
     &,0.0)
       CALL GRTX2D(1,9)
       IF(II4.EQ.1) CALL GRAN6D (' '
     &,1,' ',1,'Carbon conc. /mole frac.',24)
C...................... For boundary lines ...............
```

```
         DO 117 I=1,MM
         LENA1(I)=DISA11(I)/(TAUS+TFER)
         LENA2(I)=DISA2(I)/(TAUS+TFER)
117      CONA(I)=XA2(I)
                              XXA1(1)=0.0
                              XXA1(2)=0.022D0
                    XXA2(1)=0.0
                    XXA2(2)=0.022D0
                                   CALL GRFT5D (4,2,4,0)
         CALL GRTX3D (1, 4.0, 0.0, 0.0, 4.0)
         CALL GRTX3D (2, 4.0, 0.0, 0.0, 4.0)
         CALL GRFR6D(1)
         CALL GRLM3D(0.0D0,1.0D0,0.0D0,0.022D0)
         CALL GRLM2S (0.3,0.8,0.2,0.45)
         CALL GRTX2S(2,9)
C        ***** Define annotation *****
         CALL GRTX4S (1,'!')
         IF(FER6(II4).EQ.0) GOTO 221
          CALL GRGR6D (LG2,XXA2,2)
          CALL GRGR6D (LENA1,CONA,MM)
221      IF(II4.EQ.1) CALL GRAN5S (        0.15,0.020,'!F3!a',5,0.0)
         CALL GRTX2D(1,9)
         IF(II4.EQ.1) CALL GRAN6D (' '
        &,1,'Normalised distance',19,'Carbon conc. /mole frac.',24)
1        CONTINUE
101      DO 14 I=1,II4
         TIMS2(I)=TIMS1(I)
         FER5(I)=FER4(I)
         WRITE(6,*)TIMS2(I),FER5(I)
14       CONTINUE
         TMAX=1.0D-9
         DO 114 I=1,II4
         IF(TIMS2(I).GT.TMAX)TMAX=TIMS2(I)
114      CONTINUE
         TH=TMAX/2.0
         TH1=TMAX/5.0
         TH2=TMAX/10.0
         TMAX=TMAX+TH1
         KTEMP=KTEMP+20
10       CONTINUE
         CALL GRST9S
29       FORMAT(' TIME, s =',D12.4,'   TIME, hrs. =',F12.3)
28       FORMAT(' Diffusion coefficient in ferrite, m**2/s = ',
        &D12.4/' Diffusion coefficient in austenite, m**2/s, = ',D12.4/
        & ' Half thickness of ferrite, m =',D12.4/
        & ' Thickness of austenite, m =',D12.4/
        & ' Eq. conc. of X at interface, in ferrite, wt.% = ',D12.4/
        & ' Eq. conc. of X at interface, in austenite, wt.% = ',D12.4/
        & ' Absolute Temperature = ', F8.2, ' IAUS, IFER = ',2I9/
        & ' Austenite slice thickness, meters ',D12.4/
        & ' Ferrite slice thickness, meters   ',D12.4/
        & ' DR, dimensionless ',D12.4/
        & ' Carbon-Carbon interaction energy, J/mole = ',D12.4//)
```

142

```fortran
34        FORMAT('    HOURS     SECS     AUS     FERRITE  AVERAGE X FERS'
     &,'    AUSS')
27        FORMAT(2D12.4,F9.4, F9.6,F9.4,F9.6,2F9.6)
24        FORMAT('      No   Norm. Conc.  wt.%X in Ferrite')
25        FORMAT(' No   Norm. Conc.     wt.%X in Austenite')
7         FORMAT(F8.2,D12.4,2F10.5)
71        FORMAT(I5,D12.4,2F10.5)
11        FORMAT('--------------------------------------------------------')
12        FORMAT(' Time 0, slice 1, austenite and ferrite norm conc ',
     &2F12.4/)
          STOP
          END
C ***********************************************************************
C
          DOUBLE PRECISION FUNCTION DIFF(KTEMP)
          DOUBLE PRECISION R,KTEMP,PHI,DOTO,DTT,F
          R=8.3143
          PHI=1.0D+00-1.0/(0.5D+00*DEXP(7.2D+03*4.184/(R*KTEMP))
     &*DEXP(4.4D+00) + 1.0D+00)
          DOTO=3.3D-07*DEXP(-19.3D+03*4.184D+00/(R*KTEMP))
          DTT=3.0D-04*DEXP(-14.7D+03*4.184D+00/(R*KTEMP))
          F=0.86D+00
          DIFF=PHI*DOTO+(1.0D+00-PHI)*F*DTT+(1.0D+00-PHI)
     &*(1.0D+00-F)*DOTO
C Diffusion of carbon in ferrite, m*m/s
C Mclellan et al., Trans. Met. Soc. AIME, Vol. 233 (1965) 1938
C R     = Universal Gas Constant, J/mol/K
C KTEMP = Absolute Temperature
          RETURN
          END
C
C ***********************************************************************
C
          SUBROUTINE SOFT(A,I,J,TIMH)
          DOUBLE PRECISION A,TIMH
          IF(J .GT. 1) GOTO 3
          IF(I .EQ. 1)GOTO 1
          IF(A .LT. 0.99) GOTO 2
          GOTO 3
2         WRITE(6,10)TIMH
          J=3
10        FORMAT(' SOFT IMPINGEMENT IN FERRITE', D12.4,' hours')
          GOTO 3
1         IF(A .GT. 1.01D+00)GOTO 4
          GOTO 3
4         WRITE(6,11)TIMH
          J=3
11        FORMAT(' SOFT IMPINGEMENT IN AUSENTITE',D12.4,' hours')
3         RETURN
          END
C
C***********************************************************************
C
```

```fortran
      SUBROUTINE DIFFF(W,XBAR,XGAG,CTEMP)
C
C Program to calculate the effective diffusivity of carbon in
C austenite, taking account of the fact that this diffusivity
C is concentration dependent.  Uses Siller and McLellan theory
C to express the concentration dependence, and Lacher et al
C theory to allow for the effect of substitutional alloyingNTS
C on the activity and W of carbon in austenite.
C HH     = Planks const. Joules/sec
C KK     = Boltzmann's const. Joules/degree kelvin
C D      = Diffusivity of carbon in austenite  m*m/s
C Z      = Coordination of interstial site
C PSI    = Composition dependence of diffusion coefficient
C THETA  = No. of C atoms/ No. Fe atoms
C ACTIV  = Activity of carbon in austenite
C R      = Gas constant
C X      = Mole fraction of carbon
C T      = Absolute temperature
C SIGMA  = Site exclusion probablity
C W      = Carbon carbon interaction energy in austenite
C
      IMPLICIT REAL*8(A-H,K-Y), INTEGER(I,J,Z)
      DOUBLE PRECISION DIFF(500), CARB(500)
      HH=6.6262D-34
      KK=1.38062D-23
      Z=12
      A5=1.0D+00
      R=8.31432D+00
      T=CTEMP+273.00D+00
      II2=0
      WRITE(6,7)T,CTEMP,XBAR,XGAG
      DASH=(KK*T/HH)*DEXP(-(21230.0D+00/T))*DEXP(-31.84D+00)
      DO 9   II=1,1000
      CARB(1)=XBAR
      IF (II .GT. 1)GOTO 1
      GOTO 8
1     IF((XGAG-XBAR) .LT. 0.005)GOTO 2
      GOTO 3
2     XINCR=0.0001D+00
      GOTO 4
3     XINCR=0.001D+00
4     CARB(II)=CARB(II-1)+XINCR
      IF (CARB(II) .GT. XGAG) GOTO 5
8     X=CARB(II)
C
      IF(X .GT. 1.0/7.0)THEN
      DIFF(II) = DIFF(II-1)
      GOTO 9
      ENDIF
C  Siller and Mclellan model breaks down for Carbon > 1/7
      II2=II2+1
      THETA=X/(A5-X)
      ACTIV=CG(X,T,W,R)
```

144

```fortran
      ACTIV=DEXP(ACTIV)
      DACTIV=DCG(X,T,W,R)
      DACTIV=DACTIV*ACTIV
      DACTIV=DACTIV*A5/((A5+THETA)**2)
      SIGMA=A5-DEXP((-(W))/(R*T))
      PSI=ACTIV*(A5+Z*((A5+THETA)/(A5-(A5+Z/2)*THETA+(Z/2)*(A5+Z/2)*
     &(A5-SIGMA)*THETA*THETA)))+(A5+THETA)*DACTIV
      DIFF(II)=DASH*PSI*1.0D-04
9     CONTINUE
5     II3=0
      CALL TRAPE(CARB,DIFF,ANS,II2,ERROR,II3)
      ANS=ANS/(XGAG-XBAR)
      WRITE(6,6)ANS,ERROR
7     FORMAT(' ABSOLUTE TEMPERATURE, DEGREES KELVIN =',F8.1/
     &'            TEMPERATURE IN DEGREES CENTIGRADE =',F8.1/
     &' MOL FRAC CARBON XBAR = ',F8.4/
     &' MOL FRAC CARBON XGAG =',F8.4)
6     FORMAT(' INTEGRAL, XGAG-XBAR = ',D12.4, '   m*m/s  ',
     &8HERROR = , D12.4)
      RETURN
      END
C     ***********************************************************
C
      SUBROUTINE TRAPE(X,Y,ANS,NDIM,ERROR,II2)
C
      DOUBLE PRECISION X(1000),Y(1000),AZ(1000)
      DOUBLE PRECISION SUM1,SUM2,ANS
      SUM2=0.D+00
      IF(NDIM-1)4,3,1
C
C     INTEGRATION LOOP
1     DO 2 I=2,NDIM
      SUM1=SUM2
      SUM2=SUM2+.5D+00*(X(I)-X(I-1))*(Y(I)+Y(I-1))
2     AZ(I-1)=SUM1
3     AZ(NDIM)=SUM2
      ANS=SUM2
4     RETURN
      END
C******************************************************************************
C
      DOUBLE PRECISION FUNCTION CG(X,T,W,R)
      DOUBLE PRECISION J,DG,DUMMY,T,R,W,X
      J=1-DEXP(-W/(R*T))
      DG=DSQRT(1-2*(1+2*J)*X+(1+8*J)*X*X)
      DUMMY=5*DLOG((1-2*X)/X)+6*W/(R*T)+((38575.0)-(
     &13.48)*T)/(R*T)
      CG=DUMMY+DLOG(((DG-1+3*X)/(DG+1-3*X))**6)
      RETURN
      END
C******************************************************************************
C
      DOUBLE PRECISION FUNCTION DCG(X,T,W,R)
```

145

```
DOUBLE PRECISION J,DG,DDG,X,T,W,R
J=1-DEXP(-W/(R*T))
DG=DSQRT(1-2*(1+2*J)*X+(1+8*J)*X*X)
DDG=(0.5/DG)*(-2-4*J+2*X+16*J*X)
DCG=-((10/(1-2*X))+(5/X))+6*((DDG+3)/(DG-1+3*X
&)-(DDG-3)/(DG+1-3*X))
RETURN
END
```